CHAPTER 5

Reflection and Transmission

5.1 INTRODUCTION

In the previous chapter we discussed solutions to TEM waves in unbounded media. In real-world problems, however, the fields encounter boundaries, scatterers, and other objects. Therefore the fields must be found by taking into account these discontinuities.

In this chapter we want to discuss TEM field solutions in two semi-infinite lossless and lossy media bounded by a planar boundary of infinite extent. Reflection and transmission coefficients will be derived to account for the reflection and transmission of the fields by the boundary. These coefficients will be functions of the constitutive parameters of the two media, the direction of wave travel (angle of incidence), and the direction of the electric and magnetic fields (wave polarization).

In general, the reflection and transmission coefficients are complex quantities. It will be demonstrated that their amplitudes and phases can be varied by controlling the direction of wave travel (angle of incidence). In fact, for one wave polarization (parallel polarization) the reflection coefficient can be made equal to zero. When this occurs, the angle of incidence is known as the *Brewster angle*. This principle is used in the design of many instruments (such as binoculars).

The magnitude of the reflection coefficient can also be made equal to unity by properly selecting the wave incidence angle. This angle is known as the *critical angle*, and it is independent of wave polarization; however, in order for this angle to occur, the incident wave must exist in the denser medium. The critical angle concept plays a crucial role in the design of transmission lines (such as optical fiber, slab wave-guides, and coated conductors; the microstrip is one example).

5.2 NORMAL INCIDENCE - LOSSLESS MEDIA

We begin the discussion of reflection and transmission from planar boundaries of lossless media by assuming the wave travels perpendicular (*normal incidence*) to the planar interface formed by two semi-infinite lossless media, as shown in Figure 5-1, each characterized by the constitutive parameters of ε_1 , μ_1 and ε_2 , μ_2 . When the incident wave encounters the interface, a fraction of the wave intensity will be reflected into medium 1 and part will be transmitted into medium 2.

Assuming the incident electric field of amplitude E_0 is polarized in the x direction, we can write expressions for its incident, reflected, and transmitted electric field components, respectively, as

$$\mathbf{E}^{i} = \hat{\mathbf{a}}_{x} E_{0} e^{-j\beta_{1} z} \tag{5-1a}$$

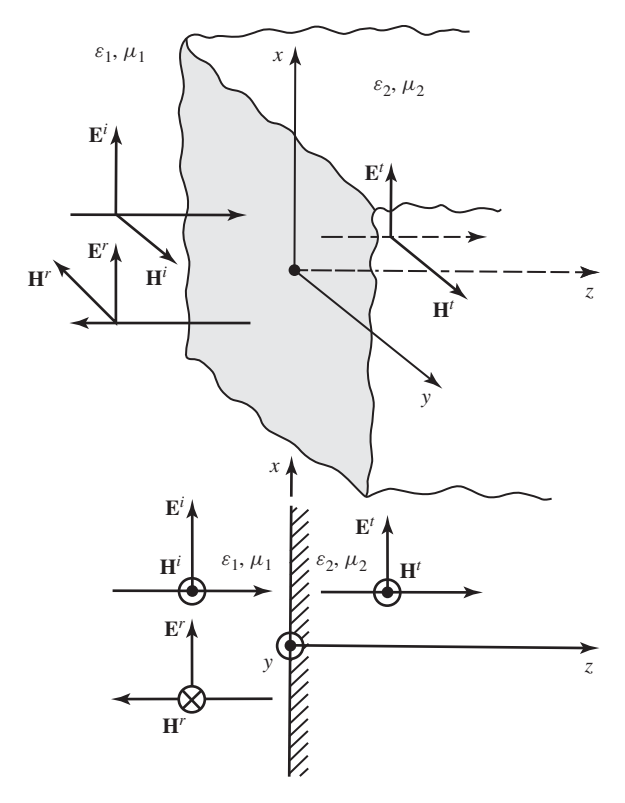


Figure 5-1 Wave reflection and transmission at normal incidence by a planar interface.

$$\mathbf{E}^r = \hat{\mathbf{a}}_x \Gamma^b E_0 e^{+j\beta_1 z} \tag{5-1b}$$

$$\mathbf{E}^t = \hat{\mathbf{a}}_x T^b E_0 e^{-j\beta_2 z} \tag{5-1c}$$

where Γ^b and T^b are used here to represent, respectively, the reflection and transmission coefficients at the interface. Presently these coefficients are unknowns and will be determined by applying boundary conditions on the fields along the interface. Since the incident fields are linearly polarized and the reflecting surface is planar, the reflected and transmitted fields will also be linearly polarized. Because we do not know the direction of polarization (positive or negative) of the reflected and transmitted electric fields, they are assumed here to be in the same direction (positive) as the incident electric fields. If that is not the case, it will be corrected by the appropriate signs on the reflection and transmission coefficients.

Using the right-hand procedure outlined in Section 4.2.1 or Maxwell's equations 4-3 or 4-3a, the magnetic field components corresponding to (5-1a) through (5-1c) can be written as

$$\mathbf{H}^{i} = \hat{\mathbf{a}}_{y} \frac{E_{0}}{\eta_{1}} e^{-j\beta_{1}z} \tag{5-2a}$$

$$\mathbf{H}^r = -\hat{\mathbf{a}}_y \frac{\Gamma^b E_0}{\eta_1} e^{+j\beta_1 z} \tag{5-2b}$$

$$\mathbf{H}^{t} = \hat{\mathbf{a}}_{y} \frac{T^{b} E_{0}}{\eta_{2}} e^{-j\beta_{2}z} \tag{5-2c}$$

The reflection and transmission coefficients will now be determined by enforcing continuity of the tangential components of the electric and magnetic fields across the interface. Using (5-1a) through (5-2c), continuity of the tangential components of the electric and magnetic fields at the interface (z = 0) leads, respectively, to

$$1 + \Gamma^b = T^b \tag{5-3a}$$

$$\frac{1}{\eta_1}(1 - \Gamma^b) = \frac{1}{\eta_2} T^b \tag{5-3b}$$

Solving these two equations for Γ^b and T^b , we can write that

$$\Gamma^{b} = \frac{\eta_{2} - \eta_{1}}{\eta_{2} + \eta_{1}} = \frac{E^{r}}{E^{i}} = -\frac{H^{r}}{H^{i}}$$
 (5-4a)

$$T^{b} = \frac{2\eta_{2}}{\eta_{1} + \eta_{2}} = 1 + \Gamma^{b} = \frac{E^{t}}{E^{i}} = \frac{\eta_{2}}{\eta_{1}} \frac{H^{t}}{H^{i}}$$
 (5-4b)

Therefore the plane wave reflection and transmission coefficients of a planar interface for normal incidence are functions of the constitutive properties, and they are given by (5-4a) and (5-4b). Since the angle of incidence is fixed at normal, the reflection coefficient cannot be equal to zero unless $\eta_2 = \eta_1$. For most dielectric material, aside from ferromagnetics, this implies that $\varepsilon_2 = \varepsilon_1$ since for them $\mu_1 \simeq \mu_2$.

Away from the interface the reflection Γ and transmission T coefficients are related to those at the boundary (Γ^b, T^b) and can be written, respectively, as

$$\left| \Gamma(z = -\ell_1) = \frac{E^r(z)}{E^i(z)} \right|_{z = -\ell_1} = \left. \frac{\Gamma^b E_0 e^{+j\beta_1 z}}{E_0 e^{-j\beta_1 z}} \right|_{z = -\ell_1} = \Gamma^b e^{-j2\beta_1 \ell_1}$$
 (5-5a)

$$T\left(\begin{array}{c} z_2 = \ell_2, \\ z_1 = -\ell_1 \end{array}\right) = \frac{E^t(z_2)|_{z_2 = \ell_2}}{E^i(z_1)|_{z_1 = -\ell_1}} = \frac{T^b E_0 e^{-j\beta_2 \ell_2}}{E_0 e^{+j\beta_1 \ell_1}} = T^b e^{-j(\beta_2 \ell_2 + \beta_1 \ell_1)}$$
(5-5b)

where ℓ_1 and ℓ_2 are positive distances measured from the interface to media 1 and 2, respectively. Associated with the electric and magnetic fields (5-1a) through (5-2c) are corresponding average power densities that can be written as

$$\mathbf{S}_{\text{av}}^{i} = \frac{1}{2} \operatorname{Re}(\mathbf{E}^{i} \times \mathbf{H}^{i^{*}}) = \hat{\mathbf{a}}_{z} \frac{|E_{0}|^{2}}{2\eta_{1}}$$
 (5-6a)

$$\mathbf{S}_{\text{av}}^{r} = \frac{1}{2} \text{Re}(\mathbf{E}^{r} \times \mathbf{H}^{r^{*}}) = -\hat{\mathbf{a}}_{z} |\Gamma^{b}|^{2} \frac{|E_{0}|^{2}}{2\eta_{1}} = -\hat{\mathbf{a}}_{z} |\Gamma^{b}|^{2} S_{\text{av}}^{i}$$
(5-6b)

$$\mathbf{S}_{\text{av}}^{t} = \frac{1}{2} \text{Re}(\mathbf{E}^{t} \times \mathbf{H}^{t^{*}}) = \hat{\mathbf{a}}_{z} |T^{b}|^{2} \frac{|E_{0}|^{2}}{2\eta_{2}} = \hat{\mathbf{a}}_{z} |T^{b}|^{2} \frac{\eta_{1}}{\eta_{2}} \frac{|E_{0}|^{2}}{2\eta_{1}}$$

$$= \hat{\mathbf{a}}_z |T^b|^2 \frac{\eta_1}{\eta_2} S_{\text{av}}^i = \hat{\mathbf{a}}_z \left(1 - |\Gamma^b|^2 \right) S_{\text{av}}^i$$
 (5-6c)

It is apparent that the ratio of the reflected to the incident power densities is equal to the square of the magnitude of the reflection coefficient. However, the ratio of the transmitted to the incident power density is not equal to the square of the magnitude of the transmission coefficient; this is one of the most common errors. Instead the ratio is proportional to the magnitude of the transmission coefficient squared and weighted by the intrinsic impedances of the two media, as given by (5-6c). Remember that the reflection and transmission coefficients relate the reflected and transmitted field intensities to the incident field intensity. Since the total tangential components of these field intensities on either side must be continuous across the boundary, the transmitted field could be greater than the incident field, which would require a transmission coefficient greater than unity. However, by the conservation of power, it is well known that the transmitted power density cannot exceed the incident power density.

Example 5-1

A uniform plane wave traveling in free space is incident normally upon a flat semi-infinite lossless medium with a dielectric constant of 2.56 (being representative of polystyrene). Determine the reflection and transmission coefficients as well as the incident, reflected, and transmitted power densities. Assume that the amplitude of the incident electric field at the interface is 1 mV/m.

Solution: Since $\varepsilon_1 = \varepsilon_0$ and $\varepsilon_2 = 2.56\varepsilon_0$,

$$\mu_1 = \mu_2 = \mu_0$$

then

$$\begin{split} \eta_1 &= \sqrt{\frac{\mu_1}{\varepsilon_1}} = \sqrt{\frac{\mu_0}{\varepsilon_0}} \\ \eta_2 &= \sqrt{\frac{\mu_2}{\varepsilon_2}} = \sqrt{\frac{\mu_0}{2.56\varepsilon_0}} = \frac{1}{1.6} \sqrt{\frac{\mu_0}{\varepsilon_0}} = \frac{\eta_1}{1.6} \end{split}$$

Thus according to (5-4a) and (5-4b)

$$\Gamma^b = \frac{\eta_2 - \eta_1}{\eta_2 + \eta_1} = \frac{\frac{1}{1.6} - 1}{\frac{1}{1.6} + 1} = \frac{1 - 1.6}{1 + 1.6} = -0.231$$

$$T^{b} = \frac{2\eta_{2}}{\eta_{1} + \eta_{2}} = \frac{2\left(\frac{1}{1.6}\right)}{1 + \frac{1}{1.6}} = \frac{2}{2.6} = 0.769$$

In addition, the incident, reflected, and transmitted power densities are obtained using, respectively, (5-6a), (5-6b), and (5-6c). Thus

$$S_{\text{av}}^{i} = \frac{|E_{0}|^{2}}{2\eta_{1}} = \frac{(10^{-3})^{2}}{2(376.73)} = 1.327 \times 10^{-9} \,\text{W/m}^{2} = 1.327 \,\text{nW/m}^{2}$$

$$S_{\text{av}}^{r} = |\Gamma^{b}|^{2} S_{\text{av}}^{i} = |-0.231|^{2} (1.327) \times 10^{-9} = 0.071 \,\text{nW/m}^{2}$$

$$S_{\text{av}}^{t} = |T^{b}|^{2} \frac{\eta_{1}}{\eta_{2}} S_{\text{av}}^{i} = |0.769|^{2} \frac{1}{1/1.6} (1.327) \times 10^{-9} = 1.256 \,\text{nW/m}^{2}$$

or

$$S_{\text{av}}^{t} = (1 - |\Gamma^{b}|^{2})S_{\text{av}}^{i} = (1 - |0.231|^{2})(1.327) \times 10^{-9} = 1.256 \,\text{nW/m}^{2}$$

In medium 1, the total field is equal to the sum of the incident and reflected fields. Thus, for the total electric and magnetic fields in medium 1, we can write that

$$\mathbf{E}^{1} = \mathbf{E}^{i} + \mathbf{E}^{r} = \hat{\mathbf{a}}_{x} \underbrace{E_{0}e^{-j\beta_{1}z}}_{\text{traveling}} \underbrace{(1 + \Gamma^{b}e^{+j2\beta_{1}z})}_{\text{standing}} = \hat{\mathbf{a}}_{x}E_{0}e^{-j\beta_{1}z} \left[1 + \Gamma(z)\right]$$
 (5-7a)

$$\mathbf{E}^{1} = \mathbf{E}^{i} + \mathbf{E}^{r} = \hat{\mathbf{a}}_{x} \underbrace{E_{0}e^{-j\beta_{1}z}}_{\text{traveling wave}} \underbrace{(1 + \Gamma^{b}e^{+j2\beta_{1}z})}_{\text{standing wave}} = \hat{\mathbf{a}}_{x} E_{0}e^{-j\beta_{1}z} \left[1 + \Gamma(z)\right]$$

$$\mathbf{H}^{1} = \mathbf{H}^{i} + \mathbf{H}^{r} = \hat{\mathbf{a}}_{y} \underbrace{(E_{0}/\eta_{1})e^{-j\beta_{1}z}}_{\text{traveling wave}} \underbrace{(1 - \Gamma^{b}e^{+j2\beta_{1}z})}_{\text{standing wave}} = \hat{\mathbf{a}}_{y} \frac{E_{0}}{\eta_{1}} e^{-j\beta_{1}z} \left[1 - \Gamma(z)\right]$$
(5-7a)
$$(5-7a)$$

In each expression the factors outside the parentheses represent the traveling wave part of the wave and those within the parentheses represent the standing wave part. Therefore the total field of two waves is the product of one of the waves times a factor that in this case is the standing wave pattern. This is analogous to the array multiplication rule in antennas where the total field of an array of identical elements is equal to the product of the field of a single element times a factor that is referred to as the array factor [1].

As discussed in Section 4.2.1D, the ratio of the maximum value of the electric field magnitude to that of the minimum is defined as the standing wave ratio (SWR), and it is given here by

SWR =
$$\frac{|\mathbf{E}^1|_{\text{max}}}{|\mathbf{E}^1|_{\text{min}}} = \frac{1 + |\Gamma^b|}{1 - |\Gamma^b|} = \frac{1 + \left|\frac{\eta_2 - \eta_1}{\eta_2 + \eta_1}\right|}{1 - \left|\frac{\eta_2 - \eta_1}{\eta_2 + \eta_1}\right|}$$
 (5-8)

For two media with identical permeabilities ($\mu_1 = \mu_2$), the SWR can be written as

$$SWR = \frac{\left|\sqrt{\varepsilon_{1}} + \sqrt{\varepsilon_{2}}\right| + \left|\sqrt{\varepsilon_{1}} - \sqrt{\varepsilon_{2}}\right|}{\left|\sqrt{\varepsilon_{1}} + \sqrt{\varepsilon_{2}}\right| - \left|\sqrt{\varepsilon_{1}} - \sqrt{\varepsilon_{2}}\right|} = \begin{cases} \sqrt{\frac{\varepsilon_{1}}{\varepsilon_{2}}}, & \varepsilon_{1} > \varepsilon_{2} \\ \sqrt{\frac{\varepsilon_{2}}{\varepsilon_{1}}}, & \varepsilon_{2} > \varepsilon_{1} \end{cases}$$
(5-9a)
$$(5-9b)$$

OBLIQUE INCIDENCE – LOSSLESS MEDIA

To analyze reflections and transmissions at oblique wave incidence, we need to introduce the plane of incidence, which is defined as the plane formed by a unit vector normal to the reflecting interface and the vector in the direction of incidence. For a wave whose wave vector is on the xz plane and is incident upon an interface that is parallel to the xy plane, as shown in Figure 5-2, the plane of incidence is the xz plane.

To examine reflections and transmissions at oblique angles of incidence for a general wave polarization, it is most convenient to decompose the electric field into its perpendicular and parallel components (relative to the plane of incidence) and analyze each one of them individually. The total reflected and transmitted field will be the vector sum of these two polarizations.

When the electric field is perpendicular to the plane of incidence, the polarization of the wave is referred to as perpendicular polarization. Since the electric field is parallel to the interface, it is also known as horizontal or E polarization. When the electric field is parallel to the plane of incidence, the polarization is referred to as parallel polarization. Because a component of the electric field is also perpendicular to the interface when the magnetic field is parallel to the interface, it is also known as vertical or H polarization. Each type of polarization will be further examined.

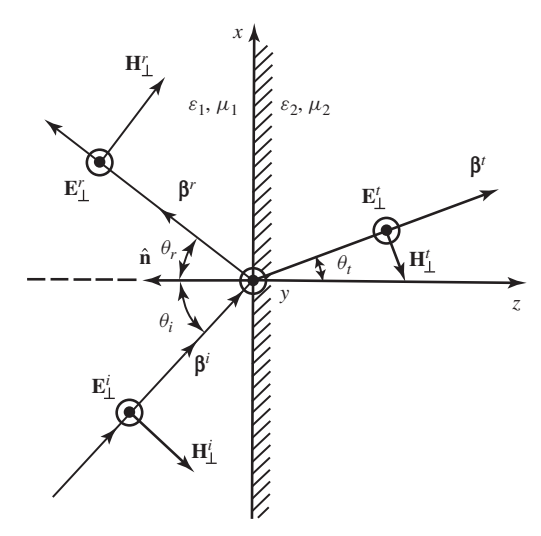


Figure 5-2 Perpendicular (horizontal) polarized uniform plane wave incident at an oblique angle on an interface.

5.3.1 Perpendicular (Horizontal or E) Polarization

Let us now assume that the electric field of the uniform plane wave incident on a planar interface at an oblique angle, as shown in Figure 5-2, is oriented perpendicularly to the plane of incidence. As previously stated, this is referred to as the perpendicular polarization.

Using the techniques outlined in Section 4.2.2, the incident electric and magnetic fields can be written as

$$\mathbf{E}_{\perp}^{i} = \hat{\mathbf{a}}_{\nu} E_{\perp}^{i} e^{-j\beta^{i} \cdot \mathbf{r}} = \hat{\mathbf{a}}_{\nu} E_{0} e^{-j\beta_{1}(x \sin \theta_{i} + z \cos \theta_{i})}$$
(5-10a)

$$\mathbf{H}_{\perp}^{i} = (-\hat{\mathbf{a}}_{x} \cos \theta_{i} + \hat{\mathbf{a}}_{z} \sin \theta_{i}) H_{\perp}^{i} e^{-j\beta^{i} \cdot \mathbf{r}}$$

$$= (-\hat{\mathbf{a}}_x \cos \theta_i + \hat{\mathbf{a}}_z \sin \theta_i) \frac{E_0}{\eta_1} e^{-j\beta_1(x \sin \theta_i + z \cos \theta_i)}$$
(5-10b)

where

$$E_{\perp}^{i} = E_{0} \tag{5-10c}$$

$$H_{\perp}^{i} = \frac{E_{\perp}^{i}}{\eta_{1}} = \frac{E_{0}}{\eta_{1}} \tag{5-10d}$$

Similarly, the reflected fields can be expressed as

$$\mathbf{E}_{\perp}^{r} = \hat{\mathbf{a}}_{y} E_{\perp}^{r} e^{-j\beta^{r} \cdot \mathbf{r}} = \hat{\mathbf{a}}_{y} \Gamma_{\perp}^{b} E_{0} e^{-j\beta_{1}(x \sin \theta_{r} - z \cos \theta_{r})}$$
(5-11a)

$$\mathbf{H}_{\perp}^{r} = (\hat{\mathbf{a}}_{x} \cos \theta_{r} + \hat{\mathbf{a}}_{z} \sin \theta_{r}) H_{\perp}^{r} e^{-j\mathbf{\beta}^{r} \cdot \mathbf{r}}$$

$$= (\hat{\mathbf{a}}_x \cos \theta_r + \hat{\mathbf{a}}_z \sin \theta_r) \frac{\Gamma_{\perp}^b E_0}{\eta_1} e^{-j\beta_1 (x \sin \theta_r - z \cos \theta_r)}$$
 (5-11b)

where

$$E_{\perp}^{r} = \Gamma_{\perp}^{b} E^{i} = \Gamma_{\perp}^{b} E_{0} \tag{5-11c}$$

$$H_{\perp}^{r} = \frac{E_{\perp}^{r}}{\eta_{1}} = \frac{\Gamma_{\perp}^{b} E_{0}}{\eta_{1}}$$
 (5-11d)

Also the transmitted fields can be written as

$$\mathbf{E}_{\perp}^{t} = \hat{\mathbf{a}}_{\mathbf{y}} E_{\perp}^{t} e^{-j\beta^{t} \cdot \mathbf{r}} = \hat{\mathbf{a}}_{\mathbf{y}} T_{\perp}^{b} E_{0} e^{-j\beta_{2}(x \sin \theta_{t} + z \cos \theta_{t})}$$
(5-12a)

$$\mathbf{H}_{\perp}^{t} = (-\hat{\mathbf{a}}_{x} \cos \theta_{t} + \hat{\mathbf{a}}_{z} \sin \theta_{t}) H_{\perp}^{t} e^{-j\mathbf{\beta}^{t} \cdot \mathbf{r}}$$

$$= (-\hat{\mathbf{a}}_x \cos \theta_t + \hat{\mathbf{a}}_z \sin \theta_t) \frac{T_{\perp}^b E_0}{n_2} e^{-j\beta_2(x \sin \theta_t + z \cos \theta_t)}$$
 (5-12b)

where

$$E_{\perp}^{t} = T_{\perp}^{b} E_{\perp}^{i} = T_{\perp}^{b} E_{0} \tag{5-12c}$$

$$H_{\perp}^{t} = \frac{E_{\perp}^{t}}{\eta_{2}} = \frac{T_{\perp}^{b} E_{0}}{\eta_{2}}$$
 (5-12d)

The reflection Γ^b_{\perp} and transmission T^b_{\perp} coefficients, and the relation between the incident θ_i , reflected θ_r , and transmission (refracted) θ_t angles can be obtained by applying the boundary conditions on the continuity of the tangential components of the electric and magnetic fields. That is

$$\left(\mathbf{E}_{\perp}^{i} + \mathbf{E}_{\perp}^{r}\right)\big|_{\substack{\tan\\r=0}} = \left(\mathbf{E}_{\perp}^{t}\right)\big|_{\substack{\tan\\r=0}} \tag{5-13a}$$

$$\left(\mathbf{H}_{\perp}^{i} + \mathbf{H}_{\perp}^{r}\right)\Big|_{\substack{\tan \\ z=0}} = \left(\mathbf{H}_{\perp}^{t}\right)\Big|_{\substack{\tan \\ z=0}}$$
 (5-13b)

Using the appropriate terms of (5-10a) through (5-12d), (5-13a) and (5-13b) can be written, respectively, as

$$e^{-j\beta_1 x \sin \theta_i} + \Gamma_{\perp}^b e^{-j\beta_1 x \sin \theta_r} = T_{\perp}^b e^{-j\beta_2 x \sin \theta_t}$$
 (5-14a)

$$\frac{1}{\eta_1} \left(-\cos\theta_i e^{-j\beta_1 x \sin\theta_i} + \Gamma_{\perp}^b \cos\theta_r e^{-j\beta_1 x \sin\theta_r} \right) = -\frac{T_{\perp}^b}{\eta_2} \cos\theta_t e^{-j\beta_2 x \sin\theta_t}$$
 (5-14b)

Whereas (5-14a) and (5-14b) represent two equations with four unknowns $(\Gamma_{\perp}^b, T_{\perp}^b, \theta_r, \theta_t)$, it should be noted that each equation is complex. By equating the corresponding real and imaginary parts of each side, each can be reduced to two equations (a total of four). If this procedure is utilized, it will be concluded that (5-14a) and (5-14b) lead to the following two relations:

$$\theta_r = \theta_i$$
 (Snell's law of reflection) (5-15a)

$$\beta_1 \sin \theta_i = \beta_2 \sin \theta_t$$
 (Snell's law of refraction) (5-15b)

Using (5-15a) and (5-15b) reduces (5-14a) and (5-14b) to

$$1 + \Gamma_{\perp}^b = T_{\perp}^b \tag{5-16a}$$

$$\frac{\cos \theta_i}{\eta_1} \left(-1 + \Gamma_{\perp}^b \right) = -\frac{\cos \theta_t}{\eta_2} T_{\perp}^b \tag{5-16b}$$

Solving (5-16a) and (5-16b) simultaneously for Γ^b_{\perp} and T^b_{\perp} leads to

$$\Gamma_{\perp}^{b} = \frac{E_{\perp}^{r}}{E_{\perp}^{i}} = \frac{\eta_{2} \cos \theta_{i} - \eta_{1} \cos \theta_{t}}{\eta_{2} \cos \theta_{i} + \eta_{1} \cos \theta_{t}} = \frac{\sqrt{\frac{\mu_{2}}{\varepsilon_{2}}} \cos \theta_{i} - \sqrt{\frac{\mu_{1}}{\varepsilon_{1}}} \cos \theta_{t}}{\sqrt{\frac{\mu_{2}}{\varepsilon_{2}}} \cos \theta_{i} + \sqrt{\frac{\mu_{1}}{\varepsilon_{1}}} \cos \theta_{t}}$$
(5-17a)

$$T_{\perp}^{b} = \frac{E_{\perp}^{t}}{E_{\perp}^{i}} = \frac{2\eta_{2}\cos\theta_{i}}{\eta_{2}\cos\theta_{i} + \eta_{1}\cos\theta_{t}} = \frac{2\sqrt{\frac{\mu_{2}}{\varepsilon_{2}}}\cos\theta_{i}}{\sqrt{\frac{\mu_{2}}{\varepsilon_{2}}}\cos\theta_{i} + \sqrt{\frac{\mu_{1}}{\varepsilon_{1}}}\cos\theta_{t}}$$
(5-17b)

 Γ^b_{\perp} and T^b_{\perp} of (5-17a) and (5-17b) are usually referred to as the plane wave *Fresnel reflection* and transmission coefficients for perpendicular polarization.

Since for most dielectric media (excluding ferromagnetic material) $\mu_1 \simeq \mu_2 \simeq \mu_0$, (5-17a) and (5-17b) reduce, by also utilizing (5-15b), to

$$\Gamma_{\perp}^{b}\big|_{\mu_{1}=\mu_{2}} = \frac{\cos\theta_{i} - \sqrt{\frac{\varepsilon_{2}}{\varepsilon_{1}}}\sqrt{1 - \left(\frac{\varepsilon_{1}}{\varepsilon_{2}}\right)\sin^{2}\theta_{i}}}{\cos\theta_{i} + \sqrt{\frac{\varepsilon_{2}}{\varepsilon_{1}}}\sqrt{1 - \left(\frac{\varepsilon_{1}}{\varepsilon_{2}}\right)\sin^{2}\theta_{i}}}$$
(5-18a)

$$T_{\perp}^{b}\big|_{\mu_{1}=\mu_{2}} = \frac{2\cos\theta_{i}}{\cos\theta_{i} + \sqrt{\frac{\varepsilon_{2}}{\varepsilon_{1}}}\sqrt{1 - \left(\frac{\varepsilon_{1}}{\varepsilon_{2}}\right)\sin^{2}\theta_{i}}}$$
 (5-18b)

Plots of $|\Gamma_{\perp}^b|$ and $|T_{\perp}^b|$ of (5-18a) and (5-18b) for $\varepsilon_2/\varepsilon_1=2.56$, 4, 9, 16, 25, and 81 as a function of θ_i are shown in Figure 5-3. It is apparent that as the relative ratio of $\varepsilon_2/\varepsilon_1$ increases, the magnitude of the reflection coefficient increases, whereas that of the transmission coefficient decreases. This is expected since large ratios of $\varepsilon_2/\varepsilon_1$ project larger discontinuities in the dielectric properties of the media along the interface. Also it is observed that for $\varepsilon_2 > \varepsilon_1$ the magnitude of the reflection coefficient never vanishes regardless of the $\varepsilon_2/\varepsilon_1$ ratio or the angle of incidence.

For $\varepsilon_2/\varepsilon_1 > 1$, both Γ^b_{\perp} and T^b_{\perp} are real with Γ^b_{\perp} being negative and T^b_{\perp} being positive for all angles of incidence. Therefore, as a function of θ_i , the phase of Γ^b_{\perp} is equal to 180° and that of the transmission coefficient T^b_{\perp} is zero. When $\varepsilon_2/\varepsilon_1 = 1$ the reflection coefficient vanishes and the transmission coefficient reduces to unity. When $\varepsilon_2/\varepsilon_1 < 1$, both Γ^b_{\perp} and T^b_{\perp} are real when the incidence angle $\theta_i \leq \theta_c$; for $\theta_i > \theta_c$, they become complex. The angle θ_i for which $|\Gamma^b_{\perp}|_{\varepsilon_2/\varepsilon_1<1}(\theta_i=\theta_c)=1$ is referred to as the *critical* angle, and it represents conditions of total internal reflection. More discussion on the critical angle $(\theta_i=\theta_c)$ and the wave propagation for $\theta_i > \theta_c$ can be found in Section 5.3.4.

In medium 1 the total electric field can be written as

$$\mathbf{E}_{\perp}^{1} = \mathbf{E}_{\perp}^{i} + \mathbf{E}_{\perp}^{r} = \hat{\mathbf{a}}_{y} \underbrace{E_{0}e^{-j\beta_{1}(x\sin\theta_{1}+z\cos\theta_{i})}}_{\text{traveling wave}} \underbrace{\left[1 + \Gamma_{\perp}^{b}e^{+j2\beta_{1}z\cos\theta_{i}}\right]}_{\text{standing wave}}$$

$$= \hat{\mathbf{a}}_{y}E_{0}e^{-j\beta_{1}(x\sin\theta_{i}+z\cos\theta_{i})} \left[1 + \Gamma_{\perp}(z)\right] \tag{5-19}$$

where

$$\Gamma_{\perp}(z) = \Gamma_{\perp}^{b} e^{+j2\beta_1 z \cos \theta_i}$$
 (5-19a)

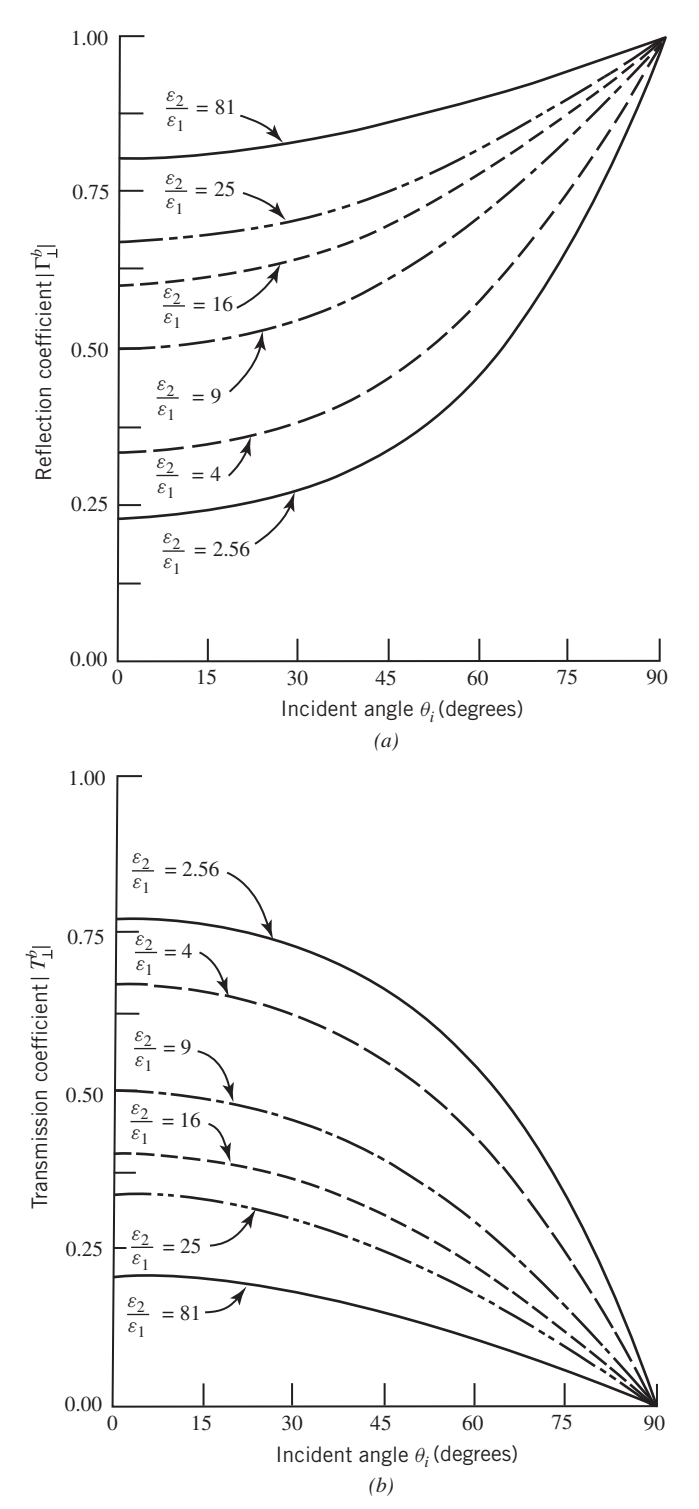


Figure 5-3 Magnitude of coefficients for perpendicular polarization as a function of incident angle. (a) Reflection. (b) Transmission.

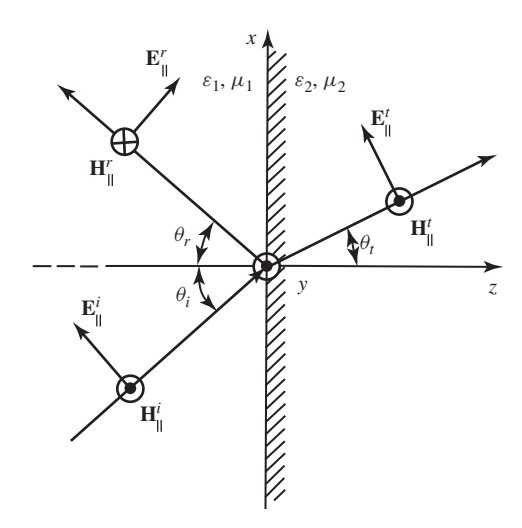


Figure 5-4 Parallel (vertical) polarized uniform plane wave incident at an oblique angle on an interface.

5.3.2 Parallel (Vertical or H) Polarization

For this polarization the electric field is parallel to the plane of incidence and it impinges upon a planar interface as shown in Figure 5-4. The directions of the incident, reflected, and transmitted electric and magnetic fields in Figure 5-4 are chosen so that for the special case of $\theta_i = 0$ they reduce to those of Figure 5-1.

Using the techniques outlined in Section 4.2.2, we can write that

$$\mathbf{E}_{\parallel}^{i} = (\hat{\mathbf{a}}_{x} \cos \theta_{i} - \hat{\mathbf{a}}_{z} \sin \theta_{i}) E_{0} e^{-j\beta^{i} \cdot \mathbf{r}}$$

$$= (\hat{\mathbf{a}}_{x} \cos \theta_{i} - \hat{\mathbf{a}}_{z} \sin \theta_{i}) E_{0} e^{-j\beta_{1}(x \sin \theta_{i} + z \cos \theta_{i})}$$
(5-20a)

$$\mathbf{H}_{\parallel}^{i} = \hat{\mathbf{a}}_{y} H_{\parallel}^{i} e^{-j\beta^{i} \cdot \mathbf{r}} = \hat{\mathbf{a}}_{y} \frac{E_{0}}{\eta_{1}} e^{-j\beta_{1}(x \sin \theta_{i} + z \cos \theta_{i})}$$
(5-20b)

where

$$E_{\parallel}^{i} = E_{0} \tag{5-20c}$$

$$H_{\parallel}^{i} = \frac{E_{\parallel}^{i}}{\eta_{1}} = \frac{E_{0}}{\eta_{1}} \tag{5-20d}$$

Similarly,

$$\mathbf{E}_{\parallel}^{r} = (\hat{\mathbf{a}}_{x} \cos \theta_{r} + \hat{\mathbf{a}}_{z} \sin \theta_{r}) E^{r} e^{-j\beta^{r} \cdot \mathbf{r}}$$

$$= (\hat{\mathbf{a}}_{x} \cos \theta_{r} + \hat{\mathbf{a}}_{z} \sin \theta_{r}) \Gamma_{\parallel}^{b} E_{0} e^{-j\beta_{1}(x \sin \theta_{r} - z \cos \theta_{r})}$$
(5-21a)

$$\mathbf{H}_{\parallel}^{r} = -\hat{\mathbf{a}}_{y} H_{\parallel}^{r} e^{-j\beta^{r} \cdot \mathbf{r}} = -\hat{\mathbf{a}}_{y} \frac{\Gamma_{\parallel}^{b} E_{0}}{\eta_{1}} e^{-j\beta_{1}(x \sin \theta_{r} - z \cos \theta_{r})}$$
(5-21b)

where

$$E_{\parallel}^{r} = \Gamma_{\parallel}^{b} E^{i} = \Gamma_{\parallel}^{b} E_{0} \tag{5-21c}$$

$$H_{\parallel}^{r} = \frac{E_{\parallel}^{r}}{\eta_{1}} = \frac{\Gamma_{\parallel}^{b} E_{0}}{\eta_{1}}$$
 (5-21d)

Also,

$$\mathbf{E}_{\parallel}^{t} = (\hat{\mathbf{a}}_{x} \cos \theta_{t} - \hat{\mathbf{a}}_{z} \sin \theta_{t}) E_{\parallel}^{t} e^{-j\beta^{t} \cdot \mathbf{r}}$$

$$= (\hat{\mathbf{a}}_{x} \cos \theta_{t} - \hat{\mathbf{a}}_{z} \sin \theta_{t}) T_{\parallel}^{b} E_{0} e^{-j\beta_{2}(x \sin \theta_{t} + z \cos \theta_{t})}$$
(5-22a)

$$\mathbf{H}_{\parallel}^{t} = \hat{\mathbf{a}}_{y} H_{\parallel}^{t} e^{-j\beta^{t} \cdot \mathbf{r}} = \hat{\mathbf{a}}_{y} \frac{T_{\parallel}^{b} E_{0}}{\eta_{2}} e^{-j\beta_{2}(x \sin \theta_{t} + z \cos \theta_{t})}$$

$$(5-22b)$$

where

$$E_{\parallel}^{t} = T_{\parallel}^{b} E^{i} = T_{\parallel}^{b} E_{0} \tag{5-22c}$$

$$H_{\parallel}^{t} = \frac{E_{\parallel}^{t}}{\eta_{2}} = \frac{T_{\parallel}^{b} E_{0}}{\eta_{2}}$$
 (5-22d)

As before, the reflection Γ_{\parallel}^b and transmission T_{\parallel}^b coefficients, and the reflection θ_r and transmission (refraction) θ_t angles are the four unknowns. These can be determined and expressed in terms of the incident angle θ_i and the constitutive parameters of the two media by applying the boundary conditions on the continuity across the interface (z=0) of the tangential components of the electric and magnetic fields as given by (5-13a) and (5-13b) and applied to parallel polarization. Using the appropriate terms of (5-20a) through (5-22d), we can write (5-13a) and (5-13b) as applied to parallel polarization, respectively, as

$$\cos \theta_i e^{-j\beta_1 x \sin \theta_i} + \Gamma_{\parallel}^b \cos \theta_r e^{-j\beta_1 x \sin \theta_r} = T_{\parallel}^b \cos \theta_t e^{-j\beta_2 x \sin \theta_t}$$
 (5-23a)

$$\frac{1}{\eta_1} \left(e^{-j\beta_1 x \sin \theta_i} - \Gamma_{\parallel}^b e^{-j\beta_1 x \sin \theta_r} \right) = \frac{1}{\eta_2} T_{\parallel}^b e^{-j\beta_2 x \sin \theta_t}$$
 (5-23b)

Following the procedure outlined in Section 5.3.1 for the solution of (5-14a) and (5-14b), it can be shown that (5-23a) and (5-23b) reduce to

$$\theta_r = \theta_i$$
 (Snell's law of reflection) (5-24a)

$$\beta_1 \sin \theta_i = \beta_2 \sin \theta_t$$
 (Snell's law of refraction) (5-24b)

$$\Gamma_{\parallel}^{b} = \frac{-\eta_{1}\cos\theta_{i} + \eta_{2}\cos\theta_{t}}{\eta_{1}\cos\theta_{i} + \eta_{2}\cos\theta_{t}} = \frac{-\sqrt{\frac{\mu_{1}}{\varepsilon_{1}}}\cos\theta_{i} + \sqrt{\frac{\mu_{2}}{\varepsilon_{2}}}\cos\theta_{t}}{\sqrt{\frac{\mu_{1}}{\varepsilon_{1}}}\cos\theta_{i} + \sqrt{\frac{\mu_{2}}{\varepsilon_{2}}}\cos\theta_{t}}$$
(5-24c)

$$T_{\parallel}^{b} = \frac{2\eta_{2}\cos\theta_{i}}{\eta_{1}\cos\theta_{i} + \eta_{2}\cos\theta_{i}} = \frac{2\sqrt{\frac{\mu_{2}}{\varepsilon_{2}}}\cos\theta_{i}}{\sqrt{\frac{\mu_{1}}{\varepsilon_{1}}}\cos\theta_{i} + \sqrt{\frac{\mu_{2}}{\varepsilon_{2}}}\cos\theta_{t}}$$
(5-24d)

 Γ^b_{\parallel} and T^b_{\parallel} of (5-24c) and (5-24d) are usually referred to as the plane wave *Fresnel reflection* and transmission coefficients for parallel polarization.

Excluding ferromagnetic material, (5-24c) and (5-24d) reduce, using also (5-24b), to

$$\Gamma_{\parallel}^{b}\big|_{\mu_{1}=\mu_{2}} = \frac{-\cos\theta_{i} + \sqrt{\frac{\varepsilon_{1}}{\varepsilon_{2}}}\sqrt{1 - \left(\frac{\varepsilon_{1}}{\varepsilon_{2}}\right)\sin^{2}\theta_{i}}}{\cos\theta_{i} + \sqrt{\frac{\varepsilon_{1}}{\varepsilon_{2}}}\sqrt{1 - \left(\frac{\varepsilon_{1}}{\varepsilon_{2}}\right)\sin^{2}\theta_{i}}}$$
(5-25a)

$$T_{\parallel}^{b}\big|_{\mu_{1}=\mu_{2}} = \frac{2\sqrt{\frac{\varepsilon_{1}}{\varepsilon_{2}}}\cos\theta_{i}}{\cos\theta_{i} + \sqrt{\frac{\varepsilon_{1}}{\varepsilon_{2}}}\sqrt{1 - \left(\frac{\varepsilon_{1}}{\varepsilon_{2}}\right)\sin^{2}\theta_{i}}}$$
(5-25b)

Plots of $|\Gamma_{\parallel}^b|$ and $|T_{\parallel}^b|$ of (5-25a) and (5-25b) for $\varepsilon_2/\varepsilon_1=2.56$, 4, 9, 16, 25, and 81 as a function of θ_i are shown in Figure 5-5. It is observed in Figure 5-5a that for this polarization there is an angle where the reflection coefficient does vanish. The angle where the reflection coefficient vanishes is referred to as the *Brewster angle*, θ_B , and it increases toward 90° as the ratio $\varepsilon_2/\varepsilon_1$ becomes larger. More discussion on the Brewster angle can be found in the next section (Section 5.3.3).

For $\varepsilon_2/\varepsilon_1 > 1$, Γ_{\parallel}^b and T_{\parallel}^b are both real. For angles of incidence less than the Brewster angle $(\theta_i < \theta_B)$, Γ_{\parallel}^b is negative, indicating a 180° phase as a function of the incident angle; for $\theta_i > \theta_B$, Γ_{\parallel}^b is positive, representing a 0° phase. The transmission coefficient T_{\parallel}^b is positive for all values of θ_i , indicating a 0° phase. When $\varepsilon_2/\varepsilon_1 = 1$, the reflection coefficient vanishes and the transmission coefficient reduces to unity. As for the perpendicular polarization, when $\varepsilon_2/\varepsilon_1 < 1$ both Γ_{\parallel}^b are real when the incident angle $\theta_i \leq \theta_c$; after that, they become complex. The angle for which $|\Gamma_{\parallel}^b|_{\varepsilon_2/\varepsilon_1 < 1}(\theta_i = \theta_c) = 1$ is again referred to as *critical* angle, and it represents conditions of total internal reflection. Further discussion of the critical angle $(\theta_i = \theta_c)$ and the wave propagation for $\theta_i > \theta_c$ can be found in Section 5.3.4. It is evident that the critical angle is not a function of polarization; it occurs only when the wave propagates from the more dense to the less dense medium.

The total electric field in medium 1 can be written as

$$\mathbf{E}_{\parallel}^{1} = \mathbf{E}_{\parallel}^{i} + \mathbf{E}_{\parallel}^{r} = \hat{\mathbf{a}}_{x} \cos \theta_{i} \underbrace{E_{0}e^{-j\beta_{1}(x \sin \theta_{i} + z \cos \theta_{i})}}_{\text{traveling wave}} \underbrace{\left[1 + \Gamma_{\parallel}^{b}e^{+j2\beta_{1}z \cos \theta_{i}}\right]}_{\text{standing wave}} \\ -\hat{\mathbf{a}}_{z} \sin \theta_{i} \underbrace{E_{0}e^{-j\beta_{1}(x \sin \theta_{i} + z \cos \theta_{i})}}_{\text{traveling wave}} \underbrace{\left[1 - \Gamma_{\parallel}^{b}e^{+j2\beta_{1}z \cos \theta_{i}}\right]}_{\text{standing wave}} \\ \mathbf{E}_{\parallel}^{1} = \mathbf{E}_{x}^{1} + \mathbf{E}_{z}^{1} = \hat{\mathbf{a}}_{x} \cos \theta_{i} E_{0}e^{-j\beta_{1}(x \sin \theta_{i} + z \cos \theta_{i})} \left[1 + \Gamma_{\parallel}(z)\right] \\ -\hat{\mathbf{a}}_{z} \sin \theta_{i} E_{0}e^{-j\beta_{1}(x \sin \theta_{i} + x \cos \theta_{i})} \left[1 - \Gamma_{\parallel}(z)\right]$$

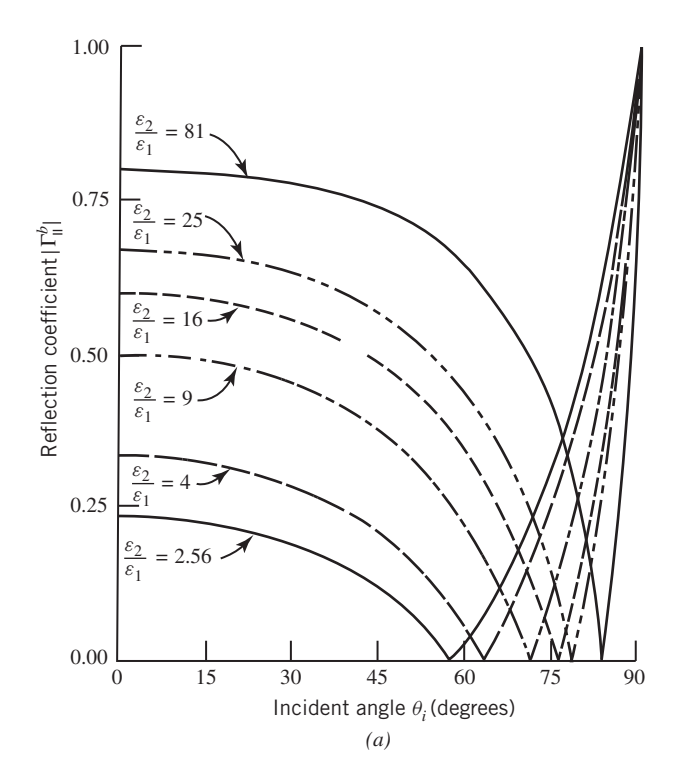
$$(5-26)$$

where

$$\Gamma_{\parallel}(z) = \Gamma_{\parallel}^b e^{+j2\beta_1 z \cos \theta_i} \tag{5-26a}$$

5.3.3 Total Transmission-Brewster Angle

The reflection and transmission coefficients for both perpendicular and parallel polarizations are functions of the constitutive parameters of the two media forming the interface, the angle of incidence, and the angle of refraction that is related to the angle of incidence through Snell's law



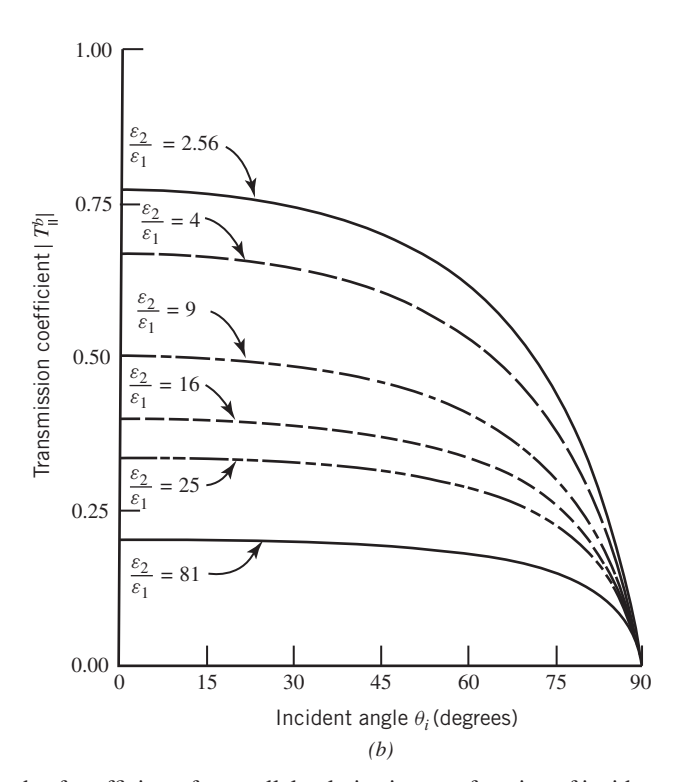


Figure 5-5 Magnitude of coefficients for parallel polarization as a function of incident angle. (*a*) Reflection. (*b*) Transmission.

of refraction. One may ask: "For a given set of constitutive parameters of two media forming an interface, is there an incidence angle that allows no reflection, i.e., $\Gamma = 0$?" To answer this we need to refer back to the expressions for the reflection coefficients as given by (5-17a) and (5-24c).

A. Perpendicular (Horizontal) Polarization To see the conditions under which the reflection coefficient of (5-17a) will vanish, we set it equal to zero, which leads to

$$\Gamma_{\perp}^{b} = \frac{\sqrt{\frac{\mu_{2}}{\varepsilon_{2}}}\cos\theta_{i} - \sqrt{\frac{\mu_{1}}{\varepsilon_{1}}}\cos\theta_{t}}{\sqrt{\frac{\mu_{2}}{\varepsilon_{2}}}\cos\theta_{i} + \sqrt{\frac{\mu_{1}}{\varepsilon_{1}}}\cos\theta_{t}} = 0$$
 (5-27)

or

$$\cos \theta_i = \sqrt{\frac{\mu_1}{\mu_2} \left(\frac{\varepsilon_2}{\varepsilon_1}\right)} \cos \theta_t \tag{5-27a}$$

Using Snell's law of refraction, as given by (5-15b), (5-27a) can be written as

$$(1 - \sin^2 \theta_i) = \frac{\mu_1}{\mu_2} \left(\frac{\varepsilon_2}{\varepsilon_1}\right) (1 - \sin^2 \theta_t)$$

$$(1 - \sin^2 \theta_i) = \frac{\mu_1}{\mu_2} \left(\frac{\varepsilon_2}{\varepsilon_1}\right) \left[1 - \frac{\mu_1}{\mu_2} \left(\frac{\varepsilon_1}{\varepsilon_2}\right) \sin^2 \theta_i\right]$$
(5-28)

or

$$\sin \theta_i = \sqrt{\frac{\frac{\varepsilon_2}{\varepsilon_1} - \frac{\mu_2}{\mu_1}}{\frac{\mu_1}{\mu_2} - \frac{\mu_2}{\mu_1}}}$$
(5-28a)

Since the sine function cannot exceed unity, (5-28a) exists only if

$$\frac{\varepsilon_2}{\varepsilon_1} - \frac{\mu_2}{\mu_1} \le \frac{\mu_1}{\mu_2} - \frac{\mu_2}{\mu_1} \tag{5-29}$$

or

$$\frac{\varepsilon_2}{\varepsilon_1} \le \frac{\mu_1}{\mu_2} \tag{5-29a}$$

If however $\mu_1 = \mu_2$, (5-28a) indicates that

$$\sin \theta_i|_{\mu_1 = \mu_2} = \infty \tag{5-29b}$$

Therefore there exists no real angle θ_i under this condition that will reduce the reflection coefficient to zero. Since the permeability for most dielectric material (aside from ferromagnetics) is almost the same and equal to that of free space $(\mu_1 \simeq \mu_2 \simeq \mu_0)$, for these materials there exists no real incidence angle that will reduce the reflection coefficient for perpendicular polarization to zero.

B. Parallel (Vertical) Polarization To examine the conditions under which the reflection coefficient for parallel polarization will vanish, we set (5-24c) equal to zero; that is

$$\Gamma_{\parallel}^{b} = \frac{-\sqrt{\frac{\mu_{1}}{\varepsilon_{1}}}\cos\theta_{i} + \sqrt{\frac{\mu_{2}}{\varepsilon_{2}}}\cos\theta_{t}}{\sqrt{\frac{\mu_{1}}{\varepsilon_{1}}}\cos\theta_{i} + \sqrt{\frac{\mu_{2}}{\varepsilon_{2}}}\cos\theta_{t}} = 0$$
 (5-30)

or

$$\cos \theta_i = \sqrt{\frac{\mu_2}{\mu_1} \left(\frac{\varepsilon_1}{\varepsilon_2}\right)} \cos \theta_t \tag{5-30a}$$

Using Snell's law of refraction, as given by (5-24b), (5-30a) can be written as

$$(1 - \sin^2 \theta_i) = \frac{\mu_2}{\mu_1} \left(\frac{\varepsilon_1}{\varepsilon_2}\right) (1 - \sin^2 \theta_t)$$

$$(1 - \sin^2 \theta_i) = \frac{\mu_2}{\mu_1} \left(\frac{\varepsilon_1}{\varepsilon_2}\right) \left[1 - \frac{\mu_1}{\mu_2} \left(\frac{\varepsilon_1}{\varepsilon_2}\right) \sin^2 \theta_i\right]$$
(5-31)

or

$$\sin \theta_{i} = \sqrt{\frac{\frac{\varepsilon_{2}}{\varepsilon_{1}} - \frac{\mu_{2}}{\mu_{1}}}{\frac{\varepsilon_{2}}{\varepsilon_{1}} - \frac{\varepsilon_{1}}{\varepsilon_{2}}}}$$
(5-31a)

Since the sine function cannot exceed unity, (5-31a) exists only if

$$\frac{\varepsilon_2}{\varepsilon_1} - \frac{\mu_2}{\mu_1} \le \frac{\varepsilon_2}{\varepsilon_1} - \frac{\varepsilon_1}{\varepsilon_2} \tag{5-32}$$

or

$$\frac{\mu_2}{\mu_1} \ge \frac{\varepsilon_1}{\varepsilon_2} \tag{5-32a}$$

If, however, $\mu_1 = \mu_2$, (5-31a) reduces to

$$\theta_i = \theta_{\rm B} = \sin^{-1}\left(\sqrt{\frac{\varepsilon_2}{\varepsilon_1 + \varepsilon_2}}\right) \tag{5-33}$$

The incident angle θ_i , as given by (5-31a) or (5-33), which reduces the reflection coefficient for parallel polarization to zero, is referred to as the Brewster angle, θ_B . It should be noted that when $\mu_1 = \mu_2$, the incidence Brewster angle $\theta_i = \theta_B$ of (5-33) exists only if the polarization of the wave is parallel (vertical).

Other forms of the Brewster angle, besides that given by (5-33), are

$$\theta_i = \theta_{\rm B} = \cos^{-1}\left(\sqrt{\frac{\varepsilon_1}{\varepsilon_1 + \varepsilon_2}}\right)$$
 (5-33a)

$$\theta_i = \theta_{\rm B} = \tan^{-1} \left(\sqrt{\frac{\varepsilon_2}{\varepsilon_1}} \right) \tag{5-33b}$$

Example 5-2

A parallel polarized electromagnetic wave radiated from a submerged submarine impinges upon a water-air planar interface. Assuming the water is lossless, its dielectric constant is 81, and the wave approximates a plane wave at the interface, determine the angle of incidence to allow complete transmission of the energy.

Solution: The angle of incidence that allows complete transmission of the energy is the Brewster angle. Using (5-33b), the Brewster angle of the water-air interface is

$$\theta_{iwa} = \theta_{Bwa} = \tan^{-1}\left(\sqrt{\frac{\varepsilon_0}{81\varepsilon_0}}\right) = \tan^{-1}\left(\frac{1}{9}\right) = 6.34^{\circ}$$

This indicates that the Brewster angle is close to the normal to the interface.

Example 5-3

Repeat the problem of Example 5-2 assuming that the same wave is radiated from a spacecraft in air, and it impinges upon the air-water interface.

Solution: The Brewster angle for an air-water interface is

$$\theta_{iaw} = \theta_{Baw} = \tan^{-1}\left(\sqrt{\frac{81\varepsilon_0}{\varepsilon_0}}\right) = \tan^{-1}(9) = 83.66^{\circ}$$

It is apparent that the sum of the Brewster angle of Example 5-2 (water-air interface) plus that of Example 5-3 (air-water interface) is equal to 90° . That is

$$\theta_{\text{Bwa}} + \theta_{\text{Baw}} = 6.34^{\circ} + 83.66^{\circ} = 90^{\circ}$$

From trigonometry, it is obvious that the preceding relation is always going to hold, no matter what two media form the interface.

5.3.4 Total Reflection-Critical Angle

In Section 5.3.3 we found the angles that allow total transmission for perpendicular, (5-28a), and parallel, (5-31a), polarizations. When the permeabilities of the two media forming the interface are the same ($\mu_1 = \mu_2$), only parallel polarized fields possess an incidence angle that allows total transmission. As before, that angle is known as the Brewster angle, and it is given by either (5-33), (5-33a), or (5-33b).

The next question we will consider is: "Is there an incident angle that allows total reflection of energy at a planar interface?" If this is possible, then $|\Gamma| = 1$. To determine the conditions under which this can be accomplished, we proceed in a similar manner as for the total transmission case of Section 5.3.3.

A. Perpendicular (Horizontal) Polarization To see the conditions under which the magnitude of the reflection coefficient is equal to unity, we set the magnitude of (5-17a) equal to

$$\frac{\left|\sqrt{\frac{\mu_2}{\varepsilon_2}}\cos\theta_i - \sqrt{\frac{\mu_1}{\varepsilon_1}}\cos\theta_t\right|}{\left|\sqrt{\frac{\mu_2}{\varepsilon_2}}\cos\theta_i + \sqrt{\frac{\mu_1}{\varepsilon_1}}\cos\theta_t\right|} = 1$$
 (5-34)

This is satisfied provided the second term in the numerator and denominator is imaginary. Using Snell's law of refraction, as given by (5-15b), the second term in the numerator and denominator can be imaginary if

$$\cos \theta_t = \sqrt{1 - \sin^2 \theta_t} = \sqrt{1 - \frac{\mu_1 \varepsilon_1}{\mu_2 \varepsilon_2} \sin^2 \theta_i} = -j \sqrt{\frac{\mu_1 \varepsilon_1}{\mu_2 \varepsilon_2} \sin^2 \theta_i - 1}$$
 (5-35)

In order for (5-35) to hold

$$\frac{\mu_1 \varepsilon_1}{\mu_2 \varepsilon_2} \sin^2 \theta_i \ge 1 \tag{5-35a}$$

or

$$\theta_i \ge \theta_c = \sin^{-1}\left(\sqrt{\frac{\mu_2 \varepsilon_2}{\mu_1 \varepsilon_1}}\right)$$
 (5-35b)

The incident angle θ_i of (5-35b) that allows total reflection is known as the *critical angle*. Since the argument of the inverse sine function cannot exceed unity, then

$$\mu_2 \varepsilon_2 \le \mu_1 \varepsilon_1 \tag{5-35c}$$

in order for the critical angle (5-35b) to be physically realizable.

If the permeabilities of the two media are the same ($\mu_1 = \mu_2$), then (5-35b) reduces to

$$\theta_i \ge \theta_c = \sin^{-1}\left(\sqrt{\frac{\varepsilon_2}{\varepsilon_1}}\right) \tag{5-36}$$

which leads to a physically realizable angle provided

$$\varepsilon_2 < \varepsilon_1$$
 (5-36a)

Therefore for two media with identical permeabilities (which is the case for most dielectrics, aside from ferromagnetic material), the critical angle exists only if the wave propagates from a more dense to a less dense medium, as stated by (5-36a).

Example 5-4

A perpendicularly polarized wave radiated from a submerged submarine impinges upon a water-air interface. Assuming the water is lossless, its dielectric constant is 81, and the wave approximates a plane wave at the interface, determine the angle of incidence that will allow complete reflection of the energy at the interface.

Solution: The angle of incidence that allows complete reflection of energy is the critical angle. Since for water $\mu_2 = \mu_0$, the critical angle is obtained using (5-36), which leads to

$$\theta_i \ge \theta_c = \sin^{-1}\left(\sqrt{\frac{\varepsilon_0}{81\varepsilon_0}}\right) = 6.38^\circ$$

Since there is a large difference between the permittivities of the two media forming the interface, the critical angle of this example is very nearly the same as the Brewster angle of Example 5-2.

The next question we will answer is: "What happens to the angle of refraction and to the propagation of the wave when the angle of incidence is equal to or greater than the critical angle?"

When the angle of incidence is equal to the critical angle, the angle of refraction reduces, through Snell's law of refraction (5-15b) and (5-35b), to

$$\theta_t = \sin^{-1} \left(\sqrt{\frac{\mu_1 \varepsilon_1}{\mu_2 \varepsilon_2}} \sin \theta_i \right) \Big|_{\theta_t = \theta_c} = \sin^{-1} \left(\sqrt{\frac{\mu_1 \varepsilon_1}{\mu_2 \varepsilon_2}} \sqrt{\frac{\mu_2 \varepsilon_2}{\mu_1 \varepsilon_1}} \right) = \sin^{-1}(1) = 90^{\circ}$$
 (5-37)

In turn the reflection and transmission coefficients reduce to

$$\Gamma^b_{\perp}|_{\theta_i = \theta_c} = 1 \tag{5-38a}$$

$$T_{\perp}^{b}|_{\theta_{i}=\theta_{c}}=2\tag{5-38b}$$

Also the transmitted fields of (5-12a) and (5-12b) can be written as

$$\mathbf{E}_{\perp}^{t} = \hat{\mathbf{a}}_{v} 2E_{0}e^{-j\beta_{2}x} \tag{5-39a}$$

$$\mathbf{H}_{\perp}^{t} = \hat{\mathbf{a}}_{z} \frac{2E_{0}}{\eta_{2}} e^{-j\beta_{2}x} \tag{5-39b}$$

which represent a plane wave that travels parallel to the interface in the +x direction as shown in Figure 5-6a. The constant phase planes of the wave are parallel to the z axis. This wave is referred to as a *surface wave* [2].

The average power density associated with the transmitted fields is given by

$$\mathbf{S}_{\text{av}}^{t}|_{\theta_{i}=\theta_{c}} = \frac{1}{2} \operatorname{Re} \left(\mathbf{E}_{\perp}^{t} \times \mathbf{H}_{\perp}^{t^{*}} \right) \Big|_{\theta_{i}=\theta_{c}} = \hat{\mathbf{a}}_{x} \frac{2|E_{0}|^{2}}{\eta_{2}}$$
 (5-40)

and it does not contain any component normal to the interface. Therefore, there is no transfer of real power across the interface in a direction normal to the boundary; thus, all power must be reflected. This is also evident by examining the magnitude of the incident and reflected average power densities associated with the fields (5-10a) through (5-11d) under critical angle incidence. These are obviously identical and are given by

$$|\mathbf{S}_{\text{av}}^{i}|_{\theta_{i}=\theta_{c}} = \left|\frac{1}{2}\operatorname{Re}\left(\mathbf{E}_{\perp}^{i} \times \mathbf{H}_{\perp}^{i^{*}}\right)\right|_{\theta_{i}=\theta_{c}} = \frac{|E_{0}|^{2}}{2\eta_{i}}|\hat{\mathbf{a}}_{x}\sin\theta_{i} + \hat{\mathbf{a}}_{z}\cos\theta_{i}| = \frac{|E_{0}|^{2}}{2\eta_{1}}$$
(5-41a)

$$|\mathbf{S}_{\text{av}}^r|_{\theta_i = \theta_c} = \left| \frac{1}{2} \text{Re} \left(\mathbf{E}_{\perp}^r \times \mathbf{H}_{\perp}^{r^*} \right) \right|_{\theta_i = \theta_c} = \frac{|E_0|^2}{2\eta_1} |\hat{\mathbf{a}}_x \sin \theta_i - \hat{\mathbf{a}}_z \cos \theta_i| = \frac{|E_0|^2}{2\eta_1}$$
(5-41b)

When the angle of incidence θ_i is greater than the critical angle $\theta_c(\theta_i > \theta_c)$, Snell's law of refraction can be written as [3]

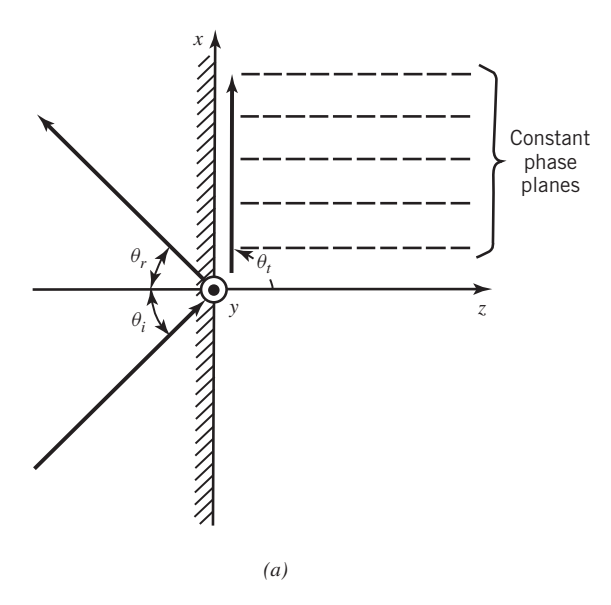
$$\sin \theta_t |_{\theta_i > \theta_c} = \frac{\beta_1}{\beta_2} \sin \theta_i \Big|_{\theta_i > \theta_c} = \sqrt{\frac{\mu_1 \varepsilon_1}{\mu_2 \varepsilon_2}} \sin \theta_i \Big|_{\theta_i > \theta_c} > 1$$
 (5-42a)

which can only be satisfied provided θ_t is complex, that is, $\theta_t = \theta_R + j\theta_X$, where $\theta_X \neq 0$. Also

$$\cos \theta_{t}|_{\theta_{i} > \theta_{c}} = \sqrt{1 - \sin^{2} \theta_{t}} \Big|_{\theta_{i} > \theta_{c}} = \sqrt{1 - \frac{\mu_{1} \varepsilon_{1}}{\mu_{2} \varepsilon_{2}} \sin^{2} \theta_{i}} \Big|_{\theta_{i} > \theta_{c}}$$

$$= \pm j \sqrt{\frac{\mu_{1} \varepsilon_{1}}{\mu_{2} \varepsilon_{2}} \sin^{2} \theta_{i} - 1} \Big|_{\theta_{i} > \theta_{c}}$$
(5-42b)

which again indicates that θ_t is complex.



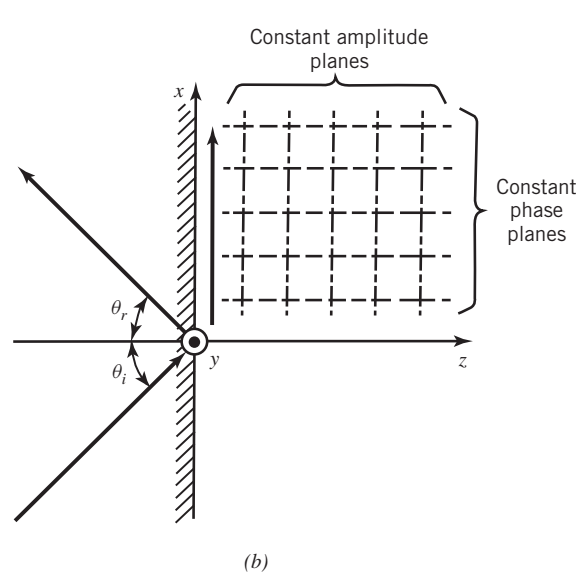


Figure 5-6 Constant phase and amplitude planes for incident angles. (a) Critical $(\theta_i = \theta_c)$. (b) Above critical $(\theta_i > \theta_c)$.

Therefore when $\theta_i > \theta_c$, there is no physically realizable angle θ_t . If not, what really does happen to the wave propagation? Since under this condition θ_t is complex and not physically realizable, this may be a clue that the wave in medium 2 is again a surface wave. To see this, let us examine the field in medium 2, the reflection and transmission coefficients, and the average power densities.

When the angle of incidence exceeds the critical angle $(\theta_i > \theta_c)$, the transmitted **E** field of (5-12a) can be written, using (5-15b) and (5-35b), as

$$\begin{split} \mathbf{E}_{\perp}^{t}|_{\theta_{i} > \theta_{c}} &= \hat{\mathbf{a}}_{y} T_{\perp}^{b} E_{0} \exp(-j \beta_{2} x \sin \theta_{t}) \exp(-j \beta_{2} z \cos \theta_{t})|_{\theta_{i} > \theta_{c}} \\ &= \hat{\mathbf{a}}_{y} T_{\perp}^{b} E_{0} \exp\left[-j \beta_{2} x \left(\sqrt{\frac{\mu_{1} \varepsilon_{1}}{\mu_{2} \varepsilon_{2}}} \sin \theta_{i}\right)\right] \exp\left(-j \beta_{2} z \sqrt{1 - \sin^{2} \theta_{t}}\right)\Big|_{\theta_{i} > \theta_{c}} \end{split}$$

$$\mathbf{E}_{\perp}^{t}|_{\theta_{i} > \theta_{c}} = \hat{\mathbf{a}}_{y} T_{\perp}^{b} E_{0} \exp \left[-j \beta_{2} x \left(\sqrt{\frac{\mu_{1} \varepsilon_{1}}{\mu_{2} \varepsilon_{2}}} \sin \theta_{i} \right) \right] \exp \left(-j \beta_{2} z \sqrt{1 - \frac{\mu_{1} \varepsilon_{1}}{\mu_{2} \varepsilon_{2}}} \sin^{2} \theta_{i} \right) \Big|_{\theta_{i} > \theta_{c}}$$

$$= \hat{\mathbf{a}}_{y} T_{\perp}^{b} E_{0} \exp \left[-j \beta_{2} x \left(\sqrt{\frac{\mu_{1} \varepsilon_{1}}{\mu_{2} \varepsilon_{2}}} \sin \theta_{i} \right) \right] \exp \left(-\beta_{2} z \sqrt{\frac{\mu_{1} \varepsilon_{1}}{\mu_{2} \varepsilon_{2}}} \sin^{2} \theta_{i} - 1 \right) \Big|_{\theta_{i} > \theta_{c}}$$

$$= \hat{\mathbf{a}}_{y} T_{\perp}^{b} E_{0} \exp \left[-\beta_{2} z \left(\sqrt{\frac{\mu_{1} \varepsilon_{1}}{\mu_{2} \varepsilon_{2}}} \sin^{2} \theta_{i} - 1 \right) \right] \exp \left[-j \beta_{2} x \left(\sqrt{\frac{\mu_{1} \varepsilon_{1}}{\mu_{2} \varepsilon_{2}}} \sin \theta_{i} \right) \right] \Big|_{\theta_{i} > \theta_{c}}$$

$$\mathbf{E}_{\perp}^{t}|_{\theta_{i} > \theta_{c}} = \hat{\mathbf{a}}_{y} T_{\perp}^{b} E_{0} e^{-\alpha_{e} z} e^{-j \beta_{e} x}$$

$$(5-43)$$

where

$$\alpha_e = \beta_2 \sqrt{\frac{\mu_1 \varepsilon_1}{\mu_2 \varepsilon_2} \sin^2 \theta_i - 1} \bigg|_{\theta_i > \theta_c} = \omega \sqrt{\mu_1 \varepsilon_1 \sin^2 \theta_i - \mu_2 \varepsilon_2} \bigg|_{\theta_i > \theta_c}$$
(5-43a)

$$\beta_e = \beta_2 \sqrt{\frac{\mu_1 \varepsilon_1}{\mu_2 \varepsilon_2}} \sin \theta_i \bigg|_{\theta_i > \theta_c} = \omega \sqrt{\mu_1 \varepsilon_1} \sin \theta_i \bigg|_{\theta_i > \theta_c}$$
 (5-43b)

$$v_{pe} = \frac{\omega}{\beta_e} = \left. \frac{\omega}{\beta_2 \sqrt{\frac{\mu_1 \varepsilon_1}{\mu_2 \varepsilon_2}} \sin \theta_i} \right|_{\theta_i > \theta_c} = \left. \frac{v_{p2}}{\sqrt{\frac{\mu_1 \varepsilon_1}{\mu_2 \varepsilon_2}} \sin \theta_i} \right|_{\theta_i > \theta_c} = \frac{1}{\sqrt{\mu_1 \varepsilon_1} \sin \theta_i} < v_{p2}$$
(5-43c)

The wave associated with (5-43) also propagates parallel to the interface with constant phase planes that are parallel to the z axis, as shown in Figure 5-6b. The effective phase velocity v_{pe} of the wave is given by (5-43c), and it is less than v_{p2} of an ordinary wave in medium 2. The wave also possesses constant amplitude planes that are parallel to the x axis, as shown in Figure 5-6b. The effective attenuation constant α_e of the wave in the z direction is that given by (5-43a). Its values are such that the wave decays very rapidly, and in a few wavelengths it essentially vanishes. This wave is also a surface wave. Since its phase velocity is less than the speed of light, it is a slow surface wave. Also since it decays very rapidly in a direction normal to the interface, it is tightly bound to the surface—i.e., it is a tightly bound slow surface wave.

Phase velocities *greater* than the intrinsic phase velocity of an ordinary plane wave in a given medium can be achieved by uniform plane waves at *real oblique angles* of propagation, as illustrated in Section 4.2.2C; phase velocities *smaller* than the intrinsic velocity can only be achieved by uniform plane waves at *complex angles* of propagation. Waves traveling at complex angles are *nonuniform* plane waves oriented so as to provide small phase velocities or large rates of change of phase in a given direction. The price for such large rates of change of phase or small velocities in one direction is associated with large attenuation at perpendicular directions.

Example 5-5

Assume that $\theta_i > \theta_c$ (so the angle of refraction $\theta_t = \theta_R + j\theta_X$ is complex, i.e. $\theta_X \neq 0$). Determine the real (θ_R) and imaginary (θ_X) parts of θ_t in terms of the constitutive parameters of the two media and the angle of incidence.

Solution: Using (5-42a)

$$\sin \theta_t = \sin(\theta_R + j\theta_X) = \sqrt{\frac{\mu_1 \varepsilon_1}{\mu_2 \varepsilon_2}} \sin \theta_i$$

or

$$\sin(\theta_R)\cosh(\theta_X) + j\cos(\theta_R)\sinh(\theta_X) = \sqrt{\frac{\mu_1\varepsilon_1}{\mu_2\varepsilon_2}}\sin\theta_i$$

Since the right side is real, then the only solution that exists is for the imaginary part of the left side to vanish and the real part to be equal to the real part of the right side. Thus

$$\cos(\theta_R)\sinh(\theta_X) = 0 \Rightarrow \theta_R = \frac{\pi}{2}$$

$$\sin(\theta_R)\cosh(\theta_X) = \sqrt{\frac{\mu_1 \varepsilon_1}{\mu_2 \varepsilon_2}}\sin\theta_i \Rightarrow \theta_X = \cosh^{-1}\left(\sqrt{\frac{\mu_1 \varepsilon_1}{\mu_2 \varepsilon_2}}\sin\theta_i\right)$$

In turn $\cos \theta_t$ is defined as

$$\cos \theta_t = \cos(\theta_R + j\theta_X) = \cos(\theta_R) \cosh(\theta_X) - j \sin(\theta_R) \sinh(\theta_X)$$

or

$$\cos \theta_t = -i \sinh(\theta_X)$$

which again is shown to be complex as was in (5-42b). When these expressions for $\sin \theta_t$ and $\cos \theta_t$ are used to represent the fields in medium 2, it will be shown that the fields are nonuniform plane waves as illustrated by (5-43).

Under the conditions where the angle of incidence is equal to or greater than the critical angle, the reflection Γ^b_{\perp} and transmission T^b_{\perp} coefficients of (5-17a) and (5-17b) reduce, respectively, to [3]

$$\begin{split} \Gamma_{\perp}^{b}|_{\theta_{i}\geq\theta_{c}} &= \frac{\sqrt{\frac{\mu_{2}}{\varepsilon_{2}}}\cos\theta_{i} - \sqrt{\frac{\mu_{1}}{\varepsilon_{1}}}\cos\theta_{t}}{\sqrt{\frac{\mu_{2}}{\varepsilon_{2}}}\cos\theta_{i} + \sqrt{\frac{\mu_{1}}{\varepsilon_{1}}}\cos\theta_{t}}\Big|_{\theta_{i}\geq\theta_{c}} \\ &= \frac{\sqrt{\frac{\mu_{2}}{\varepsilon_{2}}}\cos\theta_{i} - \sqrt{\frac{\mu_{1}}{\varepsilon_{1}}}\sqrt{1 - \sin^{2}\theta_{t}}}{\sqrt{\frac{\mu_{2}}{\varepsilon_{2}}}\cos\theta_{i} + \sqrt{\frac{\mu_{1}}{\varepsilon_{1}}}\sqrt{1 - \sin^{2}\theta_{t}}}\Big|_{\theta_{i}\geq\theta_{c}} \\ &= \frac{\sqrt{\frac{\mu_{2}}{\varepsilon_{2}}}\cos\theta_{i} - \sqrt{\frac{\mu_{1}}{\varepsilon_{1}}}\sqrt{1 - \frac{\mu_{1}\varepsilon_{1}}{\mu_{2}\varepsilon_{2}}}\sin^{2}\theta_{i}}\Big|_{\theta_{i}\geq\theta_{c}} \\ &= \frac{\sqrt{\frac{\mu_{2}}{\varepsilon_{2}}}\cos\theta_{i} + \sqrt{\frac{\mu_{1}}{\varepsilon_{1}}}\sqrt{1 - \frac{\mu_{1}\varepsilon_{1}}{\mu_{2}\varepsilon_{2}}}\sin^{2}\theta_{i}}\Big|_{\theta_{i}\geq\theta_{c}} \\ &= \frac{\sqrt{\frac{\mu_{2}}{\varepsilon_{2}}}\cos\theta_{i} + j\sqrt{\frac{\mu_{1}}{\varepsilon_{1}}}\sqrt{\frac{\mu_{1}\varepsilon_{1}}{\mu_{2}\varepsilon_{2}}}\sin^{2}\theta_{i} - 1}\Big|_{\theta_{i}\geq\theta_{c}} \\ &= \frac{\sqrt{\frac{\mu_{2}}{\varepsilon_{2}}}\cos\theta_{i} - j\sqrt{\frac{\mu_{1}}{\varepsilon_{1}}}\sqrt{\frac{\mu_{1}\varepsilon_{1}}{\mu_{2}\varepsilon_{2}}}\sin^{2}\theta_{i} - 1}\Big|_{\theta_{i}\geq\theta_{c}} \\ &\Gamma_{\perp}^{b}|_{\theta_{i}\geq\theta_{c}} = |\Gamma_{\perp}^{b}|e^{j2\psi_{\perp}} = e^{j2\psi_{\perp}} \end{split} \tag{5-44}$$

where

$$|\Gamma_{\perp}^b| = 1 \tag{5-44a}$$

$$\psi_{\perp} = \tan^{-1} \left\lceil \frac{X_{\perp}}{R_{\perp}} \right\rceil \tag{5-44b}$$

$$X_{\perp} = \sqrt{\frac{\mu_1}{\varepsilon_1}} \sqrt{\frac{\mu_1 \varepsilon_1}{\mu_2 \varepsilon_2} \sin^2 \theta_i - 1}$$
 (5-44c)

$$R_{\perp} = \sqrt{\frac{\mu_2}{\varepsilon_2}} \cos \theta_i \tag{5-44d}$$

$$T_{\perp}^{b}|_{\theta_{i} \geq \theta_{c}} = \frac{2\sqrt{\frac{\mu_{2}}{\varepsilon_{2}}}\cos\theta_{i}}{\sqrt{\frac{\mu_{2}}{\varepsilon_{2}}}\cos\theta_{i} + \sqrt{\frac{\mu_{1}}{\varepsilon_{1}}}\cos\theta_{t}}\Big|_{\theta_{i} \geq \theta_{c}}$$

$$= \frac{2\sqrt{\frac{\mu_{2}}{\varepsilon_{2}}}\cos\theta_{i}}{\sqrt{\frac{\mu_{2}}{\varepsilon_{2}}}\cos\theta_{i} + \sqrt{\frac{\mu_{1}}{\varepsilon_{1}}}\sqrt{1 - \sin^{2}\theta_{t}}}\Big|_{\theta_{i} \geq \theta_{c}}$$

$$= \frac{2\sqrt{\frac{\mu_{2}}{\varepsilon_{2}}}\cos\theta_{i} + \sqrt{\frac{\mu_{1}}{\varepsilon_{1}}}\sqrt{1 - \frac{\mu_{1}\varepsilon_{1}}{\mu_{2}\varepsilon_{2}}}\sin^{2}\theta_{i}}\Big|_{\theta_{i} \geq \theta_{c}}$$

$$= \frac{2\sqrt{\frac{\mu_{2}}{\varepsilon_{2}}}\cos\theta_{i} + \sqrt{\frac{\mu_{1}}{\varepsilon_{1}}}\sqrt{1 - \frac{\mu_{1}\varepsilon_{1}}{\mu_{2}\varepsilon_{2}}}\sin^{2}\theta_{i}}\Big|_{\theta_{i} \geq \theta_{c}}$$

$$= \frac{2\sqrt{\frac{\mu_{2}}{\varepsilon_{2}}}\cos\theta_{i} - j\sqrt{\frac{\mu_{1}}{\varepsilon_{1}}}\sqrt{\frac{\mu_{1}\varepsilon_{1}}{\mu_{2}\varepsilon_{2}}}\sin^{2}\theta_{i} - 1}\Big|_{\theta_{i} \geq \theta_{c}}$$

$$T_{\perp}^{b}|_{\theta_{i} > \theta_{c}} = |T_{\perp}^{b}|e^{j\psi_{\perp}}$$
(5-45)

where

$$|T_{\perp}^{b}| = \frac{2R_{\perp}}{\sqrt{R_{\perp}^{2} + X_{\perp}^{2}}}$$
 (5-45a)

In addition, the transmitted average power density can now be written, using (5-12a) through (5-12b) and the modified forms (5-43) through (5-43b) for the fields when the incidence angle is equal to or greater than the critical angle, as

$$\begin{split} \mathbf{S}_{\mathrm{av}}^{t}|_{\theta_{i}\geq\theta_{c}} &= \frac{1}{2}\mathrm{Re}(\mathbf{E}^{t}\times\mathbf{H}^{t^{*}})_{\theta_{i}\geq\theta_{c}} \\ &= \frac{1}{2}\mathrm{Re}\left[\left(\hat{\mathbf{a}}_{y}T_{\perp}^{b}E_{0}e^{-\alpha_{e}z}e^{-j\beta_{e}x}\right)\times\left(-\hat{\mathbf{a}}_{x}\cos\theta_{t}+\hat{\mathbf{a}}_{z}\sin\theta_{t}\right)^{*}\frac{(T_{\perp}^{b})^{*}E_{0}^{*}}{\eta_{2}}e^{-\alpha_{e}z}e^{+j\beta_{e}x}\right]_{\theta_{i}\geq\theta_{c}} \\ &= \frac{1}{2}\mathrm{Re}\left\{\left[\hat{\mathbf{a}}_{z}(\cos\theta_{t})^{*}+\hat{\mathbf{a}}_{x}(\sin\theta_{t})^{*}\right]\frac{|T_{\perp}^{b}|^{2}|E_{0}|^{2}}{\eta_{2}}e^{-2\alpha_{e}z}\right\}_{\theta_{i}\geq\theta_{c}} \\ \mathbf{S}_{\mathrm{av}}^{t}|_{\theta_{i}\geq\theta_{c}} &= \frac{1}{2}\mathrm{Re}\left\{\left[\hat{\mathbf{a}}_{z}\left(\sqrt{1-\sin^{2}\theta_{t}}\right)^{*}+\hat{\mathbf{a}}_{x}(\sin\theta_{t})^{*}\right]\frac{|T_{\perp}^{b}|^{2}|E_{0}|^{2}}{\eta_{2}}e^{-2\alpha_{e}z}\right\}_{\theta_{i}\geq\theta_{c}} \end{split}$$

$$\mathbf{S}_{\text{av}}^{t}|_{\theta_{i} \geq \theta_{c}} = \frac{1}{2} \operatorname{Re} \left\{ \left[\hat{\mathbf{a}}_{z} \left(\sqrt{1 - \frac{\mu_{1} \varepsilon_{1}}{\mu_{2} \varepsilon_{2}} \sin^{2} \theta_{i}} \right)^{*} \right] + \hat{\mathbf{a}}_{x} \left(\sqrt{\frac{\mu_{1} \varepsilon_{1}}{\mu_{2} \varepsilon_{2}}} \sin \theta_{i} \right)^{*} \right] \frac{|T_{\perp}^{b}|^{2} |E_{0}|^{2}}{\eta_{2}} e^{-2\alpha_{e}z} \right\}_{\theta_{i} \geq \theta_{c}}$$

$$= \frac{1}{2} \operatorname{Re} \left\{ \left[\hat{\mathbf{a}}_{z} \left(-j \sqrt{\frac{\mu_{1} \varepsilon_{1}}{\mu_{2} \varepsilon_{2}}} \sin^{2} \theta_{i} - 1 \right) + \hat{\mathbf{a}}_{x} \left(\sqrt{\frac{\mu_{1} \varepsilon_{1}}{\mu_{2} \varepsilon_{2}}} \sin \theta_{i} \right) \right] \frac{|T_{\perp}^{b}|^{2} |E_{0}|^{2}}{\eta_{2}} e^{-2\alpha_{e}z} \right\}_{\theta_{i} \geq \theta_{c}}$$

$$\mathbf{S}_{\text{av}}^{t}|_{\theta_{i} \geq \theta_{c}} = \hat{\mathbf{a}}_{x} \sqrt{\frac{\mu_{1} \varepsilon_{1}}{\mu_{2} \varepsilon_{2}}} \sin \theta_{i} \frac{|T_{\perp}^{b}|^{2} |E_{0}|^{2}}{2\eta_{2}} e^{-2\alpha_{e}z} \Big|_{\theta_{i} \geq \theta_{c}}$$

$$(5-46)$$

Again, from (5-46), it is apparent that there is no real power transfer across the interface in a direction normal to the boundary. Therefore all the power must be reflected into medium 1. This can also be verified by formulating and examining the incident and reflected average power densities. Doing this, using the fields (5-10a) through (5-11b) where the reflection coefficient is that of (5-44), shows that the magnitudes of the incident and reflected average power densities are those of (5-41a) and (5-41b), which are identical.

The propagation of a wave from a medium with higher density to one with lower density $(\varepsilon_2 < \varepsilon_1 \text{ when } \mu_1 = \mu_2)$ under oblique incidence can be summarized as follows.

- 1. When the angle of incidence is smaller than the critical angle $(\theta_i < \theta_c = \sin^{-1}(\sqrt{\varepsilon_2/\varepsilon_1}))$, a wave is transmitted into medium 2 at an angle θ_t , which is greater than the incident angle θ_i . Real power is transferred into medium 2, and it is directed along angle θ_t as shown in Figure 5-7a.
- 2. As the angle of incidence increases and reaches the critical angle $\theta_i = \theta_c = \sin^{-1}(\sqrt{\epsilon_2/\epsilon_1})$, the refracted angle θ_t , which varies more rapidly than the incident angle θ_i , approaches 90°. Although a wave into medium 2 exists under this condition (which is necessary to satisfy the boundary conditions), the fields form a surface wave that is directed along the x axis (which is parallel to the interface). There is no real power transfer normal to the boundary into medium 2, and all the power is reflected in medium 1 along reflected angle θ_r as shown in Figure 5-7b. The constant phase planes are parallel to the z axis.
- 3. When the incident angle θ_i exceeds the critical angle $\theta_c[\theta_i > \theta_c = \sin^{-1}(\sqrt{\epsilon_2/\epsilon_1})]$, a wave into medium 2 still exists, which travels along the x axis (which is parallel to the interface) and is heavily attenuated in the z direction (which is normal to the interface). There is no real power transfer normal to the boundary into medium 2, and all power is reflected into medium 1 along reflection angle θ_r , as shown in Figure 5-7c. Although there is no power transferred into medium 2, a wave exists there that is necessary to satisfy the boundary conditions on the continuity of the tangential components of the electric and magnetic fields. The wave in medium 2 travels parallel to the interface with a phase velocity that is less than that of an ordinary wave in the same medium [as given by (5-43c)], and it is rapidly attenuated in a direction normal to the interface with an effective attenuation constant given by (5-43a). This wave is *tightly bound* to the surface, and it is referred to as a *tightly bound slow surface wave*.

The critical angle is used to design many practical instruments and transmission lines, such as binoculars, dielectric covered ground plane (surface wave) transmission lines, fiber optic cables, etc. To see how the critical angle may be utilized, let us consider an example.

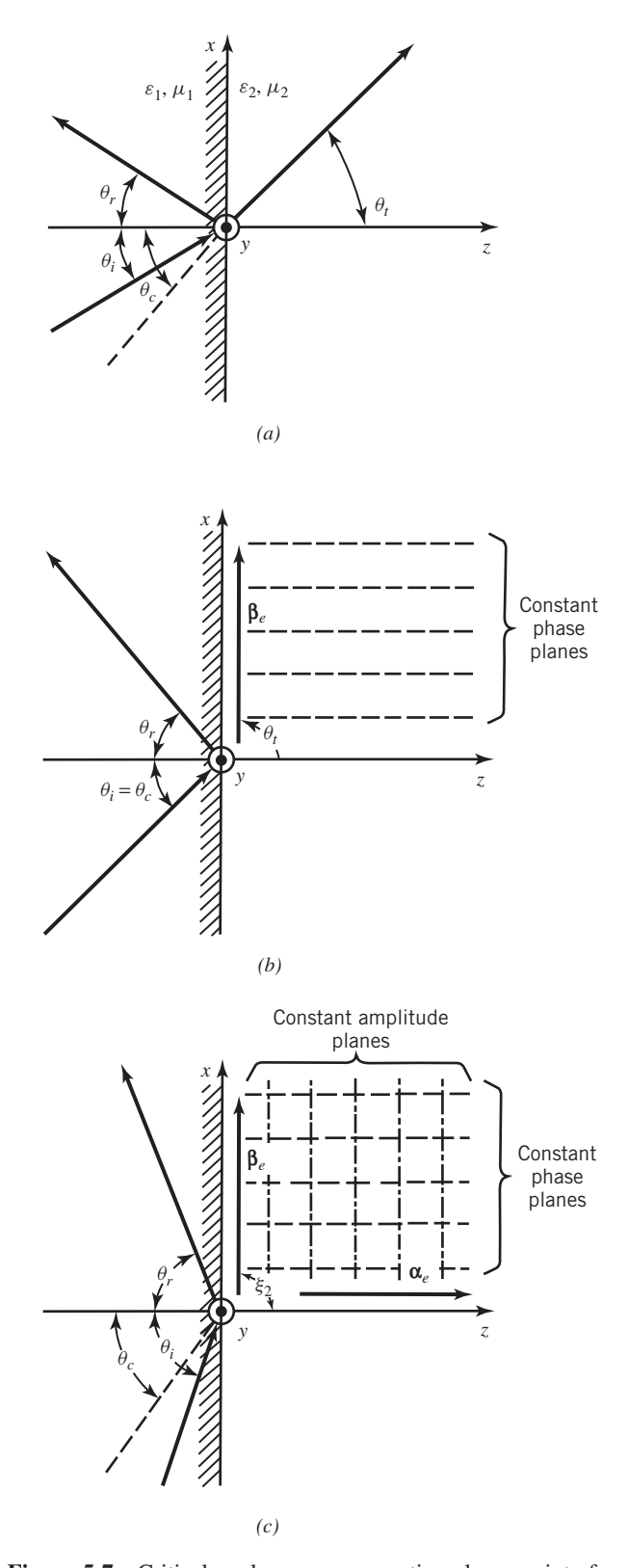


Figure 5-7 Critical angle wave propagation along an interface.

Example 5-6

Determine the range of values of the dielectric constant of a dielectric slab of thickness t so that, when a wave is incident on it from one of its ends at an oblique angle $0^{\circ} \le \theta_i \le 90^{\circ}$, the energy of the wave in the dielectric is contained within the slab. The geometry of the problem is shown in the Figure 5-8.

Solution: We assume that the slab width is infinite (two-dimensional geometry). To contain the energy of the wave within the slab, the reflection angle θ_r of the wave bouncing within the slab must be equal to or greater than the critical angle θ_c . By referring to Figure 5-8, the critical angle can be related to the refraction angle θ_t by

$$\sin \theta_r = \sin \left(\frac{\pi}{2} - \theta_t\right) = \cos \theta_t \ge \sin \theta_c = \sqrt{\frac{\varepsilon_0}{\varepsilon_r \varepsilon_0}} = \frac{1}{\sqrt{\varepsilon_r}}$$

or

$$\cos \theta_t \ge \frac{1}{\sqrt{\varepsilon_r}}$$

At the interface formed at the leading edge, Snell's law of refraction must be satisfied. That is,

$$\beta_0 \sin \theta_i = \beta_1 \sin \theta_t \Rightarrow \sin \theta_t = \frac{\beta_0}{\beta_1} \sin \theta_i = \frac{1}{\sqrt{\varepsilon_r}} \sin \theta_i$$

Using this, we can write the aforementioned $\cos \theta_t$ as

$$\cos \theta_t = \sqrt{1 - \sin^2 \theta_t} = \sqrt{1 - \frac{1}{\varepsilon_r} \sin^2 \theta_i} \ge \frac{1}{\sqrt{\varepsilon_r}}$$

or

$$\sqrt{1 - \frac{1}{\varepsilon_r} \sin^2 \theta_i} \ge \frac{1}{\sqrt{\varepsilon_r}}$$

Solving this leads to

$$\varepsilon_r - \sin^2 \theta_i > 1$$

or

$$\varepsilon_r > 1 + \sin^2 \theta_i$$

To accommodate all possible angles, the dielectric constant must be

$$\varepsilon_r \geq 2$$

since the smallest and largest values of θ_i , are, respectively, 0° and 90° . This is achievable by many practical dielectric materials such as Teflon ($\varepsilon_r \simeq 2.1$), polystyrene ($\varepsilon_r \simeq 2.56$), and many others.

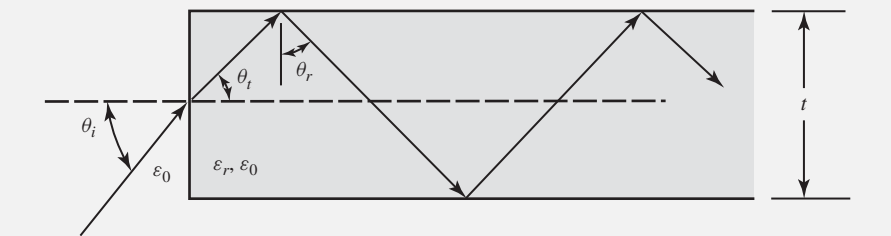


Figure 5-8 Dielectric slab of thickness t and wave containment within.

B. Parallel (Vertical) Polarization The procedure used to derive the critical angle and to examine the properties for perpendicular (horizontal) polarization can be repeated for parallel (vertical) polarization. However, it can be shown that the critical angle is not a function of polarization, and that it exists for both parallel and perpendicular polarizations. The only limitation of the critical angle is that the wave propagation be to a less dense medium ($\mu_2 \varepsilon_2 < \mu_1 \varepsilon_1$ or $\varepsilon_2 < \varepsilon_1$ when $\mu_1 = \mu_2$).

The expression for the critical angle for parallel polarization is the same as that for perpendicular polarization as given by (5-35b) or (5-36). In addition, the wave propagation phenomena that occur for perpendicular polarization when the incidence angle is less than, equal to, or greater than the critical angle are also identical to those for parallel polarization. Although the formulas for the reflection and transmission coefficients, Γ^b_{\parallel} and T^b_{\parallel} respectively, and transmitted average power density \mathbf{S}^t_{\parallel} for parallel polarization are not identical to those of perpendicular polarization as given by (5-44) through (5-46), the principles stated previously are identical here. The derivation of the specific formulas for the parallel polarization for critical angle propagation are left as an end-of-chapter exercise for the reader.

5.4 LOSSY MEDIA

In the previous sections we examined wave reflection and transmission under normal and oblique wave incidence when both media forming the interface are lossless. Let us now examine the reflection and transmission of waves under normal and oblique incidence when either one or both media are lossy [4]. Although in some cases the formulas will be the same as for the lossless cases, there are differences, especially under oblique wave incidence.

5.4.1 Normal Incidence: Conductor-Conductor Interface

When a uniform plane wave is normally incident upon a planar interface formed by two lossy media (as shown in Figure 5-1 but allowing for losses in both media through the conductivity σ), the incident, reflected, and transmitted fields, reflection and transmission coefficients, and average power densities are identical to (5-1a) through (5-6c) except that (a) an attenuation constant must be included in each field and (b) the intrinsic impedances, and attenuation and phases constants must be modified to include the conductivities of the media. Thus we can summarize the results here as

$$\mathbf{E}^{i} = \hat{\mathbf{a}}_{x} E_{0} e^{-\alpha_{1} z} e^{-j\beta_{1} z} \tag{5-47a}$$

$$\mathbf{H}^{i} = \hat{\mathbf{a}}_{y} \frac{E_{0}}{\eta_{1}} e^{-\alpha_{1} z} e^{-j\beta_{1} z}$$
 (5-47b)

$$\mathbf{E}^r = \hat{\mathbf{a}}_x \Gamma^b E_0 e^{+\alpha_1 z} e^{+j\beta_1 z} \tag{5-48a}$$

$$\mathbf{H}^{r} = -\hat{\mathbf{a}}_{y} \frac{\Gamma^{b} E_{0}}{n_{1}} e^{+\alpha_{1} z} e^{+j\beta_{1} z}$$
 (5-48b)

$$\mathbf{E}^{t} = \hat{\mathbf{a}}_{x} T^{b} E_{0} e^{-\alpha_{2} z} e^{-j\beta_{2} z} \tag{5-49a}$$

$$\mathbf{H}^{t} = \hat{\mathbf{a}}_{y} \frac{T^{b} E_{0}}{\eta_{2}} e^{-\alpha_{2} z} e^{-j\beta_{2} z}$$
 (5-49b)

$$\Gamma^b = \frac{\eta_2 - \eta_1}{\eta_2 + \eta_1} \tag{5-50a}$$

$$T^b = \frac{2\eta_2}{\eta_2 + \eta_1} \tag{5-50b}$$

$$\mathbf{S}_{\text{av}}^{i} = \hat{\mathbf{a}}_{z} \frac{|E_{0}|^{2}}{2} e^{-2\alpha_{1}z} \operatorname{Re}\left(\frac{1}{\eta_{1}^{*}}\right)$$
 (5-51a)

$$\mathbf{S}_{\text{av}}^{r} = -\hat{\mathbf{a}}_{z} |\Gamma^{b}|^{2} \frac{|E_{0}|^{2}}{2} e^{+2\alpha_{1}z} \operatorname{Re}\left(\frac{1}{\eta_{1}^{*}}\right)$$
 (5-51b)

$$\mathbf{S}'_{\text{av}} = \hat{\mathbf{a}}_z |T^b|^2 \frac{|E_0|^2}{2} e^{-2\alpha_2 z} \text{Re}\left(\frac{1}{\eta_2^*}\right)$$
 (5-51c)

For each lossy medium the attenuation constants α_i , phase constants β_i , and intrinsic impedances η_i are related to the corresponding constitutive parameters ε_i , μ_i , and σ_i , by the expressions in Table 4-1.

The total electric and magnetic fields in medium 1 can be written as

$$\mathbf{E}^{1} = \mathbf{E}^{i} + \mathbf{E}^{r} = \hat{\mathbf{a}}_{x} \underbrace{E_{0}e^{-\alpha_{1}z}e^{-j\beta_{1}z}}_{\text{traveling wave}} \underbrace{(1 + \Gamma^{b}e^{+2\alpha_{1}z}e^{+j2\beta_{1}z})}_{\text{standing wave}}$$
(5-52a)

$$\mathbf{H}^{1} = \mathbf{H}^{i} + \mathbf{H}^{r} = \hat{\mathbf{a}}_{y} \underbrace{(E_{0}/\eta_{1})e^{-\alpha_{1}z}e^{-j\beta_{1}z}}_{\text{traveling wave}} \underbrace{(1 - \Gamma^{b}e^{+2\alpha_{1}z}e^{+j2\beta_{1}z})}_{\text{standing wave}}$$
(5-52b)

In each field the factors outside the parentheses form the *traveling wave part* of the total wave; those within the parentheses form the *standing wave part*.

Example 5-7

A uniform plane wave, whose incident electric field has an x component with an amplitude at the interface of 10^{-3} V/m, is traveling in a free-space medium and is normally incident upon a lossy flat earth as shown in Figure 5-9. Assuming that the constitutive parameters of the earth are $\varepsilon_2 = 9\varepsilon_0$, $\mu_2 = \mu_0$ and $\sigma_2 = 10^{-1}$ S/m, determine the variation of the conduction current density in the earth at a frequency of 1 MHz.

Solution: At $f = 10^6 \,\text{Hz}$

$$\frac{\sigma_2}{\omega \varepsilon_2} = \frac{10^{-1}}{2\pi \times 10^6 (9 \times 10^{-9}/36\pi)} = 2 \times 10^2 \gg 1$$

which classifies the material as a very good conductor.

On either side of the interface, the total electric field is equal to

$$\mathbf{E}^{\text{total}}|_{z=0} = \hat{\mathbf{a}}_x \times 10^{-3} |1 + \Gamma^b|$$

where

$$\Gamma^b = \frac{\eta_2 - \eta_1}{\eta_2 + \eta_1} = \frac{\eta_2 - \eta_0}{\eta_2 + \eta_0}$$

$$\eta_2 \simeq \sqrt{\frac{\omega\mu}{2\sigma}} (1+j) = \sqrt{\frac{2\pi \times 10^6 (4\pi \times 10^{-7})}{2 \times 10^{-1}}} (1+j) = 2\pi (1+j)$$

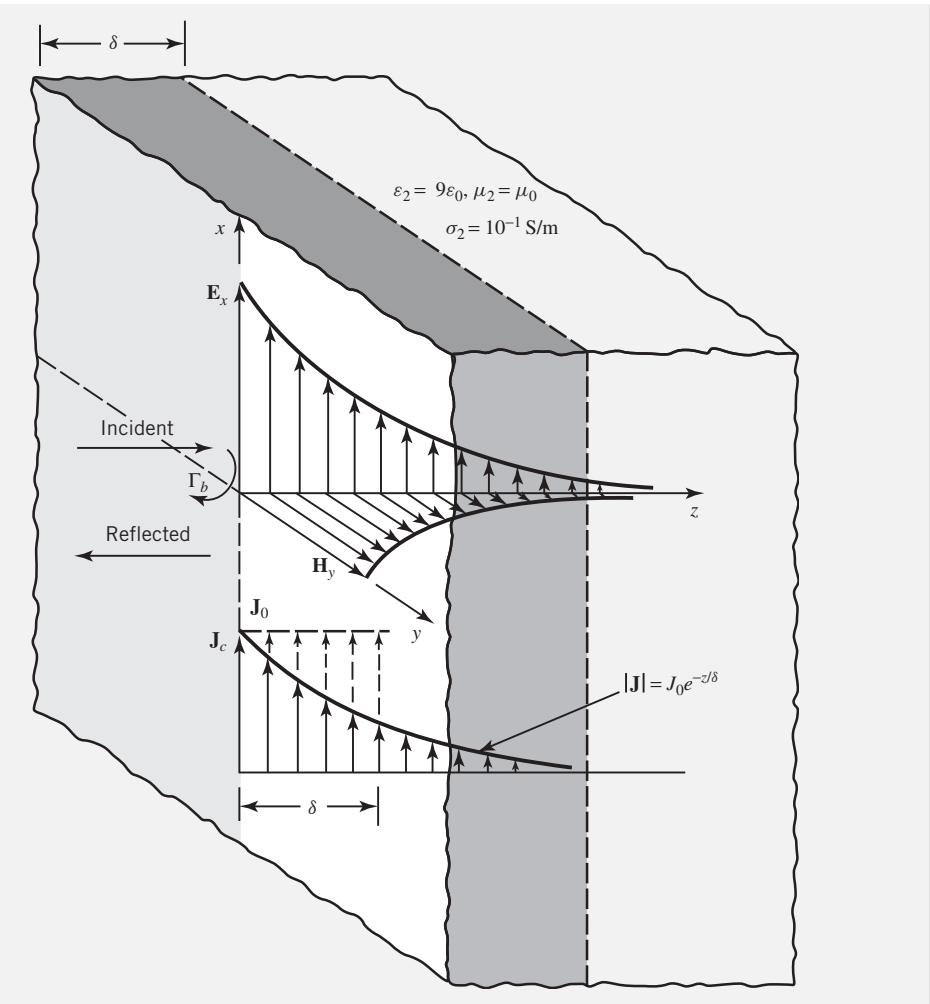


Figure 5-9 Electric and magnetic field intensities, and electric current density distributions in a lossy earth.

Thus

$$\Gamma^b = \frac{2\pi (1+j) - 377}{2\pi (1+j) + 377} = \frac{-370.72 + j2\pi}{383.28 + j2\pi}$$
$$= \frac{370.77 / 179.04^{\circ}}{383.33 / 0.94^{\circ}} = 0.967 / 178.1^{\circ}$$

and

$$\begin{aligned} \mathbf{E}^{\text{total}}|_{z=0} &= \hat{\mathbf{a}}_x \times 10^{-3} |1 + 0.967 / 178.1^{\circ}| \\ &= \hat{\mathbf{a}}_x \times 10^{-3} |0.0335 + j0.0321| = \hat{\mathbf{a}}_x (4.64 \times 10^{-5}) \end{aligned}$$

The conduction current density at the surface of the earth is equal to

$$\mathbf{J}_c|_{z=0} = \hat{\mathbf{a}}_x J_0 = \hat{\mathbf{a}}_x \sigma E^{\text{total}}|_{z=0} = \hat{\mathbf{a}}_x \times 10^{-1} (4.64 \times 10^{-5})$$
$$= \hat{\mathbf{a}}_x (4.64 \times 10^{-6})$$

or

$$J_0 = 4.64 \,\mu\text{A/m}^2$$

The magnitude of the current density varies inside the earth as

$$|J_c| = J_0|e^{-\alpha_2 z}e^{-j\beta_2 z}| = J_0e^{-\alpha_2 z} = J_0e^{-z/\delta_2}$$

where

$$\delta_2 = \text{skin depth} = \sqrt{\frac{2}{\omega \mu_2 \sigma_2}} = \sqrt{\frac{2}{2\pi \times 10^6 (4\pi \times 10^{-7}) \times 10^{-1}}}$$

$$= \frac{10}{2\pi} = 1.5915 \,\text{m}$$

The magnitude variations of the current density inside the earth are shown in Figure 5-9 and they exhibit an exponential decay. At one skin depth ($z = \delta_2 = 1.5915 \,\text{m}$), the current density has been reduced to

$$|\mathbf{J}_c|_{z=\delta_2} = J_0 e^{-1} = 0.3679 J_0 = 0.3679 (4.64 \times 10^{-6}) = 1.707 \,\mu\text{A/m}^2$$

Therefore, at one skin depth the current is reduced to 36.79% of its value at the surface. If the area under the current density curve is found, it is shown to be equal to

$$J_s = \int_0^\infty |J_c| dz = \int_0^\infty J_0 e^{-z/\delta_2} dz = -\delta_2 J_0 e^{-z/\delta_2} \Big|_0^\infty = \delta_2 J_0$$

The same answer can be obtained by assuming that the current density maintains a constant surface value J_0 to a depth equal to the skin depth and equal to zero thereafter, as shown by the dashed curve in Figure 5-9.

The area under the curve can then be interpreted as the total current density J_s (A/m) per unit width in the y direction. It can be obtained by finding the area formed by maintaining constant surface current density J_0 (A/m²) through a depth equal to the skin depth.

5.4.2 Oblique Incidence: Dielectric-Conductor Interface

Let us assume that a uniform plane wave is obliquely incident upon a planar interface where medium 1 is a perfect dielectric and medium 2 is lossy, as shown in Figure 5-10 [3]. For either the perpendicular or parallel polarization, the transmitted electric field into medium 2 can be written, using modified forms of either (5-12a) or (5-22a), as

$$\mathbf{E}^{t} = \mathbf{E}_{2} \exp \left[-\gamma_{2} (x \sin \theta_{t} + z \cos \theta_{t}) \right] = \mathbf{E}_{2} \exp \left[-(\alpha_{2} + j \beta_{2}) (x \sin \theta_{t} + z \cos \theta_{t}) \right]$$
 (5-53)

It can be shown that for lossy media, Snell's law of refraction can be written as

$$\gamma_1 \sin \theta_i = \gamma_2 \sin \theta_t \tag{5-54}$$

Therefore, for the geometry of Figure 5-10,

$$\sin \theta_t = \frac{\gamma_1}{\gamma_2} \sin \theta_i = \frac{j \beta_1}{\alpha_2 + i \beta_2} \sin \theta_i \tag{5-55a}$$

and

$$\cos \theta_t = \sqrt{1 - \sin^2 \theta_t} = \sqrt{1 - \left(\frac{j\beta_1}{\alpha_2 + i\beta_2}\right)^2 \sin^2 \theta_i} = se^{j\zeta} = s(\cos \zeta + j\sin \zeta)$$
 (5-55b)

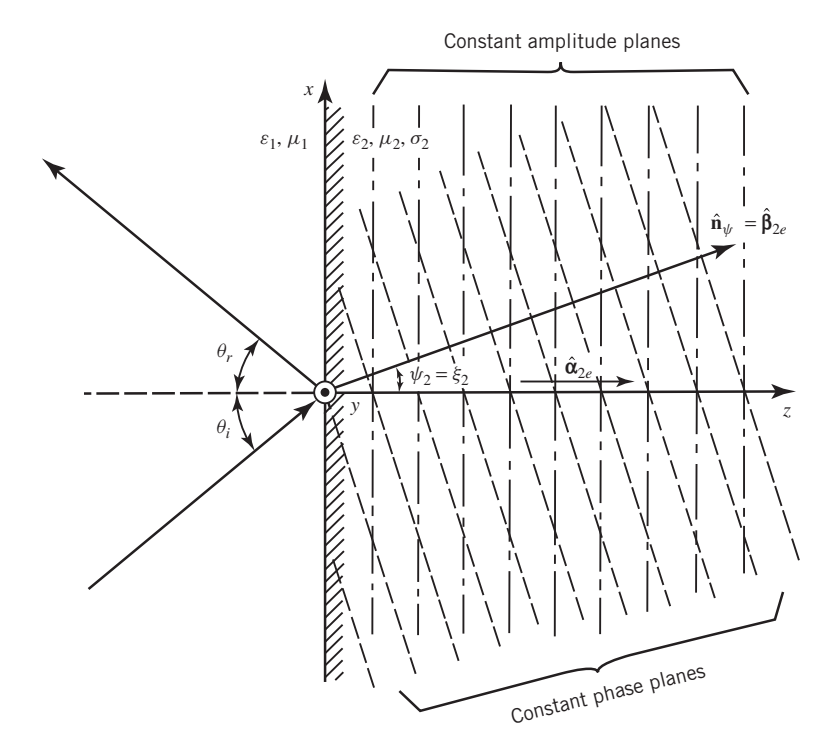


Figure 5-10 Oblique wave incidence upon a dielectric-conductor interface.

Using (5-55a) and (5-55b) we can write (5-53) as

$$\mathbf{E}^{t} = \mathbf{E}_{2} \exp \left\{ -(\alpha_{2} + j\beta_{2}) \left[x \frac{j\beta_{1}}{\alpha_{2} + j\beta_{2}} \sin \theta_{i} + zs(\cos \zeta + j\sin \zeta) \right] \right\}$$
 (5-56)

which reduces to

$$\mathbf{E}^{t} = \mathbf{E}_{2} \exp\left[-zs(\alpha_{2}\cos\zeta - \beta_{2}\sin\zeta)\right]$$

$$\times \exp\left\{-j\left[\beta_{1}x\sin\theta_{1} + zs(\alpha_{2}\sin\zeta + \beta_{2}\cos\zeta)\right]\right\}$$

$$\mathbf{E}^{t} = \mathbf{E}_{2}e^{-zp}\exp\left[-j\left(\beta_{1}x\sin\theta_{i} + zq\right)\right]$$
(5-57)

where

$$p = s(\alpha_2 \cos \zeta - \beta_2 \sin \zeta) = \alpha_{2e}$$
 (5-57a)

$$q = s(\alpha_2 \sin \zeta + \beta_2 \cos \zeta) \tag{5-57b}$$

It is apparent that (5-57) represents a nonuniform wave.

The instantaneous field of (5-57) can be written, assuming E_2 is real, as

$$\mathbf{\mathscr{E}}^{t} = \operatorname{Re}(\mathbf{E}^{t}e^{j\omega t}) = \mathbf{E}_{2}e^{-zp}\operatorname{Re}\left(\exp\left\{j\left[\omega t - (\beta_{1}x\sin\theta_{i} + zq)\right]\right\}\right)$$

$$\mathbf{\mathscr{E}}^{t} = \mathbf{E}_{2}e^{-zp}\cos\left[\omega t - (\beta_{1}x\sin\theta_{i} + zq)\right]$$
(5-58)

The constant amplitude planes (z = constant) of (5-58) are parallel to the interface, and they are shown dashed-dotted in Figure 5-10. The constant phase planes $\left[\omega t - (kx\sin\theta_i + zq) = \text{constant}\right]$ are inclined at an angle ψ_2 that is no longer θ_t , and they are indicated by the dashed lines in Figure 5-10.

To determine the constant phase we write the argument of the exponential or of the cosine function in (5-58) as

$$\omega t - (\beta_1 x \sin \theta_i + zq) = \omega t - \sqrt{(\beta_1 \sin \theta_i)^2 + q^2}$$

$$\times \left[\frac{(\beta_1 \sin \theta_i) x}{\sqrt{(\beta_1 \sin \theta_i)^2 + q^2}} + \frac{qz}{\sqrt{(\beta_1 \sin \theta_i)^2 + q^2}} \right]$$
(5-59)

If we define an angle ψ_2 such that

$$u = \beta_1 \sin \theta_i \tag{5-60a}$$

$$\sin \psi_2 = \frac{\beta_1 \sin \theta_i}{\sqrt{(\beta_1 \sin \theta_i)^2 + q^2}} = \frac{u}{\sqrt{u^2 + q^2}}$$
 (5-60b)

$$\cos \psi_2 = \frac{q}{\sqrt{(\beta_1 \sin \theta_i)^2 + q^2}} = \frac{q}{\sqrt{u^2 + q^2}}$$
 (5-60c)

or

$$\psi_2 = \tan^{-1}\left(\frac{\beta_1 \sin \theta_i}{q}\right) = \tan^{-1}\left(\frac{u}{q}\right) \tag{5-60d}$$

we can write (5-59), and in turn (5-58), as

$$\mathbf{\mathcal{E}}^{t} = \mathbf{E}_{2}e^{-zp}\operatorname{Re}\left(\exp\left\{j\left[\omega t - \sqrt{u^{2} + q^{2}}\left(\frac{ux}{\sqrt{u^{2} + q^{2}}} + \frac{qz}{\sqrt{u^{2} + q^{2}}}\right)\right]\right\}\right)$$

$$= \mathbf{E}_{2}e^{-zp}\operatorname{Re}\left(\exp\left\{j\left[\omega t - \beta_{2e}(x\sin\psi_{2} + z\cos\psi_{2})\right]\right\}\right)$$

$$\mathbf{\mathcal{E}}^{t} = \mathbf{E}_{2}e^{-zp}\operatorname{Re}\left(\exp\left\{j\left[\omega t - \beta_{2e}(\hat{\mathbf{n}}_{\psi} \cdot \mathbf{r})\right]\right\}\right)$$
(5-61)

where

$$\hat{\mathbf{n}}_{\psi} = \hat{\mathbf{a}}_{x} \sin \psi_{2} + \hat{\mathbf{a}}_{z} \cos \psi_{2} \tag{5-61a}$$

$$\beta_{2e} = \sqrt{u^2 + q^2} \tag{5-61b}$$

It is apparent from (5-60a) through (5-61a) that

- 1. The true angle of refraction is ψ_2 and not θ_t (θ_t is complex).
- 2. The wave travels along a direction defined by unit vector $\hat{\mathbf{n}}_{\psi}$.
- 3. The constant phase planes are perpendicular to unit vector $\hat{\mathbf{n}}_{\psi}$, and they are shown as dashed lines in Figure 5-10.

The phase velocity of the wave in medium 2 is obtained by setting the exponent of (5-61) to a constant and differentiating it with respect to time. Doing this, we can write the phase velocity v_p of the wave as

$$\omega(1) - \sqrt{u^2 + q^2} \left(\hat{\mathbf{n}}_{\psi} \cdot \frac{d\mathbf{r}}{dt} \right) = 0$$

$$\omega(1) - \sqrt{u^2 + q^2} \left(\hat{\mathbf{n}}_{\psi} \cdot \frac{d\mathbf{r}}{dt} \right) = \omega - \beta_{2e} (\hat{\mathbf{n}}_{\psi} \cdot \mathbf{v}_p) = 0$$
(5-62)

or

$$v_{pr} = \frac{\omega}{\beta_{2e}} = \frac{\omega}{\sqrt{u^2 + q^2}} = \frac{\omega}{\sqrt{(\beta_1 \sin \theta_i)^2 + q^2}}$$
 (5-62a)

It is evident that the phase velocity is a function of the incidence angle θ_i and the constitutive parameters of the two media.

Example 5-8

A plane wave of either perpendicular or parallel polarization traveling in air is obliquely incident upon a planar interface of copper ($\sigma = 5.76 \times 10^7$ S/m). At a frequency of 10 GHz, determine the angle of refraction and reflection coefficients for each of the two polarizations.

Solution: For copper

$$\frac{\sigma_2}{\omega \varepsilon_2} = \frac{5.8 \times 10^7 (36\pi)}{(2\pi \times 10^{10}) \times 10^{-9}} = 1.037 \times 10^8 \gg 1$$

Therefore according to Table 4-1

$$lpha_2 \simeq eta_2 \simeq \sqrt{rac{\omega \mu_2 \sigma_2}{2}}$$

Using (5-55a)

$$\sin \theta_t = \frac{j\beta_1}{\alpha_2 + j\beta_2} \sin \theta_i \simeq \frac{j\beta_1}{\sqrt{\frac{\omega\mu_2\sigma_2}{2}}(1+j)} \sin \theta_t \stackrel{\sigma_2 \gg 1}{\simeq} 0 \Rightarrow \theta_i \simeq 0$$

Therefore (5-55b), (5-57a), and (5-57b) reduce to

$$\cos \theta_t = 1 = se^{j\zeta} \Rightarrow s = 1 \qquad \zeta = 0$$

$$p = s(\alpha_2 \cos \zeta - \beta_2 \sin \zeta) \simeq \alpha_2 = \sqrt{\frac{\omega \mu_2 \sigma_2}{2}}$$

$$q = s(\alpha_2 \sin \zeta + \beta_2 \cos \zeta) \simeq \beta_2 = \sqrt{\frac{\omega \mu_2 \sigma_2}{2}}$$

Using (5-60d), the true angle of refraction is

$$\psi_2 = \tan^{-1}\left(\frac{u}{q}\right) \simeq \tan^{-1}\left(\frac{\beta_1 \sin \theta_i}{\beta_2}\right) = \tan^{-1}\left(\frac{\omega\sqrt{\mu_0\varepsilon_0}}{\sqrt{\frac{\omega\mu_0\sigma_2}{2}}}\sin \theta_i\right)$$

$$= \tan^{-1}\left(\sqrt{\frac{2\omega\varepsilon_0}{\sigma_2}}\sin \theta_i\right) \leq \tan^{-1}\left(\sqrt{\frac{2\omega\varepsilon_0}{\sigma_2}}\right) = \tan^{-1}(0.139 \times 10^{-3})$$

$$\psi_2 = \tan^{-1}(0.139 \times 10^{-3}\sin \theta_i) < 0.139 \times 10^{-3}\operatorname{rad} = (7.96 \times 10^{-3})^{\circ}$$

Using (5-17a) and (5-24c), the reflection coefficients for perpendicular and parallel polarizations reduce to

$$\begin{split} \Gamma^b_{\perp} &= \frac{\eta_2 \cos \theta_i - \eta_1 \cos \theta_t}{\eta_2 \cos \theta_i + \eta_1 \cos \theta_t} \simeq \frac{\eta_2 \cos \theta_i - \eta_1}{\eta_2 \cos \theta_i + \eta_1} = \frac{\cos \theta_i - \eta_1/\eta_2}{\cos \theta_i + \eta_1/\eta_2} \\ \Gamma^b_{\parallel} &= \frac{-\eta_1 \cos \theta_i + \eta_2 \cos \theta_t}{\eta_1 \cos \theta_i + \eta_2 \cos \theta_t} \simeq \frac{-\eta_1 \cos \theta_i + \eta_2}{\eta_1 \cos \theta_i + \eta_2} = \frac{-\cos \theta_i + \eta_2/\eta_1}{\cos \theta_i + \eta_2/\eta_1} \end{split}$$

Since

$$\frac{\eta_1}{\eta_2} = \frac{\sqrt{\frac{\mu_1}{\varepsilon_1}}}{\sqrt{\frac{j\omega\mu_2}{\sigma_2 + j\omega\varepsilon_2}}} \simeq \frac{\sqrt{\frac{\mu_0}{\varepsilon_0}}}{\sqrt{\frac{j\omega\mu_0}{\sigma_2}}} = \sqrt{\frac{\sigma_2}{j\omega\varepsilon_0}}$$

$$\frac{\eta_1}{\eta_2} \simeq 1.02 \times 10^4 e^{-j\pi/4} \gg 1 \ge \cos \theta_i$$

Then

$$\Gamma_{\perp}^{b} \simeq \frac{\cos \theta_{i} - \eta_{1}/\eta_{2}}{\cos \theta_{i} + \eta_{1}/\eta_{2}} \simeq -1$$

$$\Gamma_{\parallel}^{b} \simeq \frac{-\cos \theta_{i} + \eta_{2}/\eta_{1}}{\cos \theta_{i} + \eta_{2}/\eta_{1}} \simeq -1$$

Thus for a very good conductor, such as copper, the angle of refraction approaches zero and the magnitude of the reflection coefficients for perpendicular and parallel polarizations approach unity, and they are all essentially independent of the angle of incidence. The same will be true for all other good conductors.

5.4.3 Oblique Incidence: Conductor-Conductor Interface

In Section 5.3.4 it was shown that when a uniform plane wave is incident upon a dielectric-dielectric planar interface at an incidence angle θ_i equal to or greater than the critical angle θ_c , the transmitted wave produced into medium 2 is a nonuniform plane wave. For this plane wave, the constant amplitude planes (which are perpendicular to the α_{2_e} vector) of Figure 5-7 are perpendicular to the constant phase planes (which are perpendicular to the β_{2_e} vector), or the angle ξ_2 between the α_{2_e} and β_{2_e} vectors is 90°.

In Section 5.4.2 it was demonstrated that a uniform plane wave traveling in a lossless medium and obliquely incident upon a lossy medium also produces a nonuniform plane wave where the angle ξ_2 between the α_{2e} and β_{2e} vectors in Figure 5-10 is greater than 0° but less than 90°. In fact, for a very good conductor the angle ξ_2 between α_{2e} and β_{2e} is almost zero [for copper with $\sigma = 5.76 \times 10^7$ S/m, $\xi_2 \leq (8 \times 10^{-3})^\circ$]. As the conducting medium becomes less lossy, the angle ξ_2 increases and in the limit it approaches 90° for a lossless medium. In fact for all lossless media, the angle between the effective attenuation constant α_{2e} and phase constant β_{2e} should always be 90°, with reactive power flowing along α_{2e} and positive real power along β_{2e} [4]. This is necessary since there are no real losses associated with the wave propagation along β_{2e} . This was well illustrated in Section 5.3.4 for the nonuniform wave produced in a lossless medium when the incidence angle was equal to or greater than the critical angle.

It is very interesting to investigate the field characteristics of uniform or nonuniform plane waves that are obliquely incident upon interfaces comprised of lossy-lossy interfaces. These types of waves have been examined [5–6], but, because of the general complexity of the formulations, they will not be repeated here. The reader is referred to the literature. An excellent discussion of uniform and nonuniform plane waves propagating in lossless and lossy media and associated interfaces is found in Chapters 7 and 8 of [4].

5.5 REFLECTION AND TRANSMISSION OF MULTIPLE INTERFACES

Many applications require dielectric interfaces that exhibit specific characteristics as a function of frequency. Accomplishing this often requires multiple interfaces. The objective of this section is to analyze the characteristics of multiple layer interfaces. To reduce the complexity of the problem, we will consider only normal incidence and restrict most of our attention to lossless media. A general formulation for lossy media will also be stated.

5.5.1 Reflection Coefficient of a Single Slab Layer

Section 5.2 showed that for normal incidence the reflection coefficient Γ^b at the boundary of a single planar interface is given by (5-4a) or

$$\Gamma^b = \frac{\eta_2 - \eta_1}{\eta_2 + \eta_1} \tag{5-63}$$

and at a distance $z = -\ell$ from the boundary it is given by (5-5a) or

$$\Gamma_{\rm in}(z = -\ell) = \Gamma^b e^{-j2\beta_1 \ell} \tag{5-64}$$

Just to the right of the boundary the input impedance in the +z direction is equal to the intrinsic impedance η_2 of medium 2, that is,

$$Z_{\rm in}(z=0^+) = \eta_2 = \sqrt{\frac{\mu_2}{\varepsilon_2}}$$
 (5-65)

The input impedance at $z = -\ell$ can be found by using the field expressions (5-1a) through (5-2c). By definition $Z_{\text{in}}(z = -\ell)$ is equal to

$$Z_{\text{in}}|_{z=-\ell} = \frac{E^{\text{total}}|_{z=-\ell}}{H^{\text{total}}|_{z=-\ell}}$$
(5-66)

where

$$E^{\text{total}}|_{z=-\ell} = (E^i + E^r)|_{z=-\ell} = E_0 e^{+j\beta_1 \ell} (1 + \Gamma^b e^{-j2\beta_1 \ell}) = E_0 e^{+j\beta_1 \ell} [1 + \Gamma_{\text{in}}(\ell)]$$
(5-66a)

$$H^{\text{total}}|_{z=-\ell} = (H^{i} - H^{r})|_{z=-\ell} = \frac{E_{0}}{\eta_{1}} e^{+j\beta_{1}\ell} (1 - \Gamma^{b} e^{-j2\beta_{1}\ell}) = \frac{E_{0}}{\eta_{1}} e^{+j\beta_{1}\ell} [1 - \Gamma_{\text{in}}(\ell)]$$
(5-66b)

Therefore

$$Z_{\text{in}}|_{z=-\ell} = \eta_1 \left(\frac{1 + \Gamma^b e^{-j2\beta_1 \ell}}{1 - \Gamma^b e^{-j\beta_1 \ell}} \right) = \eta_1 \left(\frac{1 + \Gamma_{\text{in}}(\ell)}{1 - \Gamma_{\text{in}}(\ell)} \right)$$
 (5-66c)

which by using (5-63) can also be written as

$$Z_{\text{in}}|_{z=-\ell} = \eta_1 \left(\frac{1 + \Gamma^b e^{-j2\beta_1 \ell}}{1 - \Gamma^b e^{-j2\beta_1 \ell}} \right) = \eta_1 \left(\frac{1 + \Gamma_{\text{in}}(\ell)}{1 - \Gamma_{\text{in}}(\ell)} \right) = \eta_1 \left(\frac{\eta_2 + j \eta_1 \tan(\beta_1 \ell)}{\eta_1 + j \eta_2 \tan(\beta_1 \ell)} \right)$$
 (5-66d)

Equation 5-66d is analogous to the well-known impedance transfer equation that is widely used in transmission line theory [7].

Using the foregoing procedure for normal wave incidence, we can derive expressions for multiple layer interfaces [8]. Referring to Figure 5-11a the input impedance at $z = 0^+$ is equal to the intrinsic impedance η_3 of medium 3, that is

$$Z_{\rm in}(z=0^+) = \eta_3 \tag{5-67}$$

In turn, the input reflection coefficient at the same interface can be written as

$$\Gamma_{\rm in}(z=0^-) = \frac{Z_{\rm in}(0^+) - \eta_2}{Z_{\rm in}(0^+) + \eta_2} = \frac{\eta_3 - \eta_2}{\eta_3 + \eta_2}$$
 (5-67a)

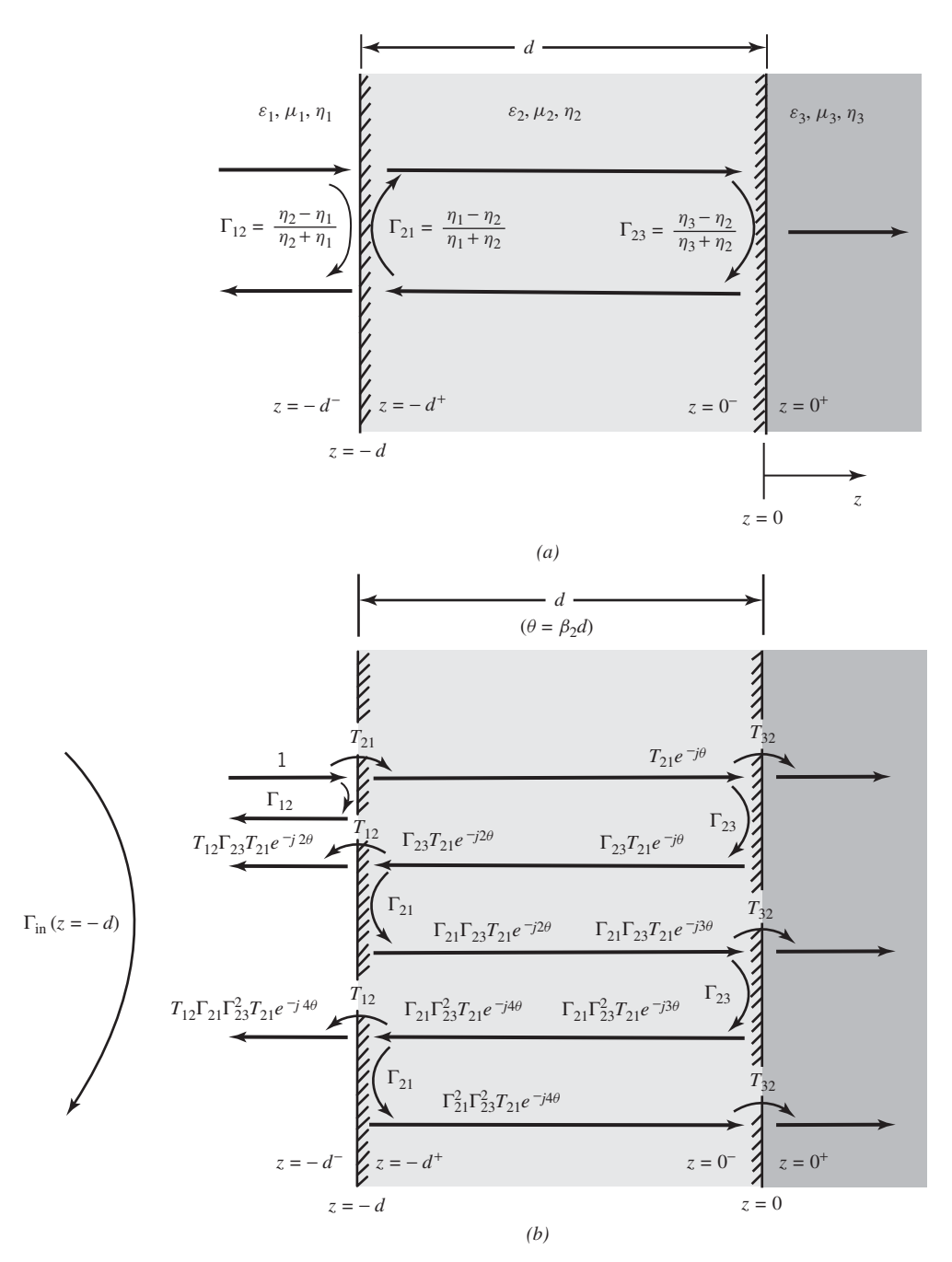


Figure 5-11 Impedances and reflection and transmission coefficients for wave propagation in dielectric slab. (a) Dielectric slab. (b) Reflection and transmission coefficients.

At $z = -d^+$ the input impedance can be written using (5-66d) as

$$Z_{\rm in}(z=-d^+) = \eta_2 \left(\frac{1 + \Gamma_{\rm in}(z=0^-)e^{-j2\beta_2 d}}{1 - \Gamma_{\rm in}(z=0^-)e^{-j2\beta_2 d}} \right) = \eta_2 \left(\frac{(\eta_3 + \eta_2) + (\eta_3 - \eta_2)e^{-j2\beta_2 d}}{(\eta_3 + \eta_2) - (\eta_3 - \eta_2)e^{-j2\beta_2 d}} \right)$$
(5-67b)

and the input reflection coefficient at $z = -d^-$ can be expressed as

$$\Gamma_{\rm in}(z = -d^{-}) = \frac{Z_{\rm in}(z = -d^{+}) - \eta_{1}}{Z_{\rm in}(z = -d^{+}) + \eta_{1}}
= \frac{\eta_{2} \left[(\eta_{3} + \eta_{2}) + (\eta_{3} - \eta_{2})e^{-j2\beta_{2}d} \right] - \eta_{1} \left[(\eta_{3} + \eta_{2}) - (\eta_{3} - \eta_{2})e^{-j2\beta_{2}d} \right]}{\eta_{2} \left[(\eta_{3} + \eta_{2}) + (\eta_{3} - \eta_{2})e^{-j2\beta_{2}d} \right] + \eta_{1} \left[(\eta_{3} + \eta_{2}) - (\eta_{3} - \eta_{2})e^{-j2\beta_{2}d} \right]}$$
(5-67c)

In Figure 5-11a we have defined individual reflection coefficients at each of the boundaries. Here these coefficients are referred to as *intrinsic* reflection coefficients, and they would exist at each boundary if two semi-infinite media form each of the boundaries (neglecting the presence of the other boundaries). Using the intrinsic reflection coefficients defined in Figure 5-11a, the input reflection coefficient of (5-67c) can also be written as

$$\Gamma_{\rm in}(z = -d^{-}) = \frac{\Gamma_{12} + \Gamma_{23}e^{-j2\beta_2 d}}{1 + \Gamma_{12}\Gamma_{23}e^{-j2\beta_2 d}}$$
 (5-67d)

Equation 5-67d can also be derived using the ray-tracing model of Figure 5-11b. At the leading interface of Figure 5-11b, Γ_{12} represents the intrinsic reflection coefficient of the initial reflection and $T_{12}\Gamma_{23}T_{21}e^{-j2\theta}$, etc., are the contributions to the input reflection due to the multiple bounces within the medium 2 slab. The total input reflection coefficient can be written as a geometric series that takes the form

$$\Gamma_{\rm in}(z=-d^-) = \Gamma_{12} + T_{12}\Gamma_{23}T_{21}e^{-j2\theta} + T_{12}\Gamma_{21}\Gamma_{23}^2T_{21}e^{-j4\theta} + \dots$$

$$\Gamma_{\rm in}(z=-d^-) = \Gamma_{12} + T_{12}\Gamma_{23}T_{21}e^{-j2\theta}[1 + \Gamma_{21}\Gamma_{23}e^{-j2\theta} + (\Gamma_{21}\Gamma_{23}e^{-j2\theta})^2 + \dots]$$

$$\Gamma_{\rm in}(z = -d^{-}) = \Gamma_{12} + \frac{T_{12}T_{21}\Gamma_{23}e^{-j2\theta}}{1 - \Gamma_{21}\Gamma_{23}e^{-j2\theta}}$$
 (5-68)

where

$$\theta = \beta_2 d \tag{5-68a}$$

Since according to (5-4a) and (5-4b)

$$\Gamma_{21} = -\Gamma_{12} \tag{5-69a}$$

$$T_{12} = 1 + \Gamma_{21} = 1 - \Gamma_{12} \tag{5-69b}$$

$$T_{21} = 1 + \Gamma_{12} \tag{5-69c}$$

(5-68) can be rewritten and reduced to the form of (5-67d).

If the magnitudes of the intrinsic reflection coefficients $|\Gamma_{12}|$ and $|\Gamma_{23}|$ are low compared to unity, (5-67d) can be approximated by the numerator

$$\Gamma_{\text{in}}(z = -d^{-}) = \frac{\Gamma_{12} + \Gamma_{23}e^{-j2\beta_{2}d}}{1 + \Gamma_{12}\Gamma_{23}e^{-j2\beta_{2}d}} \stackrel{|\Gamma_{12}| \ll 1}{\simeq} \Gamma_{12} + \Gamma_{23}e^{-j2\beta_{2}d}$$
(5-70)

The approximate form of (5-70) yields good results if the individual intrinsic reflection coefficients are low. Typically when $|\Gamma_{12}| = |\Gamma_{23}| \le 0.2$, the error of the approximate form of (5-70) is equal to or less than about 4 percent. The approximate form of (5-70) will be very convenient for representing the input reflection coefficient of multiple interfaces (> 2) when the individual intrinsic reflection coefficients at each interface are low compared to unity.

Example 5-9

A uniform plane wave at a frequency of $10\,\text{GHz}$ is incident normally on a dielectric slab of thickness d and bounded on both sides by air. Assume that the dielectric constant of the slab is 2.56.

- 1. Determine the thickness of the slab so that the input reflection coefficient at 10 GHz is zero.
- 2. Plot the magnitude of the reflection coefficient as a function of frequency between $5\,\text{GHz} \le f \le 15\,\text{GHz}$ when the dielectric slab has a thickness of 0.9375 cm.

Solution:

1. For the input reflection coefficient to be equal to zero, the reflection coefficient of (5-70) must be set equal to zero. This can be accomplished if

$$|\Gamma_{12} + \Gamma_{23}e^{-j2\beta_2 d}| = 0$$

Since

$$\Gamma_{23} = -\Gamma_{12} = \frac{\eta_1 - \eta_2}{\eta_1 + \eta_2}$$

then

$$|\Gamma_{12}||1 - e^{-j2\beta_2 d}| = 0 \Rightarrow 2\beta_2 d = 2n\pi$$
 $n = 0, 1, 2, ...$

For nontrivial solutions, the thickness must be

$$d = \frac{n\pi}{\beta_2} = \frac{\eta}{2}\lambda_2 \qquad n = 1, 2, 3, \dots$$

where λ_2 is the wavelength inside the dielectric slab. Thus the thickness of the slab must be an integral number of half wavelengths inside the dielectric. At a frequency of 10 GHz and a dielectric constant of 2.56, the wavelength inside the dielectric is

$$\lambda_2 = \frac{30 \times 10^9}{10 \times 10^9 \sqrt{2.56}} = 1.875 \,\mathrm{cm}$$

2. At a frequency of 5 GHz, the dielectric slab of thickness 0.9375 cm is equal to

$$d = \frac{0.9375\sqrt{2.56}\lambda_2}{30 \times 10^9/5 \times 10^9} = 0.25\lambda_2 \Rightarrow 2\beta_2 d = \frac{4\pi}{\lambda_2} \left(\frac{\lambda_2}{4}\right) = \pi$$

and at 15 GHz it is equal to

$$d = \frac{0.9375\sqrt{2.56}\lambda_2}{30 \times 10^9/15 \times 10^9} = 0.75\lambda_2 \Rightarrow 2\beta_2 d = \frac{4\pi}{\lambda_2} \left(\frac{3\lambda_2}{4}\right) = 3\pi$$

Since

$$\Gamma_{12} = -\Gamma_{23} = \frac{\eta_2 - \eta_1}{\eta_2 + \eta_1} = \frac{\eta_2 / \eta_1 - 1}{\eta_2 / \eta_1 + 1} = \frac{1 - \sqrt{\varepsilon_r}}{1 + \sqrt{\varepsilon_r}} = -\frac{0.6}{2.6} = -0.231$$

the input reflection coefficient of (5-70), at f=5 and 15 GHz, achieves the maximum magnitude of

$$|\Gamma_{\rm in}(z=-d^-)| = \left| \frac{-0.231 - 0.231}{1 - (-0.231)(0.231)} \right| = \frac{2(0.231)}{1 + (0.231)^2} = 0.438$$

A complete plot of $|\Gamma_{\rm in}(z=-d^-)|$ for $5\,{\rm GHz} \le f \le 15\,{\rm GHz}$ is shown in the Figure 5-12. Using the approximate form of (5-70), the magnitude of the input reflection coefficient is equal to

$$|\Gamma_{\rm in}(z=-d^-)|_{\substack{f=5,\\15\,{\rm GHz}}} \simeq |-0.231-(0.231)| = 0.462$$

The percent error of this is

percent error =
$$\left(\frac{-0.438 + 0.462}{0.438}\right) \times 100 = 5.48$$

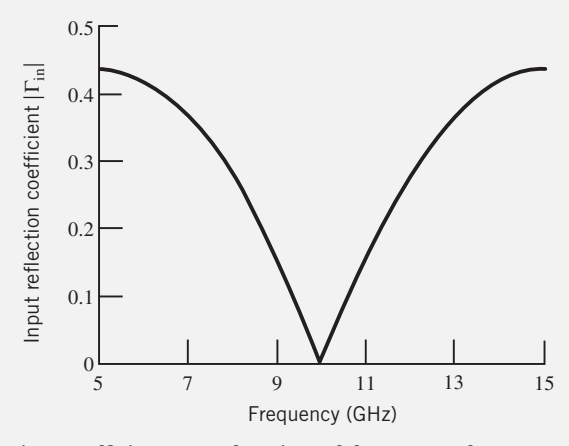


Figure 5-12 Input reflection coefficient, as a function of frequency, for wave propagation through a dielectric slab.

Example 5-10

A uniform plane wave is incident normally upon a dielectric slab whose thickness at $f_0 = 10 \, \text{GHz}$ is $\lambda_{2_0}/4$ where λ_{2_0} is the wavelength in the dielectric slab. The slab is bounded on the left side by air and on the right side by a semi-infinite medium of dielectric constant $\varepsilon_{r3} = 4$.

- 1. Determine the intrinsic impedance η_2 and dielectric constant ε_{r2} of the sandwiched slab so that the input reflection coefficient at $f_0 = 10 \, \text{GHz}$ is zero.
- 2. Plot the magnitude response of the input reflection coefficient for $0 \le f \le 20 \,\text{GHz}$ when the intrinsic impedance and physical thickness of the slab are those found in part 1.
- 3. Using the ray-tracing model of Figure 5-11b, at $f_0 = 10 \,\text{GHz}$ determine the first and next two higher-order terms that contribute to the overall input reflection coefficient. What is the input reflection coefficient using these three terms?

Solution:

1. In order for the input reflection coefficient to vanish, the magnitude of (5-70) must be equal to zero, that is

$$|\Gamma_{12} + \Gamma_{23}e^{-j2\beta_2 d}| = 0$$

Since at $f_0 = 10 \,\text{GHz}$, $d = \lambda_{2_0}/4$, then

$$2\beta_2 d|_{f=10 \text{ GHz}} = 2\left(\frac{2\pi}{\lambda_{2_0}}\right) \left(\frac{\lambda_{2_0}}{4}\right) = \pi$$

Also

$$\Gamma_{12} = \frac{\eta_2 - \eta_1}{\eta_2 + \eta_1}$$

and

$$\Gamma_{23} = \frac{\eta_3 - \eta_2}{\eta_3 + \eta_2}$$

Thus

$$\begin{split} \left| \Gamma_{12} + \Gamma_{23} e^{-j2\beta_2 d} \right|_{\substack{d = \lambda_{2_0}/4 \\ f = 10 \,\text{GHz}}} &= \left| \frac{\eta_2 - \eta_1}{\eta_2 + \eta_1} - \frac{\eta_3 - \eta_2}{\eta_3 + \eta_2} \right| \\ &= \left| \frac{(\eta_2 - \eta_1)(\eta_3 + \eta_2) - (\eta_3 - \eta_2)(\eta_2 + \eta_1)}{(\eta_2 + \eta_1)(\eta_3 + \eta_2)} \right| = 0 \end{split}$$

or

$$2|\eta_2^2 - \eta_1\eta_3| = 0 \Rightarrow \eta_2 = \sqrt{\eta_1\eta_3}$$

Since
$$\eta_1 = \sqrt{\frac{\mu_0}{\varepsilon_0}} = 377$$
 ohms and $\eta_3 = \sqrt{\frac{\mu_0}{4\varepsilon_0}} = \frac{1}{2}\eta_1 = 188.5$ ohms then

$$\eta_2 = \sqrt{\eta_1 \eta_3} = \frac{\eta_1}{\sqrt{2}} = 0.707 \eta_1 = 0.707(377) = 266.5 \text{ ohms}$$

The dielectric constant of the slab must be equal to

$$\varepsilon_{r2}=2$$

whereas the physical thickness of the dielectric is

$$d = \frac{\lambda_{2_0}}{4} = \frac{30 \times 10^9}{4(10 \times 10^9)\sqrt{2}} = 0.53 \,\mathrm{cm}$$

It is apparent then that whenever the dielectric is bounded by two semi-infinite media and its thickness is a quarter of a wavelength in the dielectric, its intrinsic impedance must always be equal to the square root of the product of the intrinsic impedances of the two media on each of its sides in order for the input reflection coefficient to vanish. This is referred to as the quarter-wavelength transformer that is so popular in transmission line design.

2. Since at $f_0 = 10$ GHz, $d = \lambda_{20}/4 = 0.53$ cm, then in the frequency range $0 \le f \le 20$ GHz

$$2\beta_2 d = 2\left(\frac{2\pi}{\lambda_2}\right) \left(\frac{\lambda_{20}}{4}\right) = \pi \left(\frac{f}{f_0}\right)$$

also

$$\Gamma_{12} = \frac{\eta_2 - \eta_1}{\eta_2 + \eta_1} = \frac{\eta_2 / \eta_1 - 1}{\eta_2 / \eta_1 + 1} = \frac{1 - \sqrt{2}}{1 + \sqrt{2}}$$

$$\Gamma_{23} = \frac{\eta_3 - \eta_2}{\eta_3 + \eta_2} = \frac{\eta_3 / \eta_2 - 1}{\eta_3 / \eta_2 + 1} = \frac{1 - \sqrt{2}}{1 + \sqrt{2}} = \Gamma_{12}$$

Therefore, the magnitude of the input reflection coefficient of (5-70) can be written now as

$$|\Gamma_{\rm in}(z=-d^-)| = \left| \frac{\Gamma_{12}(1+e^{-j\pi f/f_0})}{1+(\Gamma_{12})^2 e^{-j\pi f/f_0}} \right|$$

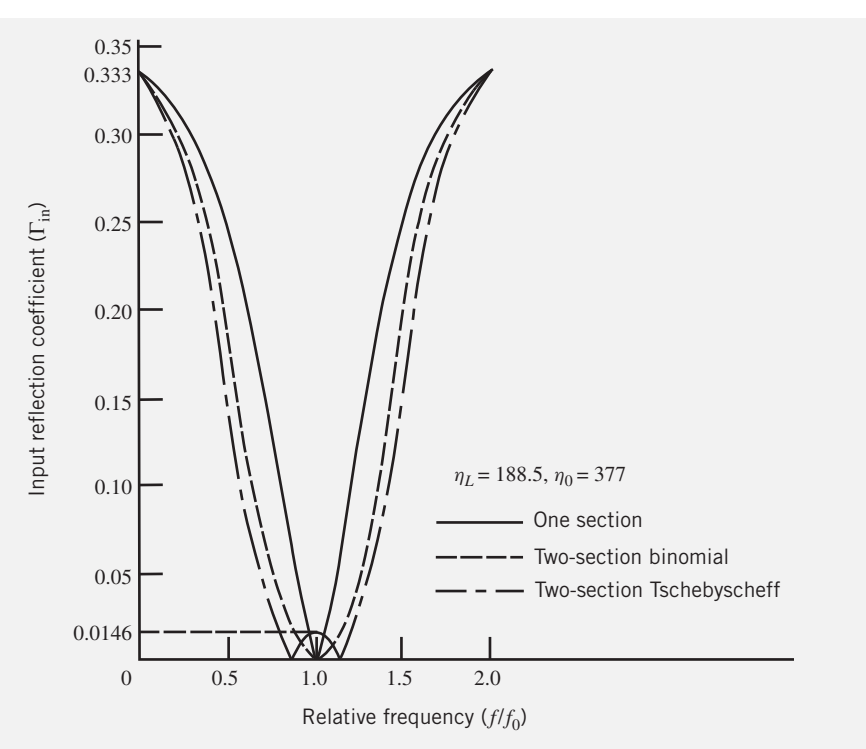


Figure 5-13 Responses of single-section, two-section binomial, and two-section Tschebyscheff quarter-wavelength transformers. (*Source:* C. A. Balanis, *Antenna Theory: Analysis and Design*, 3rd Edition. Copyright © 2005, John Wiley & Sons, Inc. Reprinted by permission of John Wiley & Sons, Inc.)

whose maximum value, which occurs when f = 0 and $2f_0 = 20 \,\text{GHz}$, is approximately equal to

$$|\Gamma_{\text{in}}(z = -d^{-})|_{\text{max}} = \frac{2|\Gamma_{12}|}{(1+|\Gamma_{12}|^{2})} = |\Gamma_{13}| = \left|\frac{\eta_{3} - \eta_{1}}{\eta_{3} + \eta_{1}}\right|$$
$$= 0.333 \simeq 2|\Gamma_{12}| = 0.3431$$

A complete plot of $|\Gamma_{\rm in}(z=-d^-)|_{d=\lambda_2/4}$ when $0 \le f \le 20$ GHz is shown in the Figure 5-13.

It is interesting to note that the magnitude of the input reflection coefficient monotonically decreases from f = 0 to f_0 , and it monotonically increases from f_0 to $2f_0$. It can also be noted that the bandwidth of the response curve near f_0 is very small, and any deviations of the frequency from f_0 will cause the reflection coefficient to rise sharply.

3. According to Figure 5-11b, the first-order term of the input reflection coefficient is

$$\Gamma_{12} = \frac{\eta_2 - \eta_1}{\eta_2 + \eta_1} = \frac{266.5 - 377}{266.5 + 377} = -0.1717$$

The next two higher terms are equal to

$$\begin{split} T_{12}\Gamma_{23}T_{21}e^{-j2\beta_2d} &= \frac{2\eta_1}{\eta_1 + \eta_2} \left(\frac{\eta_3 - \eta_2}{\eta_3 + \eta_2}\right) \left(\frac{2\eta_2}{\eta_1 + \eta_2}\right) e^{-j\pi} \\ &= -\frac{2(377)}{377 + 266.5} \left(\frac{188.5 - 266.5}{188.5 + 266.5}\right) \frac{2(266.5)}{377 + 266.5} = +0.1664 \\ T_{12}\Gamma_{21}\Gamma_{23}^2T_{21}e^{-j4\beta_2d} &= \frac{2\eta_1}{\eta_1 + \eta_2} \left(\frac{\eta_1 - \eta_2}{\eta_1 + \eta_2}\right) \left(\frac{\eta_3 - \eta_2}{\eta_3 + \eta_2}\right)^2 \left(\frac{2\eta_2}{\eta_1 + \eta_2}\right) e^{-j2\pi} \end{split}$$

$$\begin{split} T_{12}\Gamma_{21}\Gamma_{23}^2T_{21}e^{-j4\beta_2d} &= \frac{2(337)}{377 + 266.5} \left(\frac{377 - 266.5}{377 + 266.5}\right) \left(\frac{188.5 - 266.5}{188.5 + 266.5}\right)^2 \frac{2(266.5)}{377 + 266.5} \\ &= 0.0049 \\ \Gamma_{\text{in}} &\simeq \Gamma_{12} + T_{12}\Gamma_{23}\Gamma_{21}e^{-j2\beta_2d} + T_{12}\Gamma_{21}\Gamma_{23}^2T_{21}e^{-j4\beta_2d} \\ &= -0.1717 + 0.1664 + 0.0049 \\ \Gamma_{\text{in}} &\simeq -4 \times 10^{-4} \simeq 0 \end{split}$$

Thus, the first three terms, or even the first two terms, provide an excellent approximation to the exact value of zero.

The bandwidth of the response curve can be increased by flattening the curve near f_0 . This can be accomplished by increasing the number of layers bounded between the two semi-infinite media. The analysis of such a configuration will be discussed in Section 5.5.2.

If the three media of Figure 5-11 are lossy, then it can be shown that the overall reflection and transmission coefficients can be written as [3]

$$\Gamma_{\rm in} = \frac{E^r}{E^i} = \frac{(1 - Z_{12})(1 + Z_{23}) + (1 + Z_{12})(1 - Z_{23})e^{-2\gamma_2 d}}{(1 + Z_{12})(1 + Z_{23}) + (1 - Z_{12})(1 - Z_{23})e^{-2\gamma_2 d}}$$
(5-71a)

$$T = \frac{E^t}{E_i} = \frac{4}{(1 - Z_{12})(1 - Z_{23})e^{-\gamma_2 d} + (1 + Z_{12})(1 + Z_{23})e^{\gamma_2 d}}$$
(5-71b)

where

$$Z_{ij} = \frac{\mu_i \gamma_j}{\mu_j \gamma_i}$$
 $i, j = 1, 2, 3$ (5-71c)

$$\gamma_k = \pm \sqrt{j \omega \mu_k (\sigma_k + j \omega \varepsilon_k)}$$
 (5-71d)

The preceding equations are valid for lossless, lossy, or any combination of lossless and lossy media.

5.5.2 Reflection Coefficient of Multiple Layers

The results of Example 5-10 indicate that for normal wave incidence the response of a single dielectric layer sandwiched between two semi-infinite media did not exhibit very broad characteristics around the center frequency f_0 , and its overall response was very sensitive to frequency changes. The characteristics of such a response are very similar to the bandstop characteristics of a single section filter or single section quarter-wavelength impedance transformer. To increase the bandwidth of the system under normal wave incidence, multiple layers of dielectric slabs, each with different dielectric constant, must be inserted between the two semi-infinite media. Multiple section dielectric layers can be used to design dielectric filters [9]. Coating radar targets with multilayer slabs can also be used to reduce or enhance their scattering characteristics.

When N layers, each with its own thickness and constitutive parameters, are sandwiched between two semi-infinite media as shown in Figure 5-14, the analysis for the overall reflection and transmission coefficients is quite cumbersome, although it is straightforward. However, an approximate form of the input reflection coefficient for the entire system under normal wave incidence can be obtained by utilizing the approximation first introduced to represent (5-70). With this in mind, the input reflection coefficient under normal wave incidence for the system of

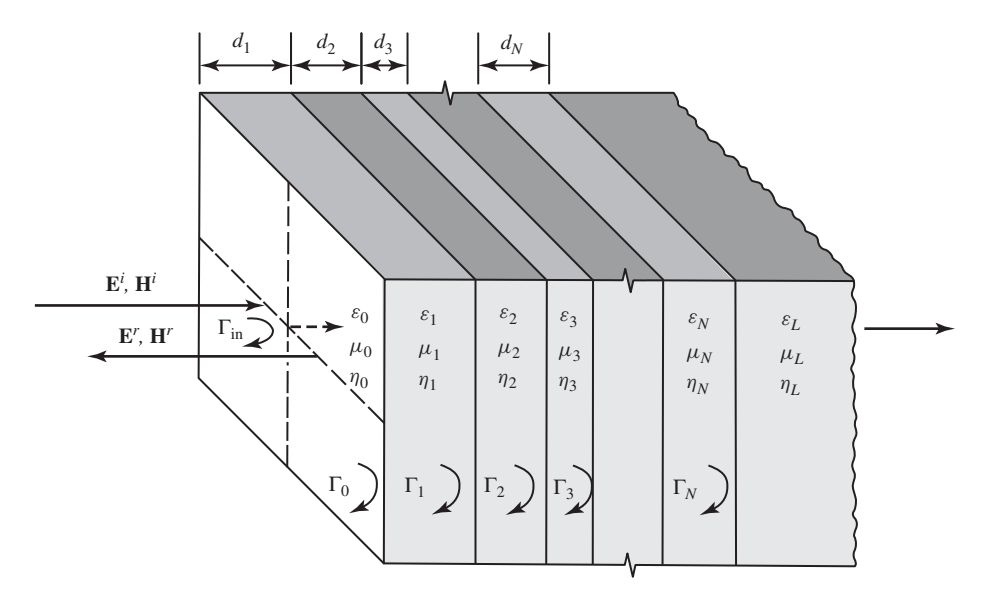


Figure 5-14 Normal wave propagation through N layers sandwiched between two media.

Figure 5-14, referenced at the boundary of the leading interface, can be written approximately as [1, 8]

$$\Gamma_{\text{in}} \simeq \Gamma_0 + \Gamma_1 e^{-j2\beta_1 d_1} + \Gamma_2 e^{-j2(\beta_1 d_1 + \beta_2 d_2)} + \dots + \Gamma_N e^{-j2(\beta_1 d_1 + \beta_2 d_2 + \dots + \beta_N d_N)}$$
(5-72)

where

$$\Gamma_0 = \frac{\eta_1 - \eta_0}{\eta_1 + \eta_0} \tag{5-72a}$$

$$\Gamma_1 = \frac{\eta_2 - \eta_1}{\eta_2 + \eta_1} \tag{5-72b}$$

$$\Gamma_2 = \frac{\eta_3 - \eta_2}{\eta_3 + \eta_2} \tag{5-72c}$$

 $\Gamma_N = \frac{\eta_L - \eta_N}{\eta_L + \eta_N}$ (5-72d)

Expression 5-72 is accurate provided that at each boundary the intrinsic reflection coefficients of (5-72a) through (5-72d) are small in comparison to unity.

A. Quarter-Wavelength Transformer Example 5-10 demonstrated that when a lossless dielectric slab of thickness $\lambda_{2_0}/4$ at a frequency f_0 is sandwiched between two lossless semi-infinite dielectric media, the input reflection coefficient at f_0 is zero provided its intrinsic impedance η_1 is equal to

$$\eta_1 = \sqrt{\eta_0 \eta_L} \tag{5-73}$$

where

 η_1 = intrinsic impedance of dielectric slab.

 η_0 = intrinsic impedance of the input semi-infinite medium.

 η_L = intrinsic impedance of the load semi-infinite medium.

However, as was illustrated in Figure 5-13, the response of the input reflection coefficient as a function of frequency was not very broad near the center frequency f_0 .

Matchings that are less sensitive to frequency variations and that provide broader bandwidths require multiple $\lambda/4$ sections. In fact the number of sections and the intrinsic impedance of each section can be designed so that the reflection coefficient follows, within the desired frequency bandwidth, prescribed variations that are symmetrical about the center frequency. This design assumes that the semi-infinite media and the dielectric slabs are all lossless so that their intrinsic impedances are all real. The discussion that follows parallels that of [1] and [8].

Referring to Figure 5-14, the total input reflection coefficient $\Gamma_{\rm in}$ for an *N*-section quarter-wavelength transformer with $\eta_L > \eta_0$ can be written, using an extension of the approximation used to represent (5-70), as [1, 8]

$$\Gamma_{\text{in}}(f) \simeq \Gamma_0 + \Gamma_1 e^{-j2\theta} + \Gamma_2 e^{-j4\theta} + \ldots + \Gamma_N e^{-j2N\theta} = \sum_{n=0}^{N} \Gamma_n e^{-j2n\theta}$$
 (5-74)

where Γ_n and θ are represented, respectively, by

$$\Gamma_n = \frac{\eta_{n+1} - \eta_n}{\eta_{n+1} + \eta_n} \tag{5-74a}$$

$$\theta = \beta_n d_n = \frac{2\pi}{\lambda_n} \left(\frac{\lambda_{n_0}}{4} \right) = \frac{\pi}{2} \left(\frac{f}{f_0} \right)$$
 (5-74b)

In (5-74) Γ_n represents the reflection coefficient at the junction of two infinite lines that have intrinsic impedances η_n and η_{n+1} , f_0 represents the designed center frequency, and f represents the operating frequency. Equation 5-74 is valid provided the Γ_n 's at each junction are small (the requirements will be met if $\eta_L \simeq \eta_0$). For lossless dielectrics, the η_n 's and Γ_n 's will all be real.

For a symmetrical transformer ($\Gamma_0 = \Gamma_N$, $\Gamma_1 = \Gamma_{N-1}$, etc.), (5-74) reduces to

$$\Gamma_{\rm in}(f) \simeq 2e^{-jN\theta} \left[\Gamma_0 \cos N\theta + \Gamma_1 \cos(N-2)\theta + \Gamma_2 \cos(N-4)\theta + \ldots \right]$$
 (5-75)

The last term in (5-75) should be

$$\Gamma_{[(N-1)/2]}\cos\theta$$
 for $N = \text{odd integer}$ (5-75a)

$$\frac{1}{2}\Gamma_{(N/2)}$$
 for $N = \text{event integer}$ (5-75b)

B. Binomial (Maximally Flat) Design One technique, used to design an N-section $\lambda/4$ transformer, requires that the input reflection coefficient (5-74) have maximally flat passband characteristics. For this method, the junction reflection coefficients (Γ_n 's) are derived using the binomial expansion and we can equate (5-74) to [1, 8]

$$\Gamma_{\text{in}}(f) \simeq \sum_{n=0}^{N} \Gamma_{n} e^{-j2n\theta} = e^{-jN\theta} \frac{\eta_{L} - \eta_{0}}{\eta_{L} + \eta_{0}} \cos^{N}(\theta)$$

$$\simeq 2^{-N} \frac{\eta_{L} - \eta_{0}}{\eta_{L} + \eta_{0}} \sum_{n=0}^{N} C_{n}^{N} e^{-j2n\theta}$$
(5-76)

where

$$C_n^N = \frac{N!}{(N-n)!n!}$$
 $n = 0, 1, 2, ..., N$ (5-76a)

From (5-76)

$$\Gamma_n = 2^{-N} \frac{\eta_L - \eta_0}{\eta_L + \eta_0} C_n^N \tag{5-77}$$

For this type of design, the fractional bandwidth $\Delta f/f_0$ is given by

$$\frac{\Delta f}{f_0} = 2 \frac{f_0 - f_m}{f_0} = 2 \left(1 - \frac{f_m}{f_0} \right) = 2 \left(1 - \frac{2}{\pi} \theta_m \right) \tag{5-78}$$

Since

$$\theta_m = \frac{2\pi}{\lambda_m} \left(\frac{\lambda_0}{4} \right) = \frac{\pi}{2} \left(\frac{f_m}{f_0} \right) \tag{5-79}$$

(5-78) reduces, using (5-76), to

$$\frac{\Delta f}{f_0} = 2 - \frac{4}{\pi} \cos^{-1} \left| \frac{\Gamma_m}{(\eta_L - \eta_0)/(\eta_L + \eta_0)} \right|^{1/N}$$
 (5-80)

where Γ_m is the magnitude of the maximum value of reflection coefficient that can be tolerated within the bandwidth.

The usual design procedure is to specify

- 1. the load intrinsic impedance η_L
- 2. the input intrinsic impedance η_0
- 3. the number of sections N
- 4. the maximum tolerable reflection coefficient Γ_m (or fractional bandwidth $\Delta f/f_0$)

and to find

- 1. the intrinsic impedance of each section
- 2. the fractional bandwidth $\Delta f/f_0$ (or maximum tolerable reflection coefficient Γ_m)

To illustrate the principle, let us consider an example.

Example 5-11

Two lossless dielectric slabs each of thickness $\lambda_0/4$ at a center frequency $f_0 = 10$ GHz are sandwiched between air to the left and a lossless semi-infinite medium of dielectric constant $\varepsilon_L = 4$ to the right. Assuming a fractional bandwidth of 0.375 and a binomial design:

- 1. Determine the intrinsic impedances, dielectric constants, and thicknesses of the sandwiched slabs so that the input reflection coefficient at $f_0 = 10 \,\text{GHz}$ is zero.
- 2. Determine the maximum reflection coefficient and SWR within the fractional bandwidth.
- 3. Plot the response of the input reflection coefficient for $0 \le f \le 20 \,\text{GHz}$ when the intrinsic impedances and physical thicknesses of the slabs are those found in part 1. Compare the response of the two-section binomial design with that of the single section of Example 5-10.

Solution:

1. Using (5-76a) and (5-77)

$$\Gamma_n = 2^{-N} \frac{\eta_L - \eta_0}{\eta_L + \eta_0} C_n^N = 2^{-N} \frac{\eta_L - \eta_0}{\eta_L + \eta_0} \frac{N!}{(N-n)!n!}$$

Since the input dielectric is air and the load dielectric has a dielectric constant $\varepsilon_L = 4$, then

$$\eta_0 = 377$$

$$\eta_L = \sqrt{\frac{\mu_0}{\varepsilon_L \varepsilon_0}} = \frac{377}{2} = 188.5$$

Therefore,

$$n = 0: \Gamma_0 = \frac{\eta_1 - \eta_0}{\eta_1 + \eta_0} = 2^{-2} \left(\frac{188.5 - 377}{188.5 + 377} \right) \frac{2!}{2!0!} = -\frac{1}{12}$$

$$\Rightarrow \eta_1 = \eta_0 \left(\frac{1 - 1/12}{1 + 1/12} \right) = 0.846 \eta_0 = 318.94 \text{ ohms}$$

$$\Rightarrow \varepsilon_{r_1} = 1.40 \qquad d_1 = \frac{\lambda_{1_0}}{4} = 0.634 \text{ cm}$$

$$n = 1: \Gamma_1 = \frac{\eta_2 - \eta_1}{\eta_2 + \eta_1} = 2^{-2} \left(\frac{188.5 - 377}{188.5 + 377} \right) \frac{2!}{1!1!} = -\frac{1}{6}$$

$$\Rightarrow \eta_2 = \eta_1 \left(\frac{1 - 1/6}{1 + 1/6} \right) = 0.714 \eta_1 = 227.72 \text{ ohms}$$

$$\Rightarrow \varepsilon_{r_2} = 2.74 \qquad d_2 = \lambda_{2_0}/4 = 0.453 \text{ cm}$$

2. For a fractional bandwidth of 0.375, the magnitude of the maximum reflection coefficient Γ_m is obtained using (5-80) or

$$\frac{\Delta f}{f_0} = 0.375 = 2 - \frac{4}{\pi} \cos^{-1} \left| \frac{\Gamma_m}{(\eta_L - \eta_0)/(\eta_L + \eta_0)} \right|^{1/2}$$

which for $\eta_L = 188.5$ and $\eta_0 = 377$ leads to

$$\Gamma_{m} = 0.028$$

The maximum standing wave ratio is

$$SWR_m = \frac{1 + \Gamma_m}{1 - \Gamma_m} = \frac{1 + 0.028}{1 - 0.028} = 1.058$$

3. The magnitude of the input reflection coefficient is given by (5-76) as

$$|\Gamma_{\rm in}| = \left| \frac{\eta_L - \eta_0}{\eta_L + \eta_0} \right| \cos^2 \theta = \frac{1}{3} \cos^2 \theta = \frac{1}{3} \cos^2 \left[\frac{\pi}{2} \left(\frac{f}{f_0} \right) \right]$$

which is shown plotted in Figure 5-13 where it is also compared with that of the one- and two-section Tschebyscheff design to be discussed next.

C. Tschebyscheff (Equal-Ripple) Design The reflection coefficient can be made to vary within the bandwidth in an oscillatory manner and have equal-ripple characteristics [10–12]. This can be accomplished by making Γ_{in} vary similarly as a Tschebyscheff (Chebyshev) polynomial. For the Tschebyscheff design, the equation that corresponds to (5-76) is [1, 8]

$$\Gamma_{\rm in}(f) = e^{-jN\theta} \frac{\eta_L - \eta_0}{\eta_L + \eta_0} \frac{T_N(\sec \theta_m \cos \theta)}{T_N(\sec \theta_m)}$$
(5-81)

where $T_N(z)$ is the Tschebyscheff polynomial of order N.

The maximum allowable reflection coefficient occurs at the edges of the passband where $\theta = \theta_m$ and $|T_N(\sec \theta_m \cos \theta)|_{\theta = \theta_m} = 1$. Thus,

$$\rho_m = \left| \frac{\eta_L - \eta_0}{\eta_L + \eta_0} \frac{1}{T_N(\sec \theta_m)} \right| \tag{5-82}$$

or

$$|T_N(\sec \theta_m)| = \left| \frac{1}{\rho_m} \frac{\eta_L - \eta_0}{\eta_L + \eta_0} \right|$$
 (5-82a)

Using (5-82), we can write (5-81) as

$$\Gamma_{in}(f) = e^{-jN\theta} \rho_m T_N \left(\sec \theta_m \cos \theta \right)$$
 (5-83)

and its magnitude as

$$|\Gamma_{in}(f)| = \rho_{in}(f) = |\rho_m T_N(\sec \theta_m \cos \theta)|$$
 (5-83a)

For this type of a design, the fractional bandwidth $\Delta f/f_o$ is also given by (5-78).

To be physical, ρ_m must be smaller than the reflection coefficient when there are no matching layers. Therefore, from (5-82),

$$\rho_m = \left| \frac{\eta_L - \eta_0}{\eta_L + \eta_0} \frac{1}{T_N \left(\sec \theta_m \right)} \right| < \left| \frac{\eta_L - \eta_0}{\eta_L + \eta_0} \right|$$
 (5-84)

or

$$|T_N(\sec \theta_m)| > 1 \tag{5-84a}$$

The Tschebyscheff polynomial can be expressed by either (6-71a) or (6-71b) of [1], or

$$T_m(z) = \cos[m\cos^{-1}(z)] \qquad -1 \le z \le +1$$
 (5-85a)

$$T_m(z) = \cosh[m\cosh^{-1}(z)] \quad z < -1, z > +1$$
 (5-85b)

Since $|T_N(\sec \theta_m)| > 1$, using (5-85b) we can express $T_N(\sec \theta_m)$ as

$$T_N(\sec \theta_m) = \cosh \left[N \cosh^{-1}(\sec \theta_m) \right]$$
 (5-86)

or by using (5-82a), as

$$|T_N(\sec \theta_m)| = \left|\cosh\left[N\cosh^{-1}(\sec \theta_m)\right]\right| = \left|\frac{1}{\rho_m}\frac{\eta_L - \eta_0}{\eta_L + \eta_0}\right|$$
(5-86a)

Thus.

$$\sec \theta_m = \cosh \left[\frac{1}{N} \cosh^{-1} \left(\left| \frac{1}{\rho_m} \frac{\eta_L - \eta_0}{\eta_L + \eta_0} \right| \right) \right]$$
 (5-87)

or

$$\theta_m = \sec^{-1} \left\{ \cosh \left[\frac{1}{N} \cosh^{-1} \left(\left| \frac{1}{\rho_m} \frac{\eta_L - \eta_0}{\eta_L + \eta_0} \right| \right) \right] \right\}$$
 (5-87a)

Using (5-83) we can write the reflection coefficient of (5-75) as

$$\Gamma_{in}(\theta) = 2e^{-jN\theta} \left\{ \rho_0 \cos(N\theta) + \rho_1 \cos[(N-2)\theta] + \ldots \right\}$$

$$= e^{-jN\theta} \rho_m T_N \left(\sec \theta_m \cos \theta \right)$$
(5-88)

For a given N, replace T_N (see $\theta_m \cos \theta$) in (5-88) by its polynomial series of (6-69) of [1] and then match terms. This will allow you to determine the intrinsic reflection coefficients $\rho'_n s$ and subsequently the $\eta'_n s$. The design procedure for the Tschebyscheff design is the same as that of the binomial design, as outlined previously.

The first few Tschebyscheff polynomials can be found in [1, 8]. For $z = \sec \theta_m \cos \theta$, the first three polynomials reduce to

$$T_{1}(\sec \theta_{m} \cos \theta) = \sec \theta_{m} \cos \theta$$

$$T_{2}(\sec \theta_{m} \cos \theta) = 2(\sec \theta_{m} \cos \theta)^{2} - 1 = \sec^{2} \theta_{m} \cos 2\theta + (\sec^{2} \theta_{m} - 1)$$

$$T_{3}(\sec \theta_{m} \cos \theta) = 4(\sec \theta_{m} \cos \theta)^{3} - 3(\sec \theta_{m} \cos \theta)$$

$$= \sec^{3} \theta_{m} \cos 3\theta + 3(\sec^{3} \theta_{m} - \sec \theta_{m}) \cos \theta$$
(5-89)

The remaining details of the analysis are found in [1, 8].

The design of Example 5-11 using a Tschebyscheff transformer is assigned as an exercise to the reader. However, its response is plotted in Figure 5-13 for comparison.

In general, multiple sections (either binomial or Tschebyscheff) provide greater bandwidths than a single section. As the number of sections increases, the bandwidth also increases. The advantage of the binomial design is that the reflection coefficient values within the bandwidth monotonically decreases from both ends toward the center. Thus the values are always smaller than an acceptable and designed value that occurs at the "skirts" of the bandwidth. For the Tschebyscheff design, the reflection coefficient values within the designed bandwidth are equal to or smaller than an acceptable and designed value. The number of times the reflection coefficient reaches the maximum value within the bandwidth is determined by the number of sections. In fact, for an even number of sections the reflection coefficient at the designed center frequency is equal to the maximum allowable value, whereas for an odd number of sections it is zero. For a maximum tolerable reflection coefficient, the *N*-section Tschebyscheff transformer provides a larger bandwidth than a corresponding *N*-section binomial design, or for a given bandwidth the maximum tolerable reflection coefficient is smaller for a Tschebyscheff design.

D. Oblique-Wave Incidence A more general formulation of the reflection and transmission coefficients can be developed by considering the geometry of Figure 5-15 where a uniform plane wave is incident at an oblique angle upon N layers of planar slabs that are bordered on either side by free space. This type of a geometry can be used to approximate the configuration of a radome whose radius of curvature is large in comparison to the wavelength. It can be shown

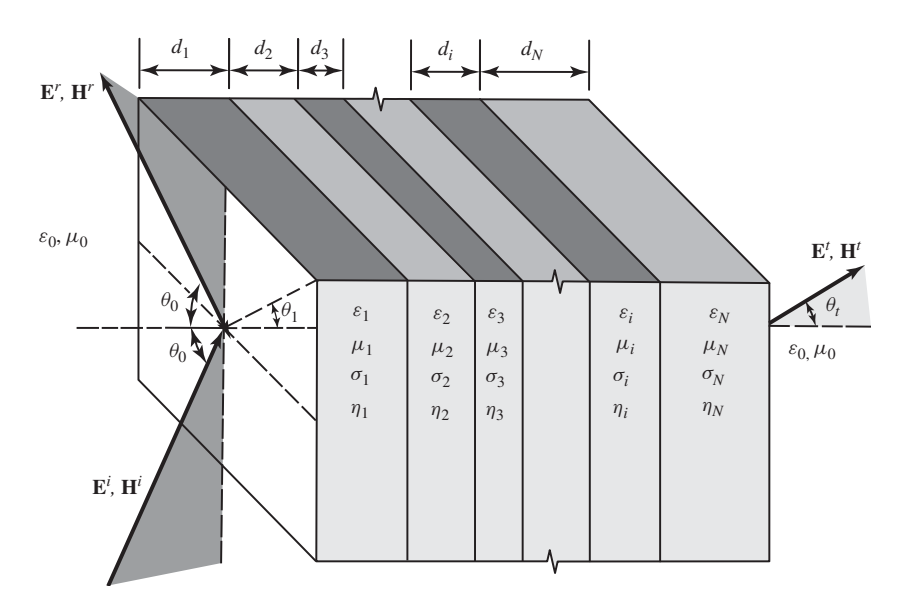


Figure 5-15 Oblique wave propagation through *N* layers of dielectric slabs.

that the overall reflection and transmission coefficients for perpendicular (horizontal) and parallel (vertical) polarizations can be written as [3]

Perpendicular (Horizontal)

$$\Gamma_{\perp} = \frac{E_{\perp}^r}{E_{\perp}^i} = \frac{B_0}{A_0} \tag{5-90a}$$

$$T_{\perp} = \frac{E_{\perp}^{t}}{E_{\perp}^{i}} = \frac{1}{A_{0}}$$
 (5-90b)

Parallel (Vertical)

$$\Gamma_{\parallel} = \frac{E_{\parallel}^{r}}{E_{\parallel}^{i}} = \frac{C_{0}}{D_{0}}$$
 (5-91a)

$$T_{\parallel} = \frac{E_{\parallel}^{I}}{E_{\parallel}^{I}} = \frac{1}{D_{0}} \tag{5-91b}$$

The functions A_0 , B_0 , C_0 , and D_0 are found using the recursive formulas

$$A_{j} = \frac{e^{\psi_{j}}}{2} [A_{j+1}(1 + Y_{j+1}) + B_{j+1}(1 - Y_{j+1})]$$
 (5-92a)

$$B_j = \frac{e^{-\psi_j}}{2} [A_{j+1}(1 - Y_{j+1}) + B_{j+1}(1 + Y_{j+1})]$$
 (5-92b)

$$C_j = \frac{e^{\psi_j}}{2} [C_{j+1}(1 + Z_{j+1}) + D_{j+1}(1 - Z_{j+1})]$$
 (5-92c)

$$D_{j} = \frac{e^{-\psi_{j}}}{2} [C_{j+1}(1 - Z_{j+1}) + D_{j+1}(1 + Z_{j+1})]$$
 (5-92d)

where

$$A_{N+1} = C_{N+1} = 1 (5-92e)$$

$$B_{N+1} = D_{N+1} = 0 (5-92f)$$

$$Y_{j+1} = \frac{\cos \theta_{j+1}}{\cos \theta_j} \sqrt{\frac{\varepsilon_{j+1} (1 - j \tan \delta_{j+1}) \mu_j}{\varepsilon_j (1 - j \tan \delta_j) \mu_{j+1}}}$$
 (5-92g)

$$Z_{j+1} = \frac{\cos \theta_{j+1}}{\cos \theta_j} \sqrt{\frac{\varepsilon_j (1 - j \tan \delta_j) \mu_{j+1}}{\varepsilon_{j+1} (1 - j \tan \delta_{j+1}) \mu_j}}$$
(5-92h)

$$\psi_j = d_j \gamma_j \cos \theta_j \tag{5-92i}$$

$$\gamma_j = \pm \sqrt{j\omega\mu_j(\sigma_j + j\omega\varepsilon_j)}$$
 (5-92j)

$$\theta_i = \text{complex angle of refraction in the } j^{\text{th}} \text{ layer}$$
 (5-92k)

where d_0 is the distance from the leading interface, which serves as the reference for the reflection and transmission coefficients [see (5-5a) and (5-5b)].

5.6 POLARIZATION CHARACTERISTICS ON REFLECTION

When linearly polarized fields are reflected from smooth flat surfaces, the reflected fields maintain their linear polarization characteristics. However, when the reflected surfaces are curved or rough, a linearly polarized component orthogonal to that of the incident field is introduced during

reflection. Therefore, the total field exhibits two components: one with the same polarization as the incident field (main polarization) and one orthogonal to it (cross polarization). During this process, the field is depolarized due to reflection.

Circularly polarized fields in free space incident upon flat surfaces:

- 1. Maintain their circular polarization but reverse their sense of rotation when the reflecting surface is perfectly conducting.
- 2. Are transformed to elliptically polarized fields of opposite sense of rotation when the flat surface is a lossless dielectric and the angle of incidence is smaller than the Brewster angle.

Similarly, elliptically polarized fields in free space upon reflection from flat surfaces

- 1. Maintain their elliptical polarization and magnitude of axial ratio but reverse their sense of rotation when reflected from a perfectly conducting surface.
- 2. Maintain their elliptical polarization but change their axial ratio and sense of rotation when the reflecting surface is a dielectric and the angle of incidence is smaller than the Brewster angle.

To analyze the polarization properties of a wave when it is reflected by a surface, let us assume that an elliptically polarized wave is obliquely incident upon a flat surface of infinite extent as shown in Figure 5-16 [7]. Using the localized coordinate system (x', y, z') of Figure 5-16, the incident electric field components can be written as

$$\mathbf{E}_{\parallel}^{i} = \hat{\mathbf{a}}_{x'} E_{\parallel}^{i} e^{-j\beta^{i} \cdot \mathbf{r}} = \hat{\mathbf{a}}_{x'} E_{\parallel}^{0} e^{-j\beta^{i} \cdot \mathbf{r}}$$
(5-93a)

$$\mathbf{E}_{\perp}^{i} = \hat{\mathbf{a}}_{y} E_{\perp}^{i} e^{-j\beta^{i} \cdot \mathbf{r}} = \hat{\mathbf{a}}_{y} E_{\perp}^{0} e^{-j(\beta^{i} \cdot \mathbf{r} - \phi_{\perp}^{i})}$$
(5-93b)

where E_{\parallel}^0 and E_{\perp}^0 are assumed to be real. For this set of field components, the Poincaré sphere angles (4-58a) through (4-59b) can be written [assuming that the ratio in (4-58a), selected here to demonstrate the procedure, satisfies the angular limits of all the Poincaré sphere angles] as

$$\gamma^{i} = \tan^{-1} \left(\frac{|E_{\perp}^{0}|}{|E_{\parallel}^{0}|} \right) \tag{5-94a}$$

$$\delta^i = \phi^i_{\perp} - \phi^i_{\parallel} = \phi^i_{\perp} \tag{5-94b}$$

$$\varepsilon^i = \cot^{-1}(AR^i) \tag{5-94c}$$

$$\tau^i$$
 = tilt angle of incident wave (5-94d)

where δ^i is the phase angle by which the perpendicular component of the incident field leads the parallel component. It is assumed that (ARi) is positive for left-hand and negative for righthand polarized fields. These two sets of angles are related to each other by (4-60a) through (4-61b), or

$$\cos(2\gamma^{i}) = \cos(2\varepsilon^{i})\cos(2\tau^{i}) \tag{5-95a}$$

$$\tan(\delta^{i}) = \frac{\tan(2\varepsilon^{i})}{\sin(2\tau^{i})}$$
 (5-95b)

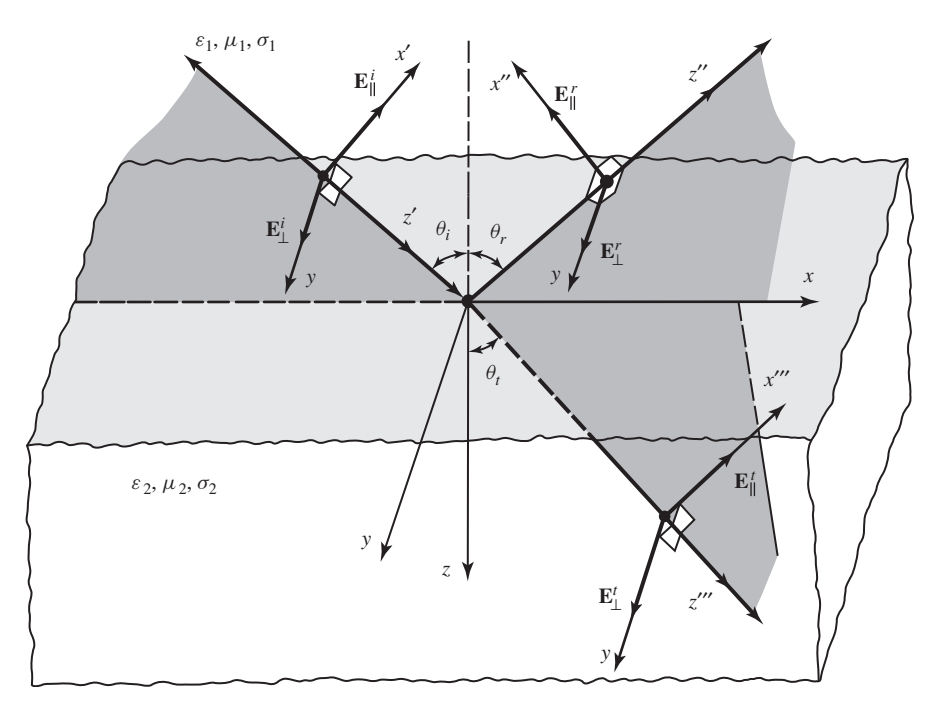


Figure 5-16 Elliptically polarized wave incident on a flat lossy surface.

or

$$\sin(2\varepsilon^{i}) = \sin(2\gamma^{i})\sin(\delta^{i}) \tag{5-95c}$$

$$\tan(2\tau^i) = \tan(2\gamma^i)\cos(\delta^i) \tag{5-95d}$$

In a similar manner, the reflected fields of the elliptically polarized wave can be written according to the localized coordinate system (x'', y, z'') of Figure 5-16 as

$$\mathbf{E}_{\parallel}^{r} = \hat{\mathbf{a}}_{x''} E_{\parallel}^{r} e^{-j\beta^{r} \cdot \mathbf{r}} = -\hat{\mathbf{a}}_{x''} \Gamma_{\parallel}^{b} E_{\parallel}^{0} e^{-j\beta^{r} \cdot \mathbf{r}} = \hat{\mathbf{a}}_{x''} |\Gamma_{\parallel}^{b}| E_{\parallel}^{0} e^{-j(\beta^{r} \cdot \mathbf{r} - \pi - \zeta_{\parallel}^{r})}$$

$$= \hat{\mathbf{a}}_{x''} |\Gamma_{\parallel}^{b}| E_{\parallel}^{0} e^{-j(\beta^{r} \cdot \mathbf{r} - \phi_{\parallel}^{r})} \tag{5-96a}$$

$$\mathbf{E}_{\perp}^{r} = \hat{\mathbf{a}}_{y} E_{\perp}^{r} e^{-j\beta^{r} \cdot \mathbf{r}} = \hat{\mathbf{a}}_{y} \Gamma_{\perp}^{b} E_{\perp}^{0} e^{-j(\beta^{r} \cdot \mathbf{r} - \phi_{\perp}^{i})} = \hat{\mathbf{a}}_{y} |\Gamma_{\perp}^{b}| E_{\perp}^{0} e^{-j(\beta^{r} \cdot \mathbf{r} - \delta^{i} - \zeta_{\perp}^{r})}$$

$$= \hat{\mathbf{a}}_{y} |\Gamma_{\perp}^{b}| E_{\perp}^{0} e^{-j(\beta^{r} \cdot \mathbf{r} - \phi_{\perp}^{r})}$$
(5-96b)

where ζ_{\parallel}^r and ζ_{\perp}^r are the phases of the reflection coefficients for parallel and perpendicular polarizations, respectively. The Poincaré sphere angles γ^r and δ^r of the reflected field can now be written by referring to (5-96a) and (5-96b) as

$$\gamma^r = \tan^{-1}\left(\frac{|\mathbf{E}_{\perp}^r|}{|\mathbf{E}_{\parallel}^r|}\right) = \tan^{-1}\left(\frac{|\Gamma_{\perp}^b|E_{\perp}^0}{|\Gamma_{\parallel}^b|E_{\parallel}^0}\right) = \tan^{-1}\left(\frac{|\Gamma_{\perp}^b|}{|\Gamma_{\parallel}^b|}\tan\gamma^i\right)$$
(5-97a)

$$\delta^{r} = \phi_{\perp}^{r} - \phi_{\parallel}^{r} = (\delta^{i} + \zeta_{\perp}^{r}) - (\pi + \zeta_{\parallel}^{r}) = (\delta^{i} - \pi) + (\zeta_{\perp}^{r} - \zeta_{\parallel}^{r})$$
 (5-97b)

where δ^r is the phase angle by which the perpendicular (y) component leads the parallel (x'') component of the reflected field. Using the angles γ^r and δ^r of (5-97a) and (5-97b), the corresponding Poincaré sphere angles ε^r , τ^r (tilt angle of ellipse) and axial ratio $(AR)^r$ of the reflected field can be found using the relations

$$\sin(2\varepsilon^r) = \sin(2\gamma^r)\sin(\delta^r) \tag{5-98a}$$

$$\tan(2\tau^r) = \tan(2\gamma^r)\cos(\delta^r) \tag{5-98b}$$

$$(AR)^r = \cot(\varepsilon^r) \tag{5-98c}$$

Following a similar procedure, the transmitted fields can be expressed as

$$\mathbf{E}_{\parallel}^{t} = \hat{\mathbf{a}}_{x'''} E_{\parallel}^{t} e^{-j\beta^{t} \cdot \mathbf{r}} = \hat{\mathbf{a}}_{x'''} T_{\parallel}^{b} E_{\parallel}^{0} e^{-j\beta^{t} \cdot \mathbf{r}} = \hat{\mathbf{a}}_{x'''} |T_{\parallel}^{b}| E_{\parallel}^{0} e^{-j(\beta^{t} \cdot \mathbf{r} - \xi_{\parallel}^{t})}$$

$$= \hat{\mathbf{a}}_{x'''} |T_{\parallel}^{b}| E_{\parallel}^{0} e^{-j(\beta^{t} \cdot \mathbf{r} - \phi_{\parallel}^{t})}$$
(5-99a)

$$\mathbf{E}_{\perp}^{t} = \hat{\mathbf{a}}_{y} E_{\perp}^{t} e^{-j\beta^{t} \cdot \mathbf{r}} = \hat{\mathbf{a}}_{y} T_{\perp}^{b} E_{\perp}^{0} e^{-j(\beta^{t} \cdot \mathbf{r} - \phi_{\perp}^{t})} = \hat{\mathbf{a}}_{y} |T_{\perp}^{b}| E_{\perp}^{0} e^{-j(\beta^{t} \cdot \mathbf{r} - \delta^{i} - \xi_{\perp}^{r})}$$

$$= \hat{\mathbf{a}}_{y} |T_{\perp}^{b}| E_{\perp}^{0} e^{-j(\beta^{t} \cdot \mathbf{r} - \phi_{\perp}^{t})}$$
(5-99b)

where ξ_{\parallel}^t , and ξ_{\perp}^t are the phases of the transmission coefficients for parallel and perpendicular polarizations, respectively. The Poincaré sphere angles δ^t and γ^t can now be written by referring to (5-99a) and (5-99b) as

$$\gamma^{t} = \tan^{-1} \left(\frac{|\mathbf{E}_{\perp}^{t}|}{|\mathbf{E}_{\parallel}^{t}|} \right) = \tan^{-1} \left(\frac{|T_{\perp}^{b}|E_{\perp}^{0}}{|T_{\parallel}^{b}|E_{\parallel}^{0}} \right) = \tan^{-1} \left(\frac{|T_{\perp}^{b}|}{|T_{\parallel}^{b}|} \tan \gamma^{i} \right)$$
 (5-100a)

$$\delta^{t} = \phi_{\perp}^{t} - \phi_{\parallel}^{t} = (\delta^{i} + \xi_{\perp}^{t}) - \xi_{\parallel}^{t} = \delta^{i} + (\xi_{\perp}^{t} - \xi_{\parallel}^{t})$$
 (5-100b)

where δ^t is the phase angle by which the perpendicular (y) component of the transmitted field leads the parallel (x''') component of the transmitted field. Using the angles γ^t and δ^t of (5-100a) and (5-100b), the corresponding Poincaré sphere angles ε^t , τ^t (tilt angle of ellipse) and axial ratio $(AR)^t$ of the transmitted field can be found using the relations

$$\sin(2\varepsilon^t) = \sin(2\gamma^t)\sin(\delta^t) \tag{5-101a}$$

$$\tan(2\tau^t) = \tan(2\gamma^t)\cos(\delta^t) \tag{5-101b}$$

$$(AR)^t = \cot(\varepsilon^t) \tag{5-101c}$$

The set of (5-96a) through (5-98c) and (5-99a) through (5-101c) can be used to find, respectively, the polarization of the reflected and transmitted fields once the polarization of the incident fields of (5-93a) through (5-94d) has been stated. A block diagram of the relations between the incident, reflected, and transmitted fields is shown in Figure 5-17. The parallel component of the incident field is taken as the reference for the phase of all of the other components.

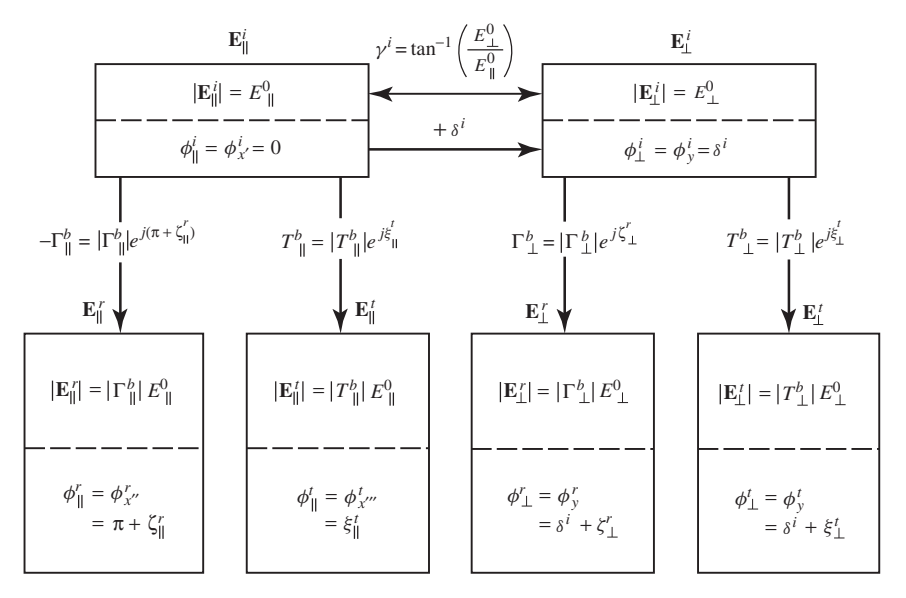


Figure 5-17 Block diagram for polarization analysis of reflected and transmitted waves.

Example 5-12

A left-hand (CCW) circularly polarized field traveling in free space at an angle of $\theta_i = 30^\circ$ is incident on a flat perfect electric conductor of infinite extent. Find the polarization of the reflected wave.

Solution: A circularly polarized wave is made of two orthogonal linearly polarized components with a 90° phase difference between them. Therefore we can assume that these two orthogonal linearly polarized components represent the perpendicular and parallel polarizations. Since the reflecting surface is perfectly conducting ($\eta_2 = 0$), the reflection coefficients of (5-17a) and (5-24c) reduce to

$$\begin{split} \Gamma^b_\perp &= -1 = 1 / \underline{\pi} \Rightarrow |\Gamma^b_\perp| = 1 \quad \zeta^r_\perp = \underline{\pi} \\ \Gamma^b_\parallel &= -1 = 1 / \underline{\pi} \Rightarrow |\Gamma^b_\parallel| = 1 \quad \zeta^r_\parallel = \underline{\pi} \end{split}$$

Since the incident field is left-hand circularly polarized, then according to (5-93a) through (5-94b)

$$\begin{split} E_{\parallel}^{0} &= E_{\perp}^{0} \\ \delta^{i} &= \phi_{\perp}^{i} = \frac{\pi}{2} \\ \gamma^{i} &= \tan^{-1} \left(\frac{E_{\perp}^{0}}{E_{\parallel}^{0}} \right) = \frac{\pi}{4} \Rightarrow \tan \gamma^{i} = 1 \end{split}$$

Thus according to (5-97a) and (5-97b)

$$\gamma^r = \tan^{-1} \left(\frac{|\Gamma_{\perp}^b|}{|\Gamma_{\parallel}^b|} \tan \gamma^i \right) = \frac{\pi}{4}$$
$$\delta^r = \delta^i - \pi + (\zeta_{\perp}^r - \zeta_{\parallel}^r) = \frac{\pi}{2} - \pi + (\pi - \pi) = -\frac{\pi}{2}$$

On the Poincaré sphere of Figure 4-20 the angles $\gamma^r = \pi/4$ and $\delta^r = -\pi/2$ define the south pole, which represents right-hand (CW) circular polarization. Therefore, the reflected field is right-hand (CW) circularly polarized, and it is opposite in rotation to that of the incident field as shown in Figure 5-18a.

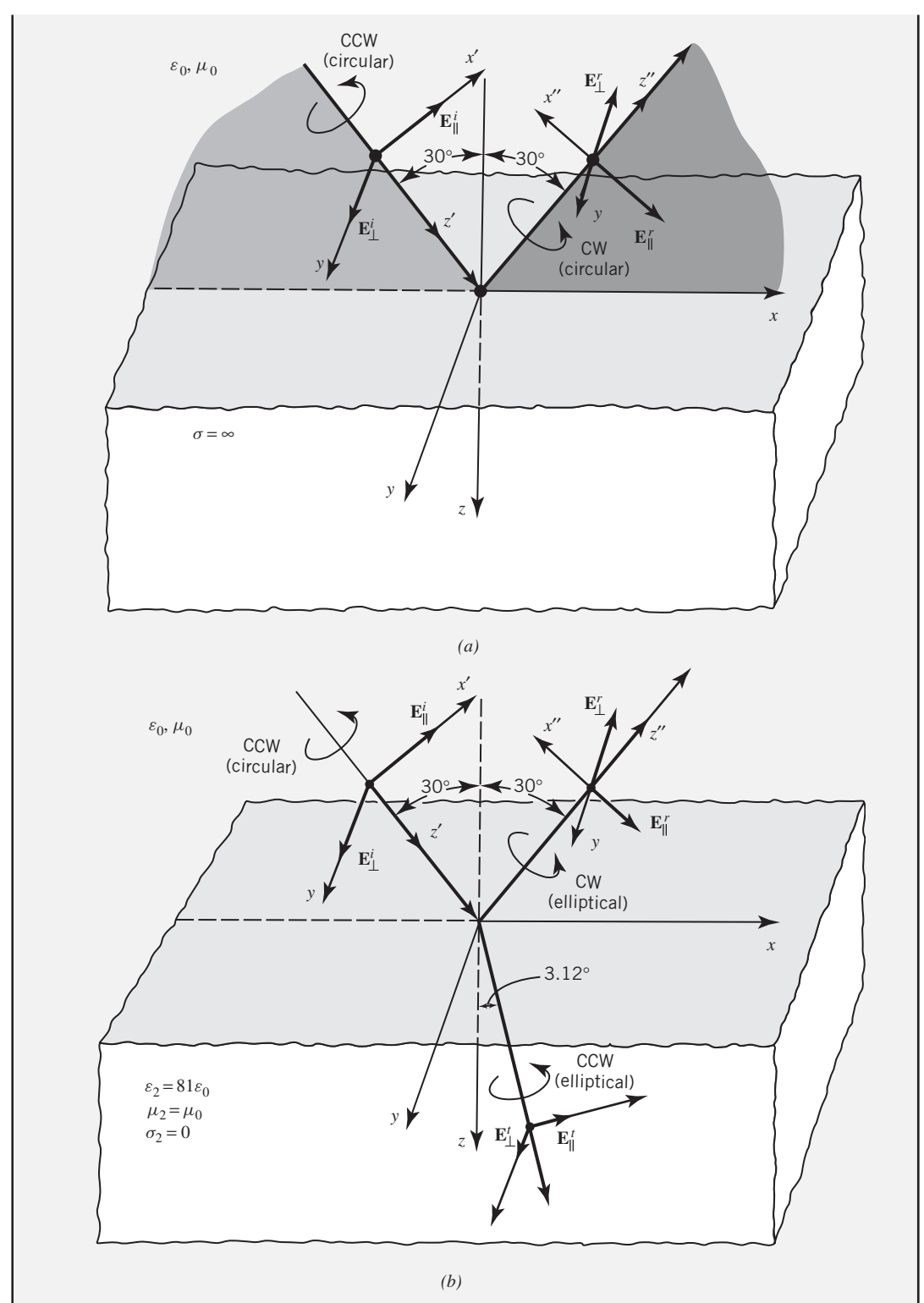


Figure 5-18 Circularly polarized wave incident upon flat surfaces with infinite and zero conductivities. (a) Infinite conductivity. (b) Lossless ocean.

Example 5-13

A left-hand (CCW) circularly polarized field traveling in free space at an angle of $\theta_i = 30^\circ$ is incident on a flat lossless ($\sigma_2 = 0$) ocean ($\varepsilon_2 = 81\varepsilon_0$, $\mu_2 = \mu_0$) of infinite extent. Find the polarization of the reflected and transmitted fields.

Solution: Since the incident field is left-hand circularly polarized, then according to (5-93a) through (5-94b)

$$\begin{split} E_\parallel^0 &= E_\perp^0 \\ \delta^i &= \phi_\perp^i = \frac{\pi}{2} \\ \gamma^i &= \tan^{-1} \left(\frac{E_\perp^0}{E_\parallel^0} \right) = \frac{\pi}{4} \Rightarrow \tan \gamma^i = 1 \end{split}$$

To find the polarization of the reflected field, we proceed as follows. Using (5-18a)

$$\begin{split} \Gamma_{\perp}^{b} &= \frac{\cos(30^{\circ}) - \sqrt{81}\sqrt{1 - \left(\frac{1}{81}\right)\sin^{2}(30^{\circ})}}{\cos(30^{\circ}) + \sqrt{81}\sqrt{1 - \left(\frac{1}{81}\right)\sin^{2}(30^{\circ})}} = \frac{0.866 - 9\sqrt{1 - \frac{1}{81}\left(\frac{1}{4}\right)}}{0.866 + 9\sqrt{1 - \frac{1}{81}\left(\frac{1}{4}\right)}} \\ &= \frac{0.866 - 8.986}{0.866 + 8.986} \\ \Gamma_{\perp}^{b} &= -0.824 \Rightarrow |\Gamma_{\perp}^{b}| = 0.824 \qquad \zeta_{\perp}^{r} = \pi \end{split}$$

Using (5-25a)

$$\begin{split} \Gamma^b_{\parallel} &= \frac{-\cos(30^\circ) + \sqrt{\frac{1}{81}}\sqrt{1 - \left(\frac{1}{81}\right)\sin^2(30^\circ)}}{\cos(30^\circ) + \sqrt{\frac{1}{81}}\sqrt{1 - \left(\frac{1}{81}\right)\sin^2(30^\circ)}} = \frac{-0.866 + \frac{1}{9}\sqrt{1 - \frac{1}{81}\left(\frac{1}{4}\right)}}{0.866 + \frac{1}{9}\sqrt{1 - \frac{1}{81}\left(\frac{1}{4}\right)}} \\ &= \frac{-0.866 + 0.111}{0.866 + 0.111} \\ \Gamma^b_{\parallel} &= -0.773 \Rightarrow |\Gamma^b_{\parallel}| = 0.773 \qquad \zeta^r_{\parallel} = \pi \end{split}$$

According to (5-97a) and (5-97b)

$$\gamma^{r} = \tan^{-1} \left(\frac{|\Gamma_{\perp}^{b}|}{|\Gamma_{\parallel}^{b}|} \tan \gamma^{i} \right) = \tan^{-1} \left(\frac{0.824}{0.773} \right) = 46.83^{\circ} = 0.817 \,\text{rad}$$
$$\delta^{r} = \delta^{i} - \pi + (\zeta_{\perp}^{r} - \zeta_{\parallel}^{r}) = \frac{\pi}{2} - \pi + (\pi - \pi) = -\frac{\pi}{2}$$

Using (5-98a) through (5-98c)

$$2\varepsilon^{r} = \sin^{-1}[\sin(2\gamma^{r})\sin(\delta^{r})]$$

$$= \sin^{-1}\left[\sin(93.66^{\circ})\sin\left(-\frac{\pi}{2}\right)\right] = -86.34^{\circ}$$

$$\Rightarrow \varepsilon^{r} = -43.17^{\circ}$$

$$2\tau^{r} = \tan^{-1}[\tan(2\gamma^{r})\cos(\delta^{r})]$$

$$= \tan^{-1}\left[\tan(93.66^{\circ})\cos\left(-\frac{\pi}{2}\right)\right] = 180^{\circ}$$

$$\Rightarrow \tau^{r} = 90^{\circ}$$

$$(AR)^r = \cot(\varepsilon^r) = \cot(-43.17^\circ) = -1.066$$

On the Poincaré sphere of Figure 4-20 the angles $\gamma^r = 0.817$ and $\delta^r = -\pi/2$ locate a point on the lower hemisphere on the principal xz plane. Therefore the reflected field is right-hand (CW) elliptically polarized, and it has an opposite sense of rotation compared to the left-hand (CCW) circularly polarized incident field as shown in Figure 5-18b. Its axial ratio is -1.066.

To find the polarization of the transmitted field we proceed as follows. Using (5-18b)

$$\begin{split} T_{\perp}^{b} &= \frac{2\cos(30^{\circ})}{\cos(30^{\circ}) + \sqrt{81}\sqrt{1 - \left(\frac{1}{81}\right)\sin^{2}(30^{\circ})}} = \frac{2(0.866)}{0.866 + 8.986} \\ &= 0.1758 \Rightarrow |T_{\perp}^{b}| = 0.1758 \qquad \xi_{\perp}^{t} = 0 \end{split}$$

Using (5-25b)

$$T_{\parallel}^{b} = \frac{2\sqrt{\frac{1}{81}}\cos(30^{\circ})}{\cos(30^{\circ}) + \sqrt{\frac{1}{81}}\sqrt{1 - \left(\frac{1}{81}\right)\sin^{2}(30^{\circ})}} = \frac{2\left(\frac{1}{9}\right)0.866}{0.866 + 0.111}$$
$$= 0.197 \Rightarrow |T_{\parallel}^{b}| = 0.197 \qquad \xi_{\parallel}^{t} = 0$$

According to (5-100a) and (5-100b)

$$\gamma^{t} = \tan^{-1} \left(\frac{|T_{\perp}^{b}|}{|T_{\parallel}^{b}|} \tan \gamma^{i} \right) = \tan^{-1} \left(\frac{0.1758}{0.197} \right) = 41.75^{\circ} = 0.729 \,\text{rad}$$
$$\delta^{t} = \delta^{i} + (\xi_{\perp}^{t} - \xi_{\parallel}^{t}) = \frac{\pi}{2} + (0 - 0) = \frac{\pi}{2}$$

Using (5-101a) through (5-101c)

$$2\varepsilon^{t} = \sin^{-1}[\sin(2\gamma^{t})\sin(\delta^{t})] = \sin^{-1}[\sin(83.5^{\circ})\sin(90^{\circ})] = 83.5^{\circ}$$

$$\Rightarrow \varepsilon^{t} = 41.75^{\circ}$$

$$2\tau^{t} = \tan^{-1}[\tan(2\gamma^{t})\cos(\delta^{t})] = \tan^{-1}[\tan(83.5^{\circ})\cos(90^{\circ})] = 0$$

$$\Rightarrow \tau^{t} = 0^{\circ}$$

$$(AR)^{t} = \cot(\varepsilon^{t}) = \cot(41.75^{\circ}) = 1.12$$

On the Poincaré sphere of Figure 4-20 the angles $\gamma^t = 0.729$ and $\delta^t = \pi/2$ locate a point on the upper hemisphere on the principal xz plane. Therefore the transmitted field is left-hand (CCW) elliptically polarized, and it is of the same sense of rotation as the left-hand (CCW) circularly polarized incident field as shown in Figure 5-18b. Its axial ratio is 1.12.

5.7 METAMATERIALS

The decades of the 1990s and 2000s had renewed interest and excitement into the field of electromagnetics, especially as they relate to the integration of a special type of artificial dielectric materials, coined metamaterials [13–18]. Using a 'broad brush,' the word metamaterials can encompass engineered textured surfaces, artificial impedance surfaces, artificial magnetic conductors, double negative materials, frequency selective surfaces, Photonic Band-Gap (PBG) surfaces, Electromagnetic Band-Gap (EBG) surfaces/structures, and even fractals or chirals. Artificial impedance surfaces are discussed in Section 8.8. In this section we want to focus

more on material structures whose constitutive parameters (permittivity and permeability) are both negative, often referred to as Double Negative (DNG). Artificial magnetic conductors can also be included in the DNG class of materials. It is the class of DNG materials that has captivated the interest and imagination of many leading researchers and practitioners, scientists and engineers, from academia, industry, and government. When electromagnetic waves interact with such materials, they exhibit some very unique and intriguing characteristics and phenomena that can be used, for example, to optimize the performance of antennas, microwave components and circuits, transmission lines, scatterers, and optical devices such as lenses. While the revitalization of metamaterials introduced welcomed renewed interest in materials for electromagnetics, it also brought along some spirited dialogue, which will be referred to in the pages that follow.

The word meta, in metamaterials, is a Greek word that means beyond/after. The term metamaterials was coined in 1999 by Dr. Rodger Walser, of the University of Texas-Austin and Metamaterial, Inc., to present materials that are artificially fabricated so that they have electromagnetic properties that go beyond those found readily in nature. In fact, the word has been used to represent materials that microscopically are intrinsically inhomogeneous and constructed from metallic arrangements that exhibit periodic formations whose period is much smaller than the free-space and/or guided wavelenth. Using Dr. Walser's own words, he defined metamaterials as 'Macroscopic composites having man-made, three-dimensional, periodic cellular architecture designed to produce an optimized combination, not available in nature, of two or more responses to specific excitation' [19]. Because of the very small period, such structures can be treated as homogeneous materials, similarly to materials found in nature, and they can then be represented using bulk constitutive parameters, such as permittivity and permeability. When the period is not small compared to the free-space or guided wavelength, then such materials can be examined using periodic analysis (i.e., the *Floquet Theorem*). Typically the construction of metamaterials is usually performed by embedding inclusions or inhomogeneities in the host medium, as shown in Figure 5-19 [13].

5.7.1 Classification of Materials

In general, materials, using their constitutive parameters ε (permittivity) and μ (permeability) as a reference, can be classified into four categories. They are those that exhibit:

- Negative ε and positive μ ; they are usually coined as **ENG** (epsilon negative) material.
- Positive ε and positive μ ; they are usually coined as **DPS** (double positive) material.

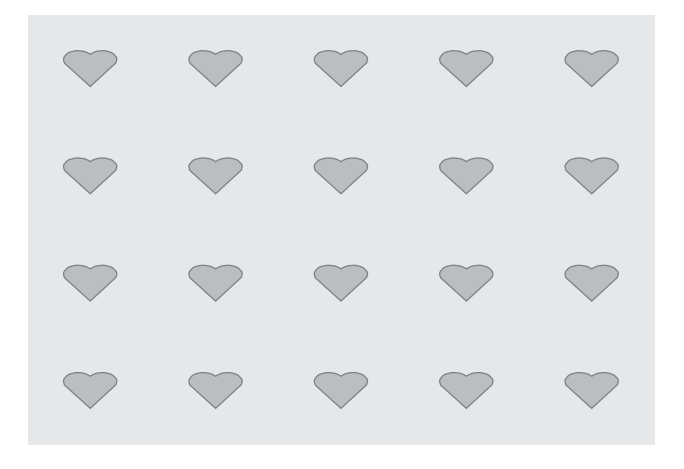


Figure 5-19 Metamaterial representation using embedded periodic inclusions (after [13]).

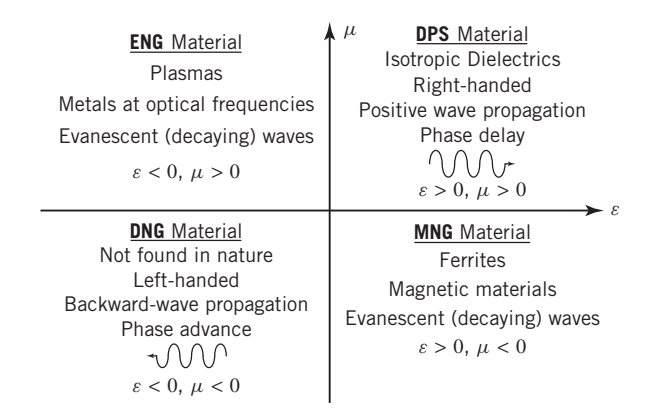


Figure 5-20 Characterization of materials according to the values of their permittivity and permeability (after [13], [17]).

- Negative ε and negative μ ; they are usually coined as **DNG** (double negative) material.
- Positive ε and negative μ ; they are usually coined as MNG (mu negative) material.

These are shown schematically in Figure 5-20.

Of the materials shown in Figure 5-20, the ones that usually are encountered in nature are those of **DPS** (double positive; first quadrant, like dielectrics such as water, glass, plastics, etc.), **ENG** (epsilon negative; second quadrant, like plasmas) and **MNG** (mu negative; fourth quadrant, like magnetic materials). Obviously the one set that is most widely familiar and used in applications is that of **DPS**, although the other two, **ENG** and **MNG**, are used in a wide range of applications.

5.7.2 Double Negative (DNG) Materials

The materials that have recently captured the attention and imagination of electromagnetic engineers and scientists are the **DNG**, which, as indicated, are not found in nature but may be artificially realizable. The **DNG** materials are also referred to as **NRI** (negative refractive index), **NIM** (negative index material), **BW** (backward) media, and left-handed (**LH**) media, to name a few. For clarity and simplicity, we will stay with the **DNG** designation. The **DNG** class has created an intense activity as many have attempted to incorporate material with such characteristics to design, enhance, or increase the performance of lenses, microwave circuits, transmission lines, antennas, phase shifters, broadband power dividers, backward and forward leaky-wave antennas, electrically small ring antennas, cloaking, plasmonic nanowires, photonic crystals, and miniaturization [13–21]. More specifically, using antennas as an example, it has been reported that the integration of materials with radiating elements can increase the radiated power, enhance the gain, and tune the frequency of operation.

While there has been a lot of activity since the recent revival of metamaterials, their introduction has also created some spirited dialogue about the negative index-of-refraction, negative refraction angle, and phase advancement [19–21]. What may have elevated this dialogue to a greater level is that some of the reported results using DNG metamaterials may have been overstated, and lacked verification, interpretation and practical physical realization [22] Appendix C of [23]. However, within the broader definition of metamaterials, there have been metamaterial structures whose performance, when combined with devices and circuits, has been validated not only by simulations but also by careful experimentation. For such structures not only good agreement between simulations and measurements has been found, but also the results have been within limits of physical reality and interpretation. Some of these have been acknowledged for their validity, and they have also often been referred to as engineered textured surfaces, artificial impedance surfaces (AIS), artificial magnetic conductors (AMC), photonic band-gap structures

(PBG), and electromagnetic band-gap structures (EBG). This class of metamaterials is discussed in Section 8.8, and the reader is referred to that section for details and references.

Because of the interest in the electromagnetic community, it is important that the topic of metamaterials be introduced to graduate students, and maybe even to undergraduates, but presented in the proper context. Because of space limitations, only an introductory overview of the subject is included in this book. A succinct chronological sequence of the basic events that led to this immense interest in metamaterials is also presented. The reader is referred to the literature for an in-depth presentation of the topic and its applications.

5.7.3 Historical Perspective

The origins of metamaterials can be traced back to the end of the 19th century, and they are outlined in many publications. Since metamaterials is a rather new designation, it is a branch of artificial dielectrics. In fact, it was indicated in 1898 that Jajadis Chunder Bose may have emulated chiral media by using man-made twisted fibers to rotate the polarization of electromagnetic waves [24]. In 1914, Lindman examined artificial chiral media when he attempted to embed into the material an ensemble of randomly oriented small wire helices [25]. In 1948, Winston E. Kock of Bell Laboratories introduced the basic principles of artificial dielectrics to design lightweight lenses in the microwave frequency range (around 3–5 GHz) [26]. His attempt was to replace at these frequencies, where the wavelength is 10-6 centimeters, heavy and bulky lenses made of natural dielectric materials. He realized his concept of artificial dielectrics by controlling the effective index-of-refraction of the materials by embedding into them, and arranging periodically, metallic disks and spheres in a concave lens shape.

The paper that revived the interest in the special class of artificial materials, now coined metamaterials and not found in nature, was that of Victor Veselago in 1968 who analyzed the propagation of uniform waves in materials that exhibited, simultaneously, both negative permittivity and permeability (DNG; double negative) [27]. Although Veselago may not have been interested in dielectric materials, he examined analytically the wave propagation through materials that exhibited, simultaneously, negative ε and negative μ . One of the materials that can be created in nature is plasma, which can exhibit negative permittivity. Plasma is an ionized gas of which a significant number of its charged particles interact strongly with electromagnetic fields and make it electrically conductive. For those that lived through the birth of the U.S. space program in the mid-1960s, led by NASA, there was a lot of interest and research in plasmas, formed beneath and around the nose of the spacecraft during re-entry that caused loss of communication with the astronauts during the final 10-15 minutes of landing. To attempt to alleviate this loss of communication (referred to then as blackout), due to the formed plasma sheath near the nose and belly of the spacecraft, NASA initiated and carried out an intense research program on plasma. The plasma was modeled with a negative dielectric constant (negative permittivity), and it was verified through many experiments.

Although Veselago may have known that negative ε can be obtained by plasma-type materials, he did not speculate, at least in [27], how and what kind of materials may exhibit DNG properties. However, he was able to show and conclude, through analytical formulation, that for wave propagation through DNG type of materials, the direction of the power density flow (Poynting vector) is opposite to the wave propagation (phase vector). He referred to such materials as *left-handed*. Based on his conclusions, the directions of power density flow and phase velocity for DPS materials (double positive, which are conventional dielectrics) and DNG materials (double negative, not found in nature) are illustrated graphically in Figure 5-21, where a uniform plane wave propagates in DPS (Figure 5-21a) and DNG (Figure 5-21b) materials. The DPS materials are also dubbed Right-Handed Materials (RHM) while the DNG materials are dubbed as Left-Handed Materials (LHM). The solid arrows represent the directions of wave vectors (phase velocities) while the dashed arrows represent power flow (Poynting vectors). While the arrows

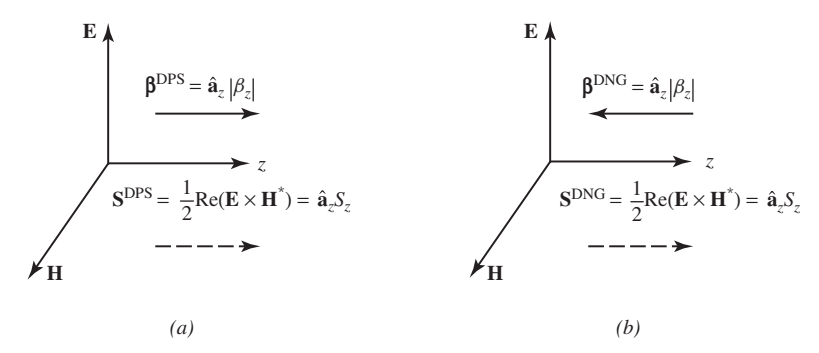


Figure 5-21 Direction of phase vector (β) and Poynting vector (S) for uniform wave propagation in double positive (DPS) and double negative (DNG) materials. (a) RHM: double positive material (DPS). (b) LHM: double negative material (DNG).

in Figure 5-21a illustrate the directions that we expect from conventional dielectrics, the arrows in Figure 5-21b point in the opposite direction, which will indicate that there is a phase advance (phase wave fronts move toward the source) for the wave in Figure 5-21b and a phase delay for the wave in Figure 5-21a, which is what we are accustomed to from conventional dielectrics. To get the phase advance of Figure 5-21b requires that the phase constant (wave number) is negative. This is accomplished by defining both the permittivity and permeability negative; thus the name of DNG material. These concepts will be presented here analytically, but first an outline will be created to lay the groundwork of metamaterials, at least as of this writing.

5.7.4 Propagation Characteristics of DNG Materials

Veselago in his seminal paper showed, using a slab of DNG material embedded into a host DPS medium (the same DPS to the left and to the right of the DNG slab), that an impinging wave emanating from a source to the left of the DNG slab will focus, creating caustics at two different points (one within the DNG slab and the other one to the right of the DNG slab), as long as the slab is sufficiently thick. This is accomplished by using, for the DNG slab, permittivity and permeability that are of the same magnitudes but opposite signs as those of the host DPS medium ($\varepsilon_2 = -\varepsilon_1$, $\mu_2 = -\mu_1$; index-of-refraction $n_2 = -n_1$). This is shown graphically in Figure 5-22, and it is often referred to as the *Veselago planar lens*. This, of course, seemed very attractive and

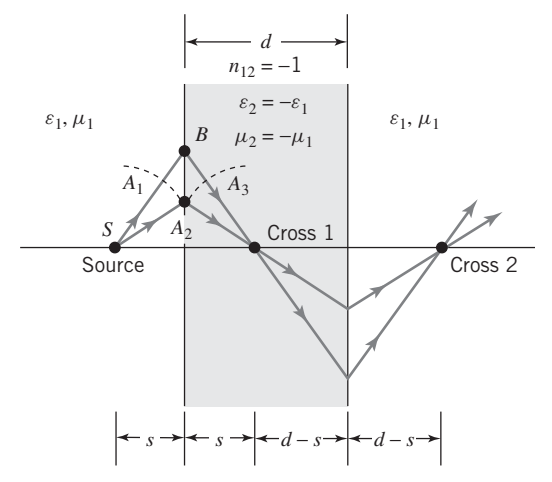


Figure 5-22 Veselago's planar/flat lens: focusing by a DNG slab between two DPS materials [19]. Reprinted with permission from John Wiley & Sons, Inc.

was probably one of the reasons the genesis of the renewed interest of modern metamaterials. However, the Veselago planar lens was also analyzed using a classical method based on Fourier transforms in the frequency domain, and the sinusoidal field exciting the lens expressed in terms of even and odd resonant surface wave modes whose amplitudes were evaluated by residues at the poles [28], Appendix D of [23]. Based on this analytical approach, the following observations were made in [28], Appendix D of [23]: A CW sinusoidal source solution to "a lossless Veselago flat lens with super resolution is not physically possible" because of the presence of surface waves that produce divergent fields over a region within and near the Veselago lens. If losses are included, the excited interfering surface wave modes will decay in a short time interval; however, the lens resolution will depend on the losses, and it will be substantially reduced if they are moderate to large [28], Appendix D of [23]. The analysis assumes that the incident field has a finite continuous frequency spectrum, and the negative epsilon and mu are frequency dispersive, which Veselago indicates are necessary for the field energy to be positive.

The time-domain solution to a frequency dispersive Veselago lens illuminated by a sinusoidal source that begins at t=0 has also been determined [29]. The time-domain fields remain finite everywhere for finite time t and approach the fields of a CW source only as $t\to\infty$. In particular, the divergent fields encountered in the CW solution to the lossless Veselago lens are caused by the infinite CW energy imparted (during the infinite amount of time between $t\to-\infty$ and the present time t) to the evanescent fields in the vicinity of the slab; analogous to the divergent fields produced by a CW source inside a lossless cavity at a resonant frequency.

The work of Veselago remained dormant for about 30 years, and it was not until the late 1990s when Pendry and his colleagues suggested that DNG materials could be created artificially by using periodic structures [30–33]. Not long after Pendry, Smith and his collaborators [34–38] built materials that exhibited DNG characteristics. This was accomplished by the use of a structure consisting of split-ring resonators and wires, a unit cell of which is shown in Figure 5-23. It was suggested that the split-ring element, of the type shown in Figure 5-23a, will contribute a negative permetability while the infinite length wire of Figure 5-23b will contribute a negative permittivity; the combination of the two will, in a periodic structure, contribute a negative index-of-refraction. An experimental array of split-ring resonators and wires is shown in Figure 5-24. In fact, Smith and his team claimed to have observed experimentally negative refraction. In [19] this phenomenon was claimed to be radiation from either a surface wave characteristic of finite periodic structures or possibly a sidelobe from the main beam [39].

Because of the immense interest in DNG materials, with negative permittivity and permeability, there were a number of subsequent experiments, in addition to that in [38], to attempt to verify the negative permittivity and permeability, and thus negative index-of-refraction. Some of these

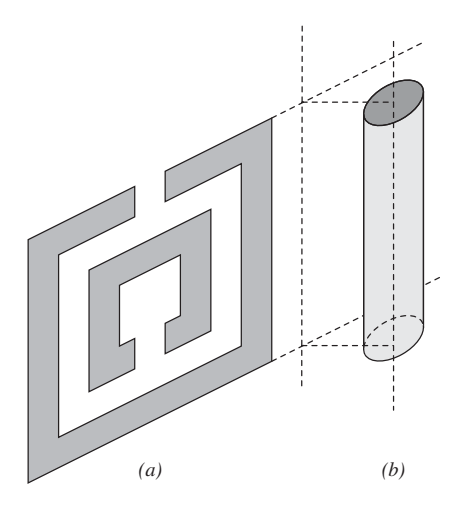


Figure 5-23 Simulation of DNG material (negative refraction) using split-ring resonators and wires. (a) Split ring. (b) Wire.

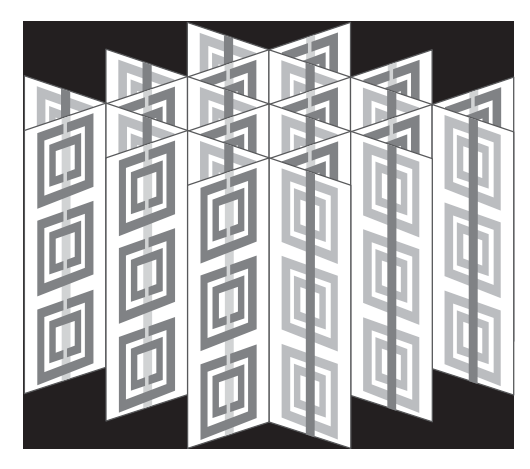


Figure 5-24 Simulation of DNG material (negative refraction) using split-ring resonators and wires [38]. "From R. A. Shelby, D. R. Smith, S. Shultz, 'Experimental verification of a negative index-of-refraction,' *Science*, vol. 292, pp. 77–79, April 2001. Reprinted with permission from AAAS."

experiments, along with the corresponding references, are summarized in [40]. For the simulations, a frequency-dispersive Drude model [13] was used to represent the negative permittivity of the infinite wires while a frequency-dispersive Lorentz model [32] was utilized for the representation of the negative permeability of the split-rings of Figure 5-23. The experiments consisted of parallel plate waveguide techniques utilizing both metamaterial slabs and prisms [40], and most of the measurements were carried out in the 4-20 GHz region. The refraction could be observed by having the slab samples rotated or by having the plane wave incident at an oblique angle. While the nearly plane wave incidence was easier to implement experimentally, the rotation of the samples yield good experimental results. The use of prisms was also an alternative and popular experiment. The metamaterial slabs and prisms were fabricated by embedding various geometrical shapes to represent the characteristics of both wire and different shape split-ring inclusions. In some of the experiments, the metamaterials included only split-ring type of inclusions to verify the negative permeability. The use of an S-shaped unit cell in the metamaterial structure provided an alternative geometry that simulated both a negative permittivity and permeability, and thus did not require the straight wire to represent the negative permittivity; alternate S-ring designs could also be used to possibly achieve dual frequency bands [40]. Gaussian beams and nearly simulated plane waves were used to perform transmission and focusing experiments to validate the negative index-of-refraction, using both dielectric and solid state structures. The solid state metamaterial structures were introduced to minimize the mismatch losses (which were greater for dielectric structures and led to low power levels), improve the mechanical fragility, and make metamaterials more attractive for industrial applications [40]. It was reported that both the transmission and focusing experiments produced results that indicated negative permittivity and permeability, and thus, the creation of a negative effective index-of-refraction [40].

The attractive performance of devices and systems that incorporated metamaterials led to the genesis of the enormous interest on the subject by many teams around the world, and the avalanche of papers published in transactions and journals, presented in symposia and conferences, and applied to numerous problems with exotic characteristics and performances. The word metamaterials became a 'household' word in the electromagnetic community in the 2000–2010 time period. This type of materials exhibit narrow bandwidths, which may have limited its applications.

5.7.5 Refraction and Propagation Through DNG Interfaces and Materials

Now that a brief historical and chronological background of the evolution of metamaterials has been outlined, we will present a special case of what initially were referred to as artificial

dielectrics, the basics from the analytical point of view as well as from a sample of simulations, and experiments. It should be pointed out, however, that what ensued after the work by Pendry and Smith was a plethora of publications which are too numerous to include here. Up to this point an attempt was made to reference some of the most basic books and papers. The reader is referred to the technical transactions, journals, and letters where most of these ensuing papers were published or presented at leading international conferences and symposia. Most of these can be found in references [41–46].

The greatest potential of the DNG materials is the creation of a structure with a negative index-of-refraction n defined as

$$n^{2} = \varepsilon_{r}\mu_{r} \Rightarrow n = \pm\sqrt{\varepsilon_{r}\mu_{r}} = \pm\sqrt{-|\varepsilon_{r}|(-|\mu_{r}|)} = \pm(j\sqrt{|\varepsilon_{r}|})(j\sqrt{|\mu_{r}|}) = \pm j^{2}\sqrt{|\varepsilon_{r}\mu_{r}|}$$

$$n = \mp\sqrt{|\varepsilon_{r}\mu_{r}|}$$
(5-102)

Which sign of n should be chosen for DNG materials (with both ε_r and μ_r negative)? It seems from (5-102) that there are two basic choices; either negative or positive n. If a positive n is selected, that resorts back to the DPS representation. If the negative value of n in (5-102) is selected, then that is the basis of DNG materials.

Materials with negative index-of-refraction have some interesting properties, some of which have been mentioned and illustrated in Figure 5-21. Now let us examine two interface options using Snell's law of refraction which is the manifest of phase match across the interface. Of particular interest are materials with negative index-of-refraction.

• Snell's law of refraction, represented by (5-15b) and (5-24b), or

$$\beta_1 \sin \theta_i = \omega \sqrt{\mu_1 \varepsilon_1} \sin \theta_i \equiv \beta_2 \sin \theta_t = \omega \sqrt{\mu_2 \varepsilon_2} \sin \theta_t$$
 (5-103)

can also be written as

$$n_1 \sin \theta_i = n_2 \sin \theta_t \tag{5-104}$$

When the index-of-refraction of both materials forming the interface is positive, then the refracted ray (transmitted wave) will be, as expected for conventional materials, on the same side (relative to the normal to the interface) as the reflected ray, as illustrated in Figure 5-25a. However, when the index-of-refraction of one material is positive while that of the other is negative, the refracted ray (transmitted wave) will be in the opposite direction of the reflected ray, as illustrated in Figure 5-25b.

• For DNG materials with a negative index-of-refraction the phase constant (wave number) of the wave traveling in the DNG material is negative, or based on the definition of (5-103)

$$\beta_2 = \omega \sqrt{\mu_2 \varepsilon_2} = -\omega \sqrt{|\mu_2| |\varepsilon_2|} \tag{5-105}$$

This implies that, for positive time, there will be a phase advance (phase wavefronts move toward the source), instead of a phase delay that we have been accustomed to. This is an interesting phenomenon, which has been part of the spirited dialogue.

So, based on the above, a negative index-of-refraction leads to:

- A refracted angle that is on the same side, relative to the normal to the interface, as the incident angle, and the power flow (Poynting vector) is outward (as expected); however, the phase vector in inward (opposite to the Poynting vector).
- Phase advance, instead of phase delay that is typical of DPS materials.

Based on the above, let us examine through an example a more general case of the planar lens that was illustrated in Figure 5-22.

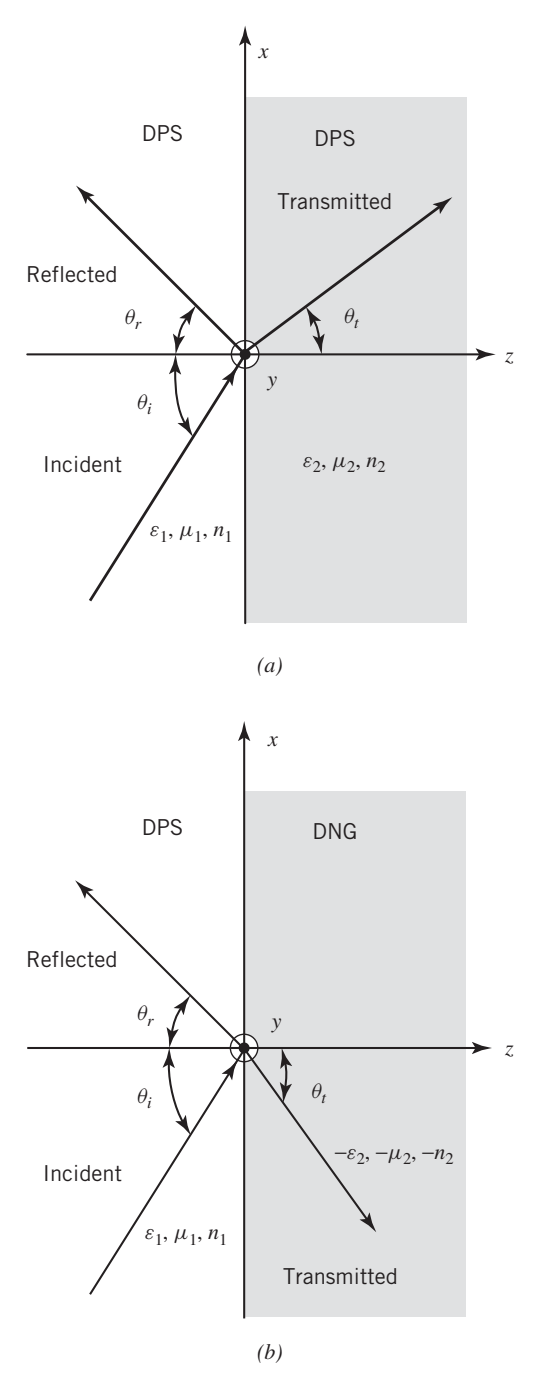


Figure 5-25 Refraction by planar interface created by double positive (DPS) and double negative (DNG) materials. (a) DPS-DPS. (b) DPS-DNG.

Example 5-14

Figure 5-22 displays Veselago's planar/flat lens. A more general one is the one of Figure 5-26 where a DNG slab is sandwiched within free space. Given the dimensions of the DNG slab of thickness d and the source position s, as shown in the Figure 5-26, determine the location of the foci (caustics) f_0 and f_1 (one within the DNG slab and one outside it) in terms of the incidence angle θ_i , position of the source s, and thickness d and index-of-refraction n_1 of the DNG slab. Assume the DNG slab possesses negative permittivity $-\varepsilon_1$, negative permeability $-\mu_1$, and negative index-of-refraction $-n_1$. Furthermore, let us assume that we are looking for a solution based on geometrical optics.

Solution: Using (5-103) through (5-105), we can write for the leading interface between free space and the DNG slab that

$$\theta_1 = \sin^{-1}\left(\frac{1}{|n_1|}\sin\theta_i\right)$$

Also from Figure 5-26

$$\tan \theta_i = \frac{h_1}{s} \Rightarrow h_1 = s \tan \theta_i$$

$$\tan \theta_1 = \frac{h_1}{f_0} \Rightarrow h_1 = f_0 \tan \theta_1$$

Equating the two previous equations leads to

$$s \tan \theta_i = f_0 \tan \theta_1 \Rightarrow f_0 = s \frac{\tan \theta_i}{\tan \theta_1} \Rightarrow \tan \theta_1 = \frac{s}{f_0} \tan \theta_i$$

From Figure 5-26

$$\tan \theta_0 = \frac{h_2}{f_1} \Rightarrow h_2 = f_1 \tan \theta_0$$

$$\tan \theta_1 = \frac{h_2}{d - f_0} \Rightarrow h_2 = (d - f_0) \tan \theta_1$$

Equating the last two equations leads to

$$f_1 \tan \theta_0 = (d - f_0) \tan \theta_1 \Rightarrow f_1 = (d - f_0) \frac{\tan \theta_1}{\tan \theta_0}$$

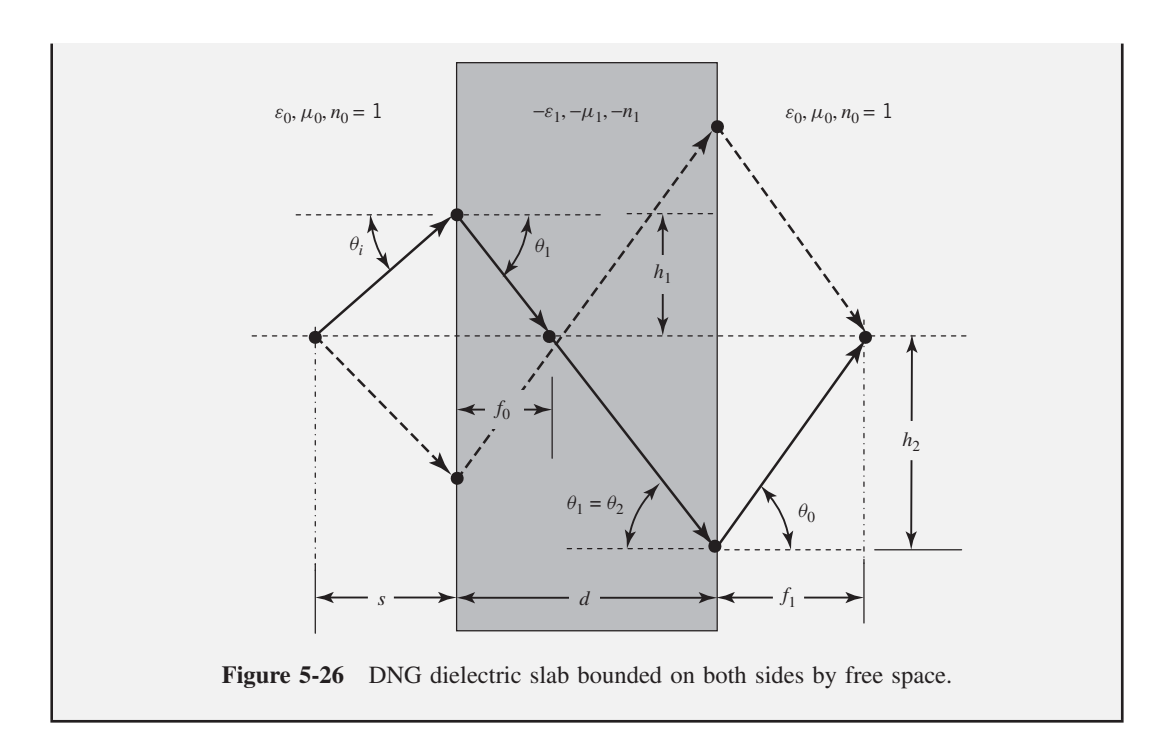
which can also be expressed, assuming $d > f_0$, as

$$f_1 = (d - f_0) \frac{\tan \theta_1}{\tan \theta_0} = (d - f_0) \frac{s}{f_0} \frac{\tan \theta_i}{\tan \theta_0}$$

Since $\theta_0 = \theta_i$, the above equation reduces to

$$f_1 = (d - f_0) \frac{s}{f_0}$$

As the magnitude of $-\varepsilon_1$ approaches that of free space (that is $|-\varepsilon_1| \to |\varepsilon_0| \Rightarrow |-n_1| \to |n_0| = 1$), the focal distance f_0 approaches $s(f_0 \to s)$ and f_1 approaches $d - s(f_1 \to d - s)$. Then Figure 5-26 reduces, in this limiting case, to Figure 5-22. When s becomes very large (approaching infinity), the incident wave reduces to near normal incidence. In this case the focusing moves toward infinity (ideally no focusing).



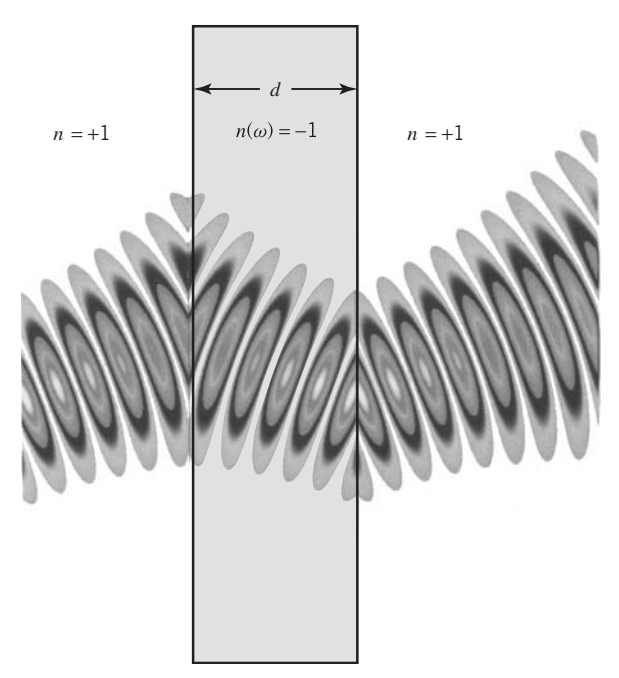


Figure 5-27 Negative refraction from a DNG slab [48]. Copyright © by The Optical Society of America. Permission and courtesy of R. W. Ziolkowski.

To illustrate the DNG refraction, a simulation has been performed, using the Finite-Difference Time-Domain method, of a 30 GHz perpendicularly polarized CW Gaussian beam incident at 20° on a DNG slab bordered from the left and right by free space, as shown in Figure 5-27 [48]. Because the incident wave is a plane wave, there is no focusing. The index-of-refraction of the

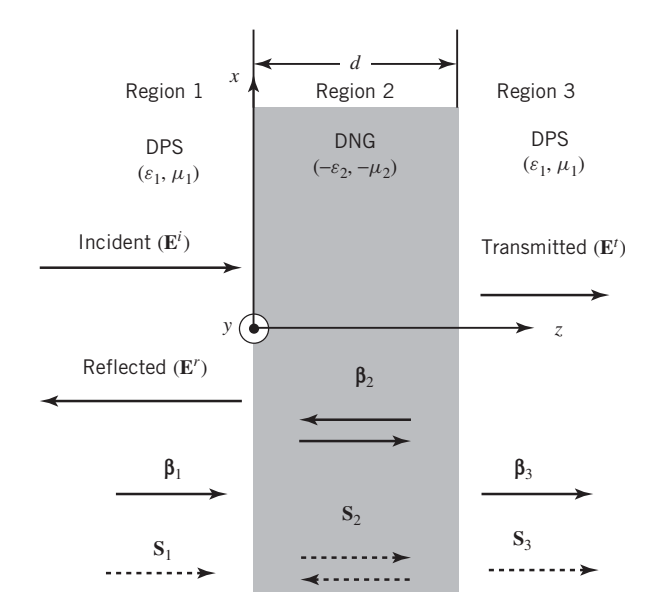


Figure 5-28 Reflection and transmission through a DNG slab.

DNG slab is n = -1, and it was chosen to minimize reflections. Identical electric and magnetic Drude models were selected with parameters chosen so that only small losses were considered [13, 48]. Assuming the stated parameters of the media, the negative refraction is visible at the leading and trailing interfaces.

Another interesting observation will be to illustrate, through an example, the propagation of a plane wave through a slab of metamaterial, of thickness d, when it is embedded into a conventional dielectric material, as shown in Figure 5-28. This is similar to the problem for ordinary dielectrics, illustrated in Figure 5-11. For convenience, it is assumed that in Figure 5-28 the media to the left and right of the metamaterial DNG slab are both conventional dielectrics and *identical*. Also, at first we examine wave propagation at normal incidence, which is similar to that of conventional dielectrics, shown in Figure 5-11. The phase vectors β (\longrightarrow) and Poynting vectors S (\longrightarrow) in each region are also indicated by their respective arrows. The analytical formulation of the reflection and transmission coefficients follows.

Example 5-15

For the DNG geometry of Figure 5-28, derive a simplified expression for the total input reflection at the initial interface and the total transmission coefficient through the entire DNG slab.

Solution: Using (5-67d), the total input reflection coefficient at the leading edge of the slab can be written as

$$\Gamma = \frac{E^r}{E^t} = \frac{\Gamma_{12} + \Gamma_{23}e^{-j2\beta_2d}}{1 + \Gamma_{12}\Gamma_{23}e^{-j2\beta_2d}} = \frac{\Gamma_{23} - \Gamma_{12}}{m_3 - n_1} \frac{\Gamma_{12} \left(1 - e^{-j2\beta_2d}\right)}{1 - (\Gamma_{12})^2 e^{-j2\beta_2d}}$$

which for a DNG slab, based on (5-105), reduces to

$$\Gamma = \frac{E^r}{E^t} = \frac{\Gamma_{12} + \Gamma_{23}e^{+j2|\beta_2|d}}{1 + \Gamma_{12}\Gamma_{23}e^{+j2|\beta_2|d}} \frac{\Gamma_{23} = -\Gamma_{12}}{\frac{\eta_3 = \eta_1}{\eta_3}} \frac{\Gamma_{12}\left(1 - e^{+j2|\beta_2|d}\right)}{1 - (\Gamma_{12})^2e^{+j2|\beta_2|d}}$$

since

$$\Gamma_{12} = \left[\frac{\eta_2 - \eta_1}{\eta_2 + \eta_1}\right] = -\Gamma_{23}$$

Similarly, it can be shown that the transmission coefficient can be written as [13]

$$T = \frac{E^{t}}{E^{i}} = \frac{4\eta_{2}\eta_{3}e^{-j\beta_{2}d}}{(\eta_{1} + \eta_{2})(\eta_{2} + \eta_{3})} \frac{1}{(1 + \Gamma_{12}\Gamma_{23}e^{-j\beta_{2}d})}$$

$$T = \frac{E^{t}}{E^{i}} \frac{\Gamma_{23} = -\Gamma_{12}}{\eta_{3} = \eta_{1}} \frac{4\eta_{2}\eta_{1}e^{-j\beta_{2}d}}{(\eta_{1} + \eta_{2})^{2}} \frac{1}{[1 - (\Gamma_{12})^{2}e^{-j\beta_{2}d}]}$$

which for the DNG slab reduces to

$$T = \frac{E^{t}}{E^{i}} \frac{\frac{\Gamma_{23} = -\Gamma_{12}}{\eta_{3} = \eta_{1}}}{\frac{4\eta_{2}\eta_{1}e^{+j2|\beta_{2}|d}}{(\eta_{1} + \eta_{2})^{2}}} \frac{1}{\left[1 - (\Gamma_{12})^{2}e^{+j2|\beta_{2}|d}\right]}$$

An interesting observation is made if the DNG dielectric slab of Example 5-15 is matched to the medium it is embedded; that is, if $\eta_2 = \eta_1$. For this case, $\Gamma_{12} = 0$, and the total input reflection and the transmission coefficients of Example 5-15 reduce, respectively, to

$$\Gamma = 0 \tag{5-106a}$$

$$T = e^{+j2|\beta_2|d} (5-106b)$$

The transmission coefficient of (5-106b) indicates a phase advance (phase wavefront moving toward the source), instead of a phase delay as we are accustomed for wave propagation through conventional materials. This wave propagation through DNG materials is a unique feature that can be taken advantage of in various applications. As an example, the usual phase delay in conventional dielectric slabs and/or transmission lines can be compensated by phase advance in DNG type of slabs and/or transmission lines [13, 15, 16, 47] and others.

Now consider a uniform plane wave propagating at oblique incidence through a planar interface consisting of two materials. The case where both media are DPS has been treated in Section 5.3.1 for perpendicular polarization (Figure 5-2) and in Section 5.3.2 for parallel polarization (Figure 5-4). Now we will examine the wave propagation through a DNG medium; in this case medium 2 is DNG, when the first medium is DPS. However, before this is done, the interface formed by two DPS materials will be examined first. The planar interface formed by one DPS and one DNG material is examined afterwards. Only the perpendicular polarization of Figure 5-2 is considered. The same procedure can be applied to Figure 5-4 for the parallel polarization.

Based on the geometry of Figure 5-2, the vector wavenumbers for the incident, reflected, and transmitted fields can be written as

$$\mathbf{\beta}_i = \beta_1 \left(\hat{\mathbf{a}}_x \sin \theta_i + \hat{\mathbf{a}}_z \cos \theta_i \right) = n_1 \frac{\omega}{v_0} \left(\hat{\mathbf{a}}_x \sin \theta_i + \hat{\mathbf{a}}_z \cos \theta_i \right)$$
 (5-107a)

$$\mathbf{\beta}_r = \beta_1 \left(\hat{\mathbf{a}}_x \sin \theta_i - \hat{\mathbf{a}}_z \cos \theta_i \right) = n_1 \frac{\omega}{v_0} \left(\hat{\mathbf{a}}_x \sin \theta_i - \hat{\mathbf{a}}_z \cos \theta_i \right)$$
 (5-107b)

$$\boldsymbol{\beta}_t = \beta_2 \left(\hat{\boldsymbol{a}}_x \sin \theta_t + \hat{\boldsymbol{a}}_z \cos \theta_t \right) = n_2 \frac{\omega}{v_0} \left(\hat{\boldsymbol{a}}_x \sin \theta_t + \hat{\boldsymbol{a}}_z \cos \theta_t \right)$$
 (5-107c)

Using the expressions for the electric and magnetic fields of (5-10a) through (5-12b), the Poynting vectors for the respective three fields (incident, reflected, and refracted) can be written as

$$\mathbf{S}_i = \frac{1}{2} \frac{|E_0|^2}{\eta_1} \left(\hat{\mathbf{a}}_x \sin \theta_i + \hat{\mathbf{a}}_z \cos \theta_i \right)$$
 (5-108a)

$$\mathbf{S}_r = \frac{1}{2} \frac{|\Gamma E_0|^2}{\eta_1} \left(\hat{\mathbf{a}}_x \sin \theta_i - \hat{\mathbf{a}}_z \cos \theta_i \right)$$
 (5-108b)

$$\mathbf{S}_t = \frac{1}{2} \frac{|TE_0|^2}{\eta_2} \left(\hat{\mathbf{a}}_x \sin \theta_t + \hat{\mathbf{a}}_z \cos \theta_t \right)$$
 (5-108c)

This is left as end-of-the-chapter exercises for the reader. It is apparent, from the vectors within the parentheses in (5-107a) through (5-108c), that for a DPS-DPS interface the phase vectors and the Poynting vectors for all three fields (incident, reflected, and refracted) are all parallel to each other and in the same directions.

Now let us consider the same oblique incidence upon a DPS-DNG interface, as shown in Figure 5-29. Snell's law of refraction, which is given by (5-103) and (5-104), can be expressed as

$$\sin \theta_t = \frac{\omega \sqrt{\mu_1 \varepsilon_1}}{\omega \sqrt{\mu_2 \varepsilon_2}} \sin \theta_i = \frac{n_1}{n_2} \sin \theta_i \Rightarrow \theta_t = \sin^{-1} \left(\frac{n_1}{n_2} \sin \theta_i \right)$$
 (5-109)

For positive n_1 and n_2 , the angle θ_t is positive, and everything follows what we already have experienced with DPS materials. However, when n_1 and n_2 have opposite signs, the angle θ_t is negative, as indicated in Figures 5-25, 5-26, and 5-29, and simulated in Figure 5-27. Based on these figures, whose interface is formed by a DPS and a DNG material (which leads to a negative angle of refraction), we will examine the directions of the phase vectors of (5-107) and Poynting vectors of (5-108) for the perpendicular polarization. The same can be done for the parallel polarization. This is left as an end-of-the-chapter exercise for the reader.

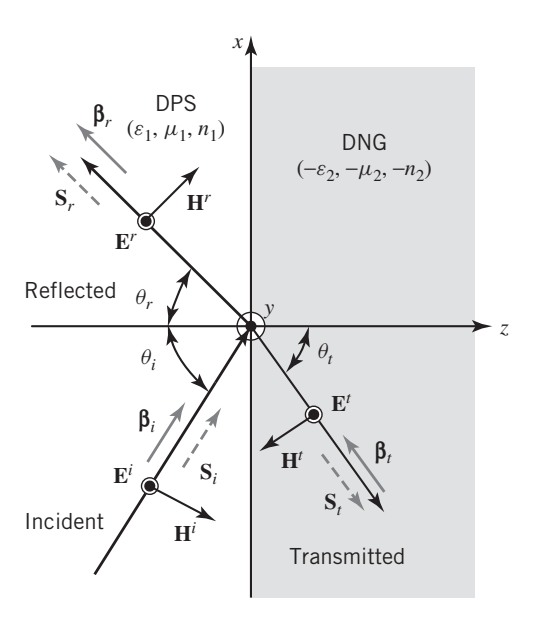


Figure 5-29 Uniform plane wave reflection and refraction of perpendicular polarization by a planar interface formed by DPS and DNG materials.

Since for the interface of Figure 5-29 the index-of-refraction of medium 2 is negative and the wavenumber is also negative, as expressed by (5-105), the wave vectors of (5-107a) and the Poynting vectors of (5-108a) can now be written, respectively, as

$$\mathbf{\beta}_i = \beta_1 \left(\hat{\mathbf{a}}_x \sin \theta_i + \hat{\mathbf{a}}_z \cos \theta_i \right) = n_1 \frac{\omega}{v_0} \left(\hat{\mathbf{a}}_x \sin \theta_i + \hat{\mathbf{a}}_z \cos \theta_i \right)$$
 (5-110a)

$$\boldsymbol{\beta}_r = \beta_1 \left(\hat{\mathbf{a}}_x \sin \theta_i - \hat{\mathbf{a}}_z \cos \theta_i \right) = n_1 \frac{\omega}{v_0} \left(\hat{\mathbf{a}}_x \sin \theta_i - \hat{\mathbf{a}}_z \cos \theta_i \right)$$
 (5-110b)

$$\mathbf{\beta}_t = |\beta_2| \left(\hat{\mathbf{a}}_x \sin |\theta_t| - \hat{\mathbf{a}}_z \cos |\theta_t| \right) = |n_2| \frac{\omega}{v_0} \left(\hat{\mathbf{a}}_x \sin |\theta_t| - \hat{\mathbf{a}}_z \cos |\theta_t| \right)$$
 (5-110c)

$$\mathbf{S}_i = \frac{1}{2} \frac{|E_0|^2}{\eta_1} \left(\hat{\mathbf{a}}_x \sin \theta_i + \hat{\mathbf{a}}_z \cos \theta_i \right)$$
 (5-111a)

$$\mathbf{S}_r = \frac{1}{2} \frac{|\Gamma E_0|^2}{\eta_1} \left(\hat{\mathbf{a}}_x \sin \theta_i - \hat{\mathbf{a}}_z \cos \theta_i \right)$$
 (5-111b)

$$\mathbf{S}_t = \frac{1}{2} \frac{|TE_0|^2}{\eta_2} \left(-\hat{\mathbf{a}}_x \sin|\theta_t| + \hat{\mathbf{a}}_z \cos|\theta_t| \right)$$
 (5-111c)

While the wave and Poynting vectors of the incident and reflected fields are unaffected by the presence of the DNG material forming the interface in Figure 5-29 [they are the same as in (5-107) and (5-108)], those of the transmitted fields, as represented by (5-110c) and (5-111c) are different from the corresponding ones of (5-107c) and (5-108c) in two ways.

The first difference is that the wave vector of (5-110c) is antiparallel to the Poynting vector of (5-111c), whereas they were parallel for (5-107c) and (5-108c). Also, for positive time, the wavenumber of (5-107c) leads to a phase delay, but the wavenumber of (5-110c) leads to a phase advance. In addition, while the phase vector of (5-107c) and the Poynting vector of (5-108c) are both directed away from the source (point of refraction in the first quadrant), the Poynting vector of (5-111c) is also directed away from the source, but in the fourth quadrant. These are also illustrated graphically in Figures 5-21a and 5-21b. These are some of the similarities and differences in the transmitted fields for DPS-DPS and DPS-DNG interfaces.

5.7.6 Negative-Refractive-Index (NRI) Transmission Lines

Another application of the DNG material is the design of Negative-Refractive-Index Transmission Lines (NRI-TL) [15, 16, 47]. This concept can be used to design:

- nonradiating phase-shifting lines that can produce either positive or negative phase shift
- broadband series power dividers
- forward leaky-wave antennas

and other applications [16]. When a wave propagates through a DPS medium, like in a conventional dielectric slab of thickness d_1 , it will accumulate phase lag $|\phi_1|$ of $\beta_1 d_1(\phi_1 = -\beta_1 d_1)$, also referred to as negative phase shift, where β_1 is the phase constant (wave number). This negative phase shift can be compensated by a positive phase shift ϕ_2 ($\phi_2 = +|\beta_2|d_2$) through a DNG slab that follows the DPS slab. In fact, ideally, the negative phase shift accumulated through propagation in the DPS slab ($\phi_1 = -\beta_1 d_1$) can be totally eliminated if the positive phase ϕ_2 ($\phi_2 = +|\beta_2|d_2$) can be created by propagation through the DNG slab such that $|\phi_1| = |\phi_2|$ so that the total phase ϕ by wave propagation through both slabs is equal to zero ($\phi = \phi_1 + \phi_2 = 0$). Such an arrangement is shown graphically in Figure 5-30 where the arrows are used to designate

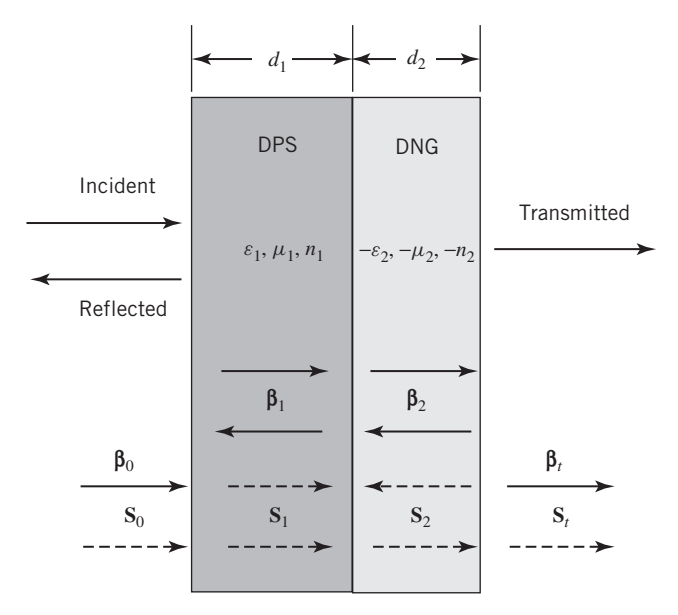


Figure 5-30 Wave propagation through two successive dielectric slabs, one made of DPS material and the other, of DNG material, for phase wave compensation.

the directions of the phase vectors β and the Poynting vectors S. This phase compensation can also be used to create any other desired total phase shift by appropriately choosing the phase constants and thicknesses of the DPS and DNG slabs. The special case of zero phase shift of wave propagation through both slabs is accomplished provided

$$|\phi_1| = \omega \sqrt{\mu_1 \varepsilon_1} d_1 = |\phi_2| = \omega \sqrt{|\mu_2| |\varepsilon_2|} d_2 \Rightarrow n_1 d_1 = n_2 d_2 \Rightarrow \frac{d_1}{d_2} = \frac{n_1}{n_2}$$
 (5-112)

A graphical illustration of such phase compensation of the electric field intensity of a perpendicularly polarized field, simulated using the FDTD method, is exhibited in Figure 5-31 [13]. The incident field is a Gaussian beam traveling in a free-space medium and normally incident upon the DPS slab followed by a DNG slab. The indices of refraction were chosen to be $n_{\rm real}(\omega) = +3$ for the DPS slab and $n_{\rm real}(\omega) = -3$ for the DNG slab. Observing the phase fronts of the beam inside the two slabs, it is evident that the beam expands (diverges) in the DPS slab while it refocuses (converges) in the DNG slab. Ultimately, the phase fronts of the exiting beam in the free-space medium to the right of the DNG slab begin to expand and match those of the incident field to the left of the DPS slab. According to [13], there was only 0.323 dB attenuation of wave propagation through the two slabs that span a total distance of $4\lambda_0$. However, the total phase accumulation from the leading edge of the DPS slab to the trailing edge of the DNG slab is zero. Thus, the output field exits the trailing edge, along the symmetry line of the source/beam which is perpendicular to the interface, with the same phase as the input field and with only a slight attenuation in the peak value of about of 0.323 dB, which is due to a small loss in the medium and to the Gaussian beam diverging from the source. While the negative (second) layer refocuses the beam, the small loss by the first layer is not totally compensated by the second layer and leads to the slight attenuation at the output face of the system. Such an arrangement of slabs is usually referred to, for obvious reasons, as a beam translator [13].

This phase compensation concept can also be applied to compensate for negative phase shift by wave propagation through a conventional DPS transmission line followed by a NRI line with DNG material, often referred to as BW (backward-wave) line, as shown graphically in Figure 5-32 [16].

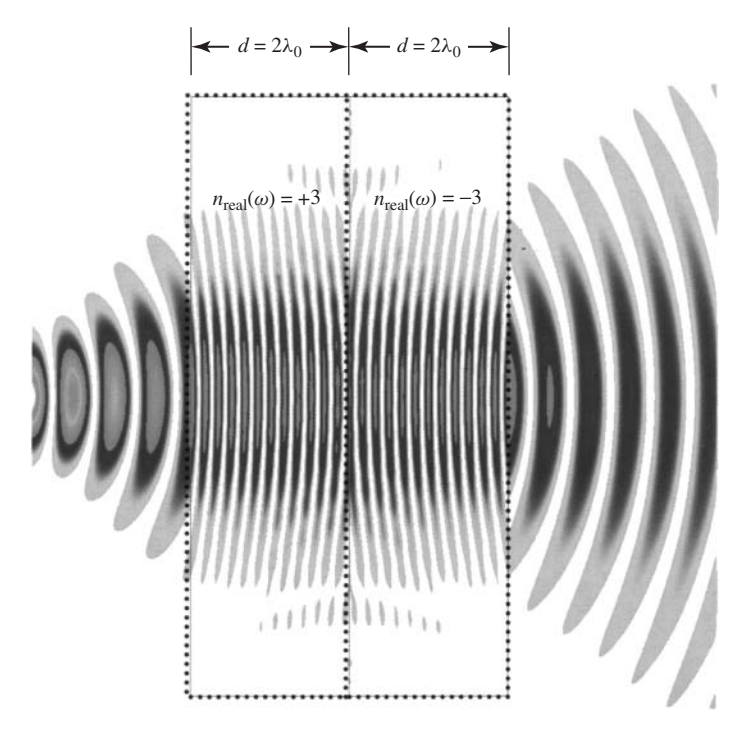


Figure 5-31 Phase compensation by successive conventional DPS and DNG slabs [13]. Reprinted with permission from John Wiley & Sons, Inc. Original courtesy of R. W. Ziolkowski.

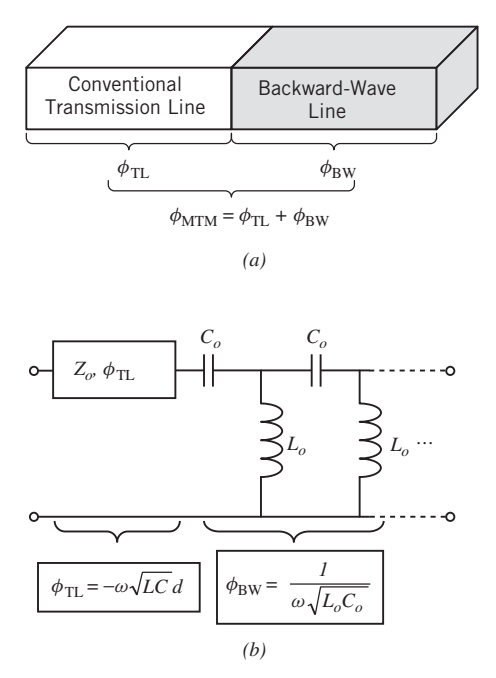
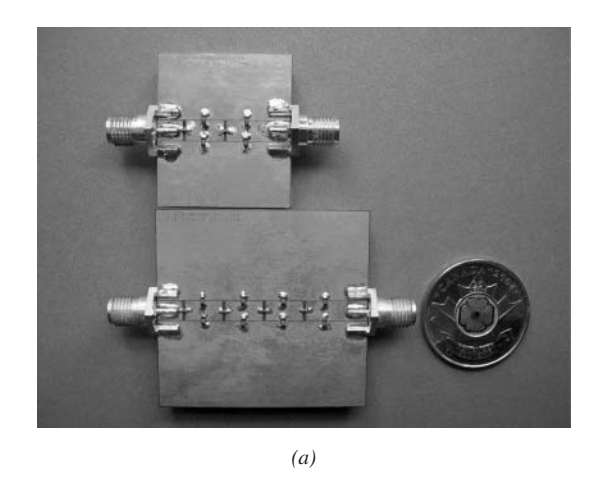
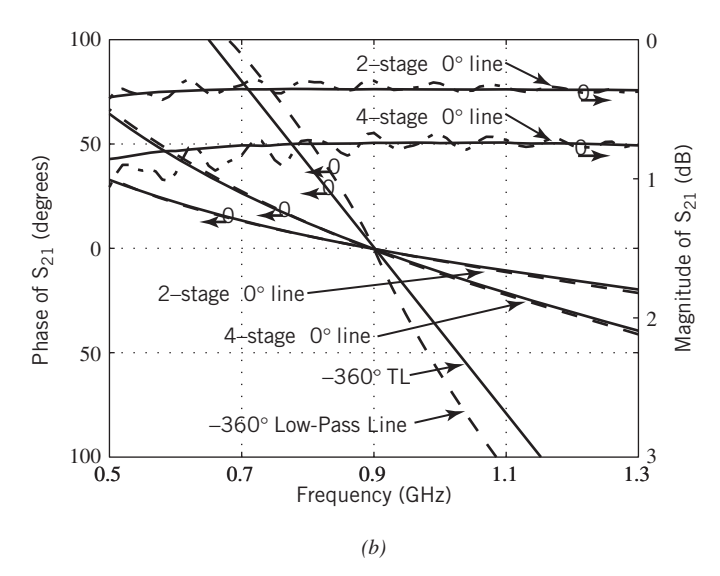


Figure 5-32 Phase compensation by successive conventional and backward-wave transmission lines [16]. Reprinted with permission from John Wiley & Sons, Inc. Originals courtesy of G. V. Eleftheriades and M. Antoniades. (a) Conventional transmission line followed by a backward-wave line. (b) Equivalent circuit of conventional transmission line followed by a backward-wave line.





In Figure 5-32b the equivalent circuit of BW line indicates that the phase advance through the unit cell of a BW line is given by

$$\phi_{\rm BW} = \frac{1}{\omega \sqrt{L_o C_o}} \tag{5-113}$$

which is representative of the phase through a high-pass LC filter of the type shown in the unit cell of the BW line in Figure 5-32b. Such a backward type of a wave, for the equivalent circuit of the backward section of the line, has also been addressed in [49], which states that "a wave in which the phase velocity and group velocity have opposite signs is known as a backward wave. Conditions for these may seem unexpected or rare, but they are not." In fact, it is also stated

in [49] that many filter type of lines have backward waves and that periodic circuits exhibit an equal number of forward and backward "space harmonics."

The low-pass filter (regular transmission line) and high-pass filter (backward-wave line) characteristics can be verified using the Brillouin dispersion diagram [49, 50], which is a plot of ω vs. β with the phase velocity defined as

$$v_p = \frac{\omega}{\beta} \tag{5-114}$$

while the group velocity is defined as

$$v_g = \frac{\partial \omega}{\partial \beta} \tag{5-115}$$

For the regular transmission type line v_p and v_g have the same sign while for the backward-wave type of line, v_p and v_g have opposite signs.

Therefore, it seems that in Figure 5-32 there is a low-pass filter (conventional) line followed by a high-pass filter (BW line) with a total phase shift for the two of

$$\phi_{\text{MTM}} = \phi_{\text{TL}} + \phi_{\text{BW}} = -\omega \sqrt{LC} d + \frac{1}{\omega \sqrt{L_o C_o}}$$
 (5-116)

The transmission line is of the delay type while the backward-wave line is of the phase advance type.

Various one-dimensional phase-shifting lines were constructed at 0.9 GHz using coplanar waveguide (CPW) technology [16]. Two such units, one a two-stage and the other a four-stage phase shifters, are shown in Figure 5-33a. The corresponding simulated and measured phase responses of both units are shown in Figure 5-33b where they are compared with the phase responses of a conventional -360° TL line and a -360° low-pass loaded line. The corresponding magnitudes of both units of 0° phase shift are also indicated in Figure 5-33b. A good comparison is observed between the simulated and measured results and confirms the broadband nature of the phase shifting lines which also exhibit rather small losses [16].

5.8 MULTIMEDIA

On the website that accompanies this book, the following multimedia resources are included for the review, understanding, and presentation of the material of this chapter.

- MATLAB computer programs:
 - a. **SWR_Animation_** Γ **_SWR_Impedance:** Animates the standing wave pattern of a plane wave traveling in a semi-infinite lossless medium and impinging, at normal incidence, upon a planar interface formed by two semi-infinite planar media; the second medium can be lossy (see Figure 5-1). It also computes the input reflection coefficient Γ , SWR, and input impedance.
 - b. **QuarterWave_Match:** Designs a quarter-wavelength impedance transformer of *N* slabs to match a given semi-infinite medium (input) to another semi-infinite medium (load).
 - c. **Single_Slab:** Characterizes the reflection and transmission characteristics of a single layer slab bounded on both sides by two semi-infinite media.
 - d. **Refl_Trans_Multilayer:** Computes the reflection and transmission coefficients of a uniform plane wave incident at oblique angle upon *N* layers of planar slabs bordered on either side by free space.
 - e. **Polarization_Refl_Trans:** Computes the Poincaré sphere angles, and thus, the polarization, of a plane wave incident at oblique angles upon a planar interface.
- Power Point (PPT) viewgraphs, in multicolor.

REFERENCES

- 1. C. A. Balanis, *Antenna Theory: Analysis and Design*, Third Edition, John Wiley & Sons, New York, 2005.
- 2. M. A. Plonus, Applied Electromagnetics, McGraw-Hill, New York, 1978.
- 3. D. T. Paris and F. K. Hurd, Basic Electromagnetic Theory, McGraw-Hill, New York, 1969.
- 4. R. B. Adler, L. J. Chu, and R. M. Fano, *Electromagnetic Energy Transmission and Radiation*, Chapters 7 and 8, John Wiley & Sons, New York, 1960.
- 5. J. J. Holmes and C. A. Balanis, "Refraction of a uniform plane wave incident on a plane boundary between two lossy media," *IEEE Trans. Antennas Propagat.*, vol. AP-26, no. 5, pp. 738–741, September 1978.
- R. D. Radcliff and C. A. Balanis, "Modified propagation constants for nonuniform plane wave transmission through conducting media," IEEE Trans. Geoscience Remote Sensing, vol. GE-20, no. 3, pp. 408–411, July 1982.
- 7. J. D. Kraus, Electromagnetics, Fourth Edition, McGraw-Hill, New York, 1992.
- 8. R. E. Collin, Foundations for Microwave Engineering, Second Edition, McGraw-Hill, New York, 1992.
- 9. R. E. Collin and J. Brown, "The design of quarter-wave matching layers for dielectric surfaces," *Proc. IEE*, vol. 103, Part C, pp. 153–158, March 1956.
- 10. S. B. Cohn, "Optimum design of stepped transmission line transformers," *IRE Trans. Microwave Theory Tech.*, vol. MTT-3, pp. 16–21, April 1955.
- 11. L. Young, "Optimum quarter-wave transformers," *IRE Trans. Microwave Theory Tech.*, vol. MTT-8, pp. 478–482, September 1960.
- 12. G. L. Matthaei, L. Young, and E. M. T. Jones, *Microwave Filters, Impedance-Matching Networks and Coupling Structures*, McGraw-Hill, New York, 1964.
- 13. N. Engheta and R. W. Ziolkowski (editors), *Metamaterials: Physics and Engineering Explorations*, N. Engheta, R. W. Ziolkowski, Editors, IEEE Press, Wiley Inter-Science, New York, 2006.
- 14. IEEE Transactions on Antennas and Propagation, Special Issue on Metamaterials, vol. 51, no. 10, October 2003.
- 15. G. V. Eleftheriades and K. G. Balmain (editors), Negative-Refraction Metamaterials: Fundamental Principles and Applications, John Wiley & Sons, New York, 2005.
- 16. G.V. Eleftheriades and M. A. Antoniades, "Antenna Application of Negative Refractive Index Transmission Line (NRI-TL) Metamaterials," Chapter 14, in *Modern Antenna Handbook*, C. A. Balanis (editor), John Wiley & Sons, pp. 677–736, 2008.
- 17. C. Caloz and T. Itoh, *Electromagnetic Metamaterials: Transmission Line Theory and Microwave Applications*, John Wiley & Sons, New York, 2006.
- 18. R. Marques, F. Martin, and M. Sorolla, *Metamaterials with Negative Parameters: Theory, Design and Microwave Applications*, John Wiley & Sons, New York, 2008.
- 19. B. A. Munk, Metamaterials: Critique and Alternatives, John Wiley & Sons, New York, 2009.
- 20. B. E. Spielman, S. Amari, C. Caloz, G. V. Eleftheriades, T. Itoh, D. R. Jackson, R. Levy, J. D. Rhodes and R. V. Snyder, "Metamaterials face-off. Metamaterials: A rich opportunity for discovery or an overhyped gravy train!," *IEEE Microwave Magazine*, pp. 8–10, 12, 14, 16–17, 22, 26, 28, 30, 32, 34, 36, 38, 42, May 2009.
- 21. P. M. Valanju, R. M. Walser, and A. P. Valanju, "Wave refraction in negative-index media: always positive and very inhomogeneous," *Phys. Rev. Lett.*, vol. 88, no. 18, 187401:1–4, May 2002.
- 22. G. K. Karawas and R. E. Collin, "Spherical shell of ENG metamaterial surrounding a dipole," Military Communications Conference 2008 (MILCOM 2008), pp. 1–7, San Diego, CA, November 2008.
- 23. R. C. Hansen and R. E. Collin, Small Antenna Handbook, John Wiley & Sons, Hoboken, NJ, 2011.
- 24. J. C. Bose, "On the rotation of plane of polarization of electric wave by a twisted structure," *Proc. Roy. Soc.*, vol. 63, pp. 146–152, 1898.
- 25. I. V. Lindell, A. H. Sihvola and J. Kurkijarvi, "Karl F. Lindman: The last Hertzian and a Harbinger of electromagnetic chirality," *IEEE Antennas Propagat. Magazine*, vol. 34, no. 3, pp. 24–30, 1992.
- 26. W. E Kock, "Metallic delay lines," Bell Sys. Tech. J., Vol. 27, pp. 58-82, 1948.

- 27. V. G. Veselago, "The electrodynamics of substances with simultaneous negative values of ε and μ ," Sov. Phys.-Usp., vol. 47, pp. 509–514, Jan.-Feb. 1968.
- 28. R. E. Collin, "Frequency dispersion limits resolution in Veselago lens," *Progress in Electromagnetic Research*, vol. 19, pp. 233–261, 2010.
- 29. A.D. Yaghjian and T.B. Hansen, "Plane-wave solutions to frequency-domain and time-domain scattering from magnetodielectric slabs," *Phys. Rev. E*, 73, 046608, April 2006; erratum, 76, 049903, October 2007.
- 30. J. B. Pendry, A. J. Holden, W. J. Stewart and I. Youngs, "Extremely, low-frequency plasmons in metallic mesostructure," *Phys. Rev. Letters.*, vol. 76, pp. 4773–4776, June 1996.
- 31. J. B. Pendry, A. J. Holden, D. J. Robbins, and W. J. Stewart, "Low-frequency plasmons in thin wire structures," *J. Phys., Condens. Matter*, vol. 10, pp. 4785–4809, 1998.
- 32. J. B. Pendry, A. J. Holden, D. J. Robbins, and W. J. Stewart, "Magnetism from conductors and enhanced nonlinear phenomena," *IEEE Trans. Microwave Theory Tech.*, vol. 47, no. 11, pp. 2075–2081, Nov. 1999.
- 33. J. B. Pendry, "Negative refraction makes a perfect lens," *Phys. Rev. Lett.*, vol. 85, pp. 3966–3969, Oct. 2000.
- 34. D. R. Smith, W. J. Padilla, D. C. Vier, S.C. Nemat-Nasser, and S. Schultz, "Composite medium with simultaneously negative permeability and permittivity," *Phys. Rev. Lett.*, vol. 84, pp. 4184–4187, May 2000.
- 35. D. R. Smith, D. C. Vier, N. Kroll, and S. Schultz, "Direct calculation of the permeability and permittivity for left-handed metamaterials," *Appl. Phys. Lett.*, vol. 77, pp. 2246–2248, Oct. 2000.
- 36. D. R. Smith and N. Kroll, "Negative refractive index in left-handed materials," *Phys. Rev. Lett.*, vol. 85, pp. 2933–2936, Oct. 2000.
- 37. R. A. Shelby, D. R. Smith, S. C. Nemat-Nasser, and S. Schultz, "Microwave transmission through a two-dimensional, isotropic, left-handed metamaterial," *Appl. Phys. Lett.*, 78, pp. 489–491, Jan. 2001.
- 38. A. Shelby, D. R. Smith, and S. Schultz, "Experimental verification of a negative index-of-refraction," *Science*, vol. 292, pp. 77–79, April 2001.
- 39. B. A. Munk, Finite Antenna Arrays and FSS, John Wiley & Sons, Hoboken, NJ, 2003.
- 40. T. M. Grzegorczyk, J. A. Kong, and R. Lixin, "Refraction experiments in waveguide environments," *Chapter 4 in Metamaterials: Physics and Engineering Explorations* N. Engeta and R. W. Ziolkowski (editors), Wiley-Interscience, 2006.
- 41. IEEE Transactions on Antennas and Propagation.
- 42. IEEE Transactions on Microwave Theory and Techniques.
- 43. IEEE Antennas and Wireless Propagation Letters.
- 44. IEEE Microwave and Wireless Components Letters.
- 45. Physical Review Letters.
- 46. Journal of Applied Physics.
- 47. G. V. Eleftheriades, "EM transmission-line metamaterials," *Materials Today*, vol. 12, no. 3, pp. 30–41, March 2009.
- 48. R. W. Ziolkowski, "Pulsed and CW Gaussian beam interactions with double negative material slabs," *Opt. Express*, Vol. 11, pp. 662–681, April 2003.
- 49. S. Ramo, J. R. Whinnery and T. Van Duzer, *Fields and Waves in Communication Electronics*, Third Edition, John Wiley & Sons, New York, 1994.
- 50. D. M. Pozar, Microwave Engineering, Second Edition, John Wiley & Sons, New York, 2004.

PROBLEMS

5.1. A uniform plane wave traveling in a dielectric medium with $\varepsilon_r = 4$ and $\mu_r = 1$ is incident normally upon a free-space medium. If the incident electric field is given by

$$\mathbf{E}^i = \hat{\mathbf{a}}_{v} 2 \times 10^{-3} e^{-j\beta z} \, \text{V/m}$$

write the:

- (a) Corresponding incident magnetic field.
- (b) Reflection and transmission coefficients.

- (c) Reflected and transmitted electric and magnetic fields.
- (d) Incident, reflected, and transmitted power densities.

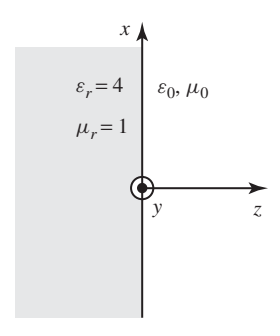


Figure P5-1

- **5.2.** The dielectric constant of water is 81. Calculate the percentage of power density reflected and transmitted when a uniform plane wave traveling in air is incident normally upon a calm lake. Assume that the water in the lake is lossless.
- **5.3.** A uniform plane wave propagating in a medium with relative permittivity of 4 is incident normally upon a dielectric medium with dielectric constant of 9. Assuming both media are nonferromagnetic and lossless, determine the:
 - (a) Reflection and transmission coefficients.
 - (b) Percentage of incident power density that is reflected and transmitted.
- **5.4.** A vertical interface is formed by having free space to its left and a lossless dielectric medium to its right with $\varepsilon=4\varepsilon_0$ and $\mu=\mu_0$, as shown in Figure P5-4. The incident electric field of a uniform plane wave traveling in the free-space medium and incident normally upon the interface has a value

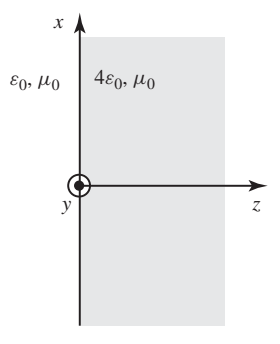


Figure P5-4

- of 2×10^{-3} V/m right before it strikes the boundary. At a frequency of 3 GHz, find the:
- (a) Reflection coefficient.
- (b) SWR in the free-space medium.
- (c) Positions (in meters) in the free-space medium where the electric field maxima and minima occur.
- (d) Maximum and minimum values of the electric field in the free-space medium.
- **5.5.** A uniform plane wave traveling in air is incident upon a flat, lossless, and infinite in extent dielectric interface with a dielectric constant of 4. In the air medium, a standing wave is formed. If the normalized magnitude of the incident E-field is $E_o = 1$, determine the:
 - (a) Maximum value of the E-field standing wave pattern in air.
 - (b) Shortest distance l (in λ_o) from the interface where the first maximum in the E- field standing wave pattern will occur (normalized to the incident field).
 - (c) Minimum value of the E-field standing wave pattern in air (normalized to the incident field).
 - (d) Shortest distance l (in λ_o) in air from the interface where the first minimum in the E-field standing wave pattern will occur (normalized to the incident field).
 - (e) Standing Wave Ratio (SWR) measured in the air medium.
 - (f) Input wave impedance inside the air medium where the:
 - 1. First maximum in the E-field standing wave pattern occurs.
 - 2. First minimum in the E-field standing wave pattern occurs.
- **5.6.** A CW circularly-polarized wave of $f = 100 \,\mathrm{MHz}$ of the form

$$\mathbf{E}^{i}(z) = \left(\hat{\mathbf{a}}_{x} - j\,\hat{\mathbf{a}}_{y}\right)e^{-j\,6\pi z}$$

where z is in meters, is traveling inside a lossless dielectric medium and is normally incident upon a flat planar interface formed by the dielectric medium and air. The interface is on the xy-plane. Assuming the permeability of the dielectric medium is the same as free space, determine the:

- (a) Dielectric constant (relative permittivity) of the dielectric medium.
- (b) Reflection coefficients for the $\hat{\mathbf{a}}_x$ and $\hat{\mathbf{a}}_y$ components.

- (c) Transmission coefficients for the $\hat{\mathbf{a}}_x$ and $\hat{\mathbf{a}}_y$ components.
- (d) Polarization (linear, circular or elliptical) of the reflected field.
- (e) Sense of polarization rotation, if any, of the reflected field.
- (f) Polarization (linear, circular or elliptical) of the transmitted field.
- (g) Sense of polarization rotation, if any, of the transmitted field.

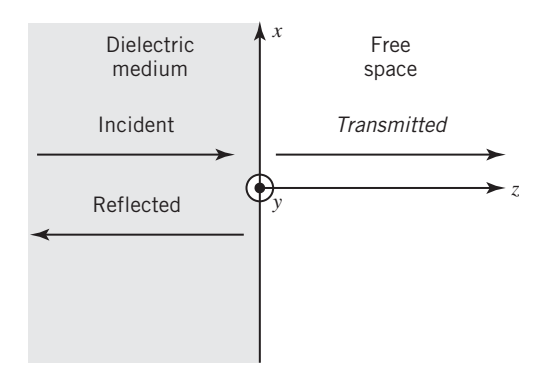


Figure P5-6

- **5.7.** The field radiated by an antenna along the +z axis is a uniform plane wave whose polarization is right-hand circularly-polarized (RHC). The field radiated by the antenna impinges, at normal incidence, upon a perfectly electric conducting (PEC) flat and infinite in extend ground plane. Determine the:
 - (a) Polarization of the field reflected by the ground plane toward the antenna, including the sense of rotation (if any). Justify your answer.
 - (b) Normalized output voltage (dimensionless and in dB) at the transmitting antenna, which is now acting as a receiving antenna, based on its reception of the reflected field. Justify your answer. Is it what you are expecting or is it a surprise?

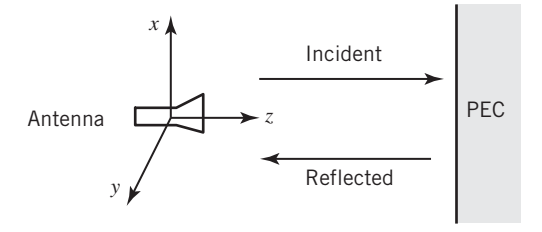


Figure P5-7

5.8. A time-harmonic electromagnetic wave traveling in free space is incident normally upon a perfect conducting planar surface, as shown in Figure P5-8. Assuming the incident electric field is given by

$$\mathbf{E}^{i} = \hat{\mathbf{a}}_{x} E_{0} e^{-j\beta_{0}z}$$

find the (a) reflected electric field, (b) incident and reflected magnetic fields, and (c) current density J_s induced on the conducting surface.

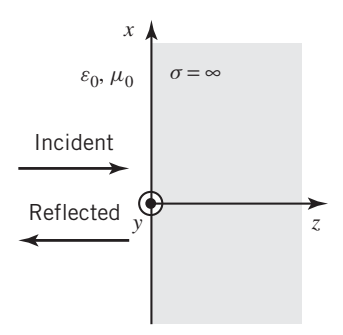


Figure P5-8

5.9. A uniform plane wave traveling in air is incident normally on a half space occupied by a lossless dielectric medium of relative permittivity of 4. The reflections can be eliminated by placing another dielectric slab, $\lambda_1/4$ thick, between the air and the original dielectric medium, as shown in Figure P5-9. To accomplish this, the intrinsic impedance η_1 of the slab must be equal to $\sqrt{\eta_0\eta_2}$ where η_0 and η_2 are, respectively, the intrinsic impedances of air and the original dielectric medium. Assuming that the relative permeabilities of all the media are unity, what should the relative permittivity of the dielectric slab be to accomplish this?

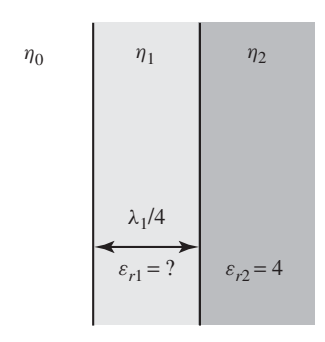


Figure P5-9

5.10. A uniform plane wave traveling in free space is incident normally upon a lossless dielectric slab of thickness *t*, as shown in Figure P5-10. Free space is found on the other side of the slab. Derive expressions for the total reflection and transmission coefficients in terms of the media constitutive electrical parameters and thickness of the slab.

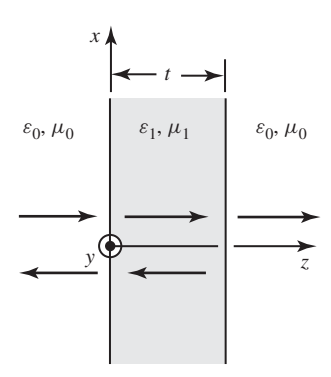
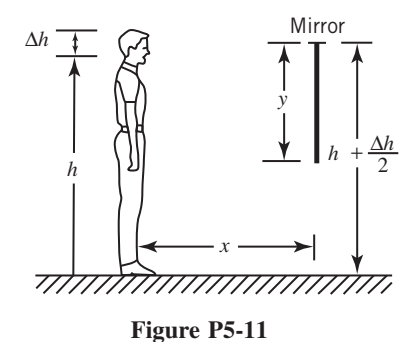


Figure P5-10

5.11. The vertical height from the ground to a person's eyes is h, and from his eyes to the top of his head is Δh . A flat mirror of height y is hung vertically at a distance x from the person. The top of the mirror is at a height of $h + (\Delta h/2)$ from the ground, as shown in Figure P5-11. What is the minimum length of the mirror in the vertical direction so that the person *only* sees his entire image in the mirror?



5.12. A linearly polarized wave is incident on an isosceles right triangle (prism) of glass, and it exits as shown in Figure P5-12. Assuming that the dielectric constant of the prism is 2.25, find the ratio of the exited average power density S_e to that of the incident S_i .

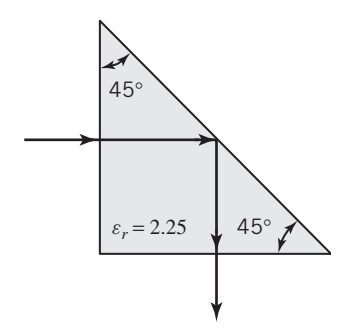


Figure P5-12

5.13. A uniform plane wave is obliquely incident at an angle of 30° on a dielectric slab of thickness d with $\varepsilon = 4\varepsilon_0$ and $\mu = \mu_0$ that is embedded in free space, as shown in Figure P5-13. Find the angles θ_2 and θ_3 (in degrees).

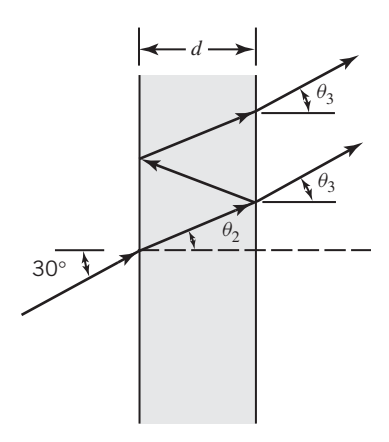


Figure P5-13

- **5.14.** A perpendicularly polarized uniform plane wave traveling in free space is obliquely incident on a dielectric with a relative permittivity of 4, as shown in Figure 5-2. What should the incident angle be so that the reflected power density is 25% of the incident power density?
- **5.15.** Repeat Problem 5-14 for a parallel polarized uniform plane wave.
- **5.16.** Find the Brewster angles for the interfaces whose reflection coefficients are plotted in Figure 5-5.
- **5.17.** A parallel-polarized uniform plane wave is incident obliquely on a lossless dielectric slab that is embedded in a free-space medium, as shown in Figure P5-17. Derive

expressions for the total reflection and transmission coefficients in terms of the electrical constitutive parameters, thickness of the slab, and angle of incidence.

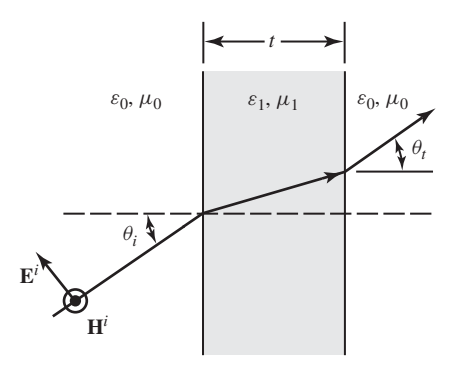


Figure P5-17

5.18. Repeat Problem 5-17 for a perpendicularly polarized plane wave, as shown in Figure P5-18.

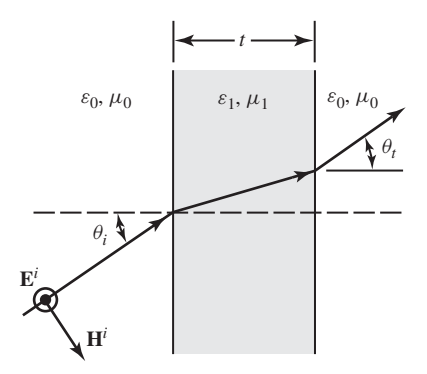


Figure P5-18

- **5.19.** A perpendicularly polarized plane wave traveling in a dielectric medium with relative permittivity of 9 is obliquely incident on another dielectric with relative permittivity of 4. Assuming that the permeabilities of both media are the same, find the incident angle (measured from the normal to the interface) that results in total reflection.
- **5.20.** Calculate the Brewster and critical angles for a parallel-polarized wave when the plane interface is:
 - (a) Water to air (ε_r of water is 81).
 - (b) Air to water.
 - (c) High density glass to air (ε_r) of glass is 9).

- **5.21.** A uniform plane wave traveling in a lossless dielectric is incident normally on a flat interface formed by the presence of air. For ε_r 's of 2.56, 4, 9, 16, 25, and 81:
 - (a) Determine the critical angles.
 - (b) Find the Brewster angles if the wave is of parallel polarization.
 - (c) Compare the critical and Brewster angles found in parts (a) and (b).
 - (d) Plot the magnitudes of the reflection coefficients for both perpendicular, $|\Gamma_{\perp}|$, and parallel, $|\Gamma_{\parallel}|$, polarizations versus incidence angle.
 - (e) Plot the phase (in degrees) of the reflection coefficients for both perpendicular and parallel polarizations versus incidence angle.
- 5.22. The transmitting antenna of a ground-to-air communication system is placed at a height of 10 m above the water, as shown in Figure P5-22. For a ground separation of 10 km between the transmitter and the receiver, which is placed on an airborne platform, find the height *h*₂ above water of the receiving system so that the wave reflected by the water does not possess a parallel polarized component. Assume that the water surface is flat and lossless.

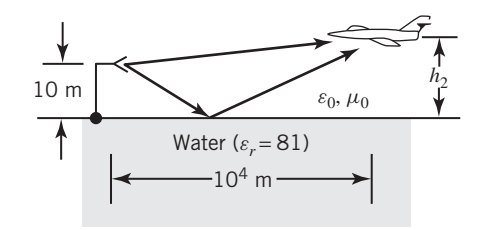


Figure P5-22

- **5.23.** For the geometry of Problem 5-22, the transmitter is radiating a right-hand circularly polarized wave. Assuming the aircraft is at a height of 1,101.11 m, give the polarization (linear, circular, or elliptical) and sense of rotation (right or left hand) of the following.
 - (a) A wave reflected by the sea and intercepted by the receiving antenna.
 - (b) A wave transmitted, at the same reflection point as in part (a), into the sea.
- **5.24.** The heights above the earth of a transmitter and receiver are, respectively, 100 and 10 m, as shown in Figure P5-24. Assuming that the transmitter radiates both perpendicular and parallel polarizations, how far

apart (in meters) should the transmitter and receiver be placed so that the reflected wave has no parallel polarization? Assume that the reflecting medium is a lossless flat earth with a dielectric constant of 16.

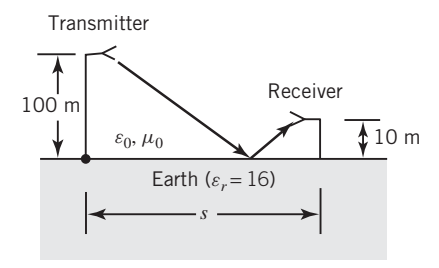


Figure P5-24

5.25. A light source that shines isotropically is submerged at a depth *d* below the surface of water, as shown in Figure P5-25. How far in the *x* direction (both positive and negative) can an observer (just above the water interface) go and still see the light? Assume that the water is flat and lossless with a dielectric constant of 81.

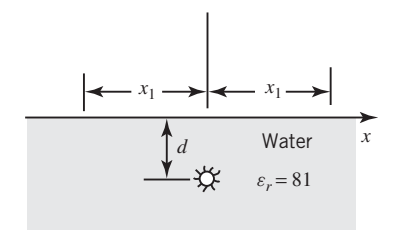


Figure P5-25

- **5.26.** The 30° to 60° dielectric prism shown in Figure P5-26 is surrounded by free space.
 - (a) What is the minimum value of the prism's dielectric constant so that there is no time-average power density transmitted across the hypotenuse when a

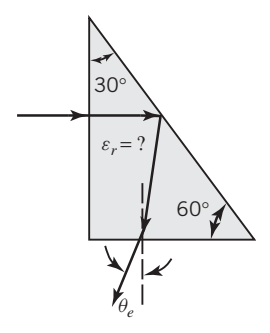


Figure P5-26

- plane wave is incident on the prism, as shown in the figure?
- (b) What is the exiting angle θ_e if the dielectric constant of the prism is that found in part (a)?
- 5.27. A uniform plane wave of parallel polarization, traveling in a lossless dielectric medium with relative permittivity of 4, is obliquely incident on a free-space medium. What is the angle of incidence so that the wave results in a complete (a) transmission into the free-space medium and (b) reflection from the free-space medium?
- **5.28.** A fish is swimming in water beneath a circular boat of diameter *D*, as shown in Figure P5-28.
 - (a) Find the largest included angle $2\theta_c$ of an imaginary cone within which the fish can swim and not be seen by an observer at the surface of the water.
 - (b) Find the smallest height of the cone. Assume that light strikes the boat at grazing incidence $\theta_i = \pi/2$ and refracts into the water.

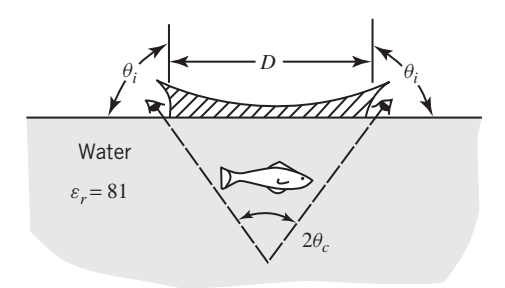


Figure P5-28

5.29. Any object above absolute zero temperature $(0 \text{ K or } -273^{\circ}\text{C})$ emits electromagnetic radiation. According to the reciprocity theorem, the amount of electromagnetic energy emitted by the object toward an angle θ_i is equal to the energy received by the object when an electromagnetic wave is incident at an angle θ_i , as shown in Figure P5-29. The electromagnetic power emitted by the object is sensed by a microwave remote detection system as a brightness temperature T_B given by

$$T_B = eT_m = (1 - |\Gamma|^2)T_m$$

where

e = emissivity of the object (dimensionless)

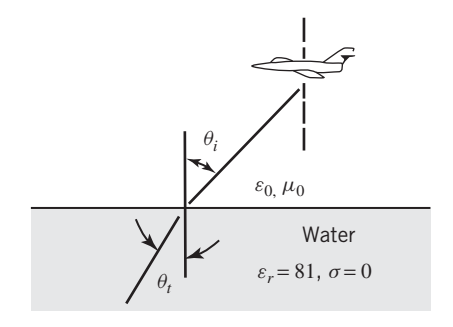


Figure P5-29

 Γ = reflection coefficient for the interface

 T_m = thermal (molecular) temperature of object (water)

It is desired to make the brightness temperature T_B equal to the thermal (molecular) temperature T_m .

- (a) State the polarization (perpendicular, parallel, or both) that will accomplish this.
- (b) At what angle θ_i (in degrees) will this occur when the object is a flat water surface?
- **5.30.** A uniform plane wave at a frequency of 10^4 Hz is traveling in air, and it is incident normally on a large body of salt water with constants of $\sigma = 3$ S/m and $\varepsilon_r = 81$. If the magnitude of the electric field on the salt water side of the interface is 10^{-3} V/m, find the depth (in meters) inside the salt water at which the magnitude of the electric field has been reduced to 0.368×10^{-3} V/m.
- **5.31.** At large observation distances, the field radiated by a satellite antenna that is attempting to communicate with a submerged submarine is locally TEM (also assume uniform plane wave), as shown in Figure P5-31. Assuming the incident electric field before

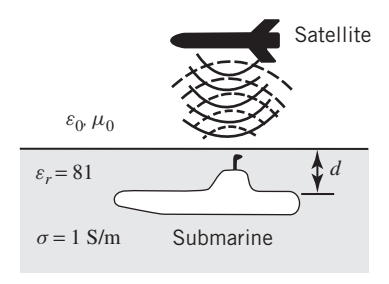


Figure P5-31

it impinges on the water is 1 mV/m and the submarine is directly below the satellite, find at 1 MHz the:

- (a) Intensity of the reflected E field.
- (b) SWR created in air.
- (c) Incident and reflected power densities.
- (d) Intensity of the transmitted E field.
- (e) Intensity of the transmitted power density.
- (f) Depth *d* (in meters) of the submarine where the intensity of the transmitted electric field is 0.368 of its value immediately after it enters the water.
- (g) Depth (in meters) of the submarine so that the distance from the surface of the ocean to the submarine is 20λ (λ in water).
- (h) Time (in seconds) it takes the wave to travel from the surface of the ocean to the submarine at a depth of 100 m.
- (i) Ratio of velocity of the wave in water to that in air (v/v_0) .
- **5.32.** A uniform plane wave traveling inside a good conductor with conductivity σ_1 is incident normally on another good conductor with conductivity σ_2 , where $\sigma_1 > \sigma_2$. Determine the ratio of σ_1/σ_2 so that the SWR inside medium 1 near the interface is 1.5.
- **5.33.** A right-hand circularly polarized uniform plane wave traveling in air is incident normally on a flat and smooth water surface with $\varepsilon_r = 81$ and $\sigma = 0.1$ S/m, as shown in Figure P5-33. Assuming a frequency of 1 GHz and an incident electric field of

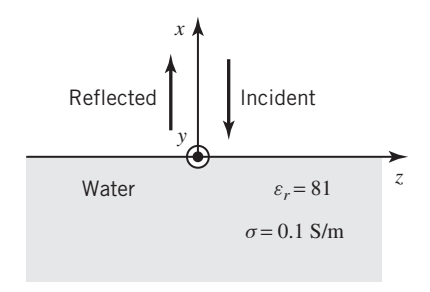


Figure P5-33

$$\mathbf{E}^{i} = (\hat{\mathbf{a}}_{y} + \hat{\mathbf{a}}_{z}e^{j\psi})E_{0}e^{j\beta_{0}x}$$

do the following.

- (a) Determine the value of ψ .
- (b) Write an expression for the corresponding incident magnetic field.

- (c) Write expressions for the reflected electric and magnetic fields.
- (d) Determine the polarization (including sense of rotation) of the reflected wave.
- (e) Write expressions for the transmitted electric and magnetic fields.
- (f) Determine the polarization (including sense of rotation) of the transmitted
- (g) Determine the percentage (compared to the incident) of the reflected and transmitted power densities.
- **5.34.** A right-hand circularly polarized wave is incident normally on a perfect conducting flat surface ($\sigma = \infty$).
 - (a) What is the polarization and sense of rotation of the reflected field?
 - (b) What is the normalized (maximum unity) output voltage if the reflected wave is received by a right-hand circularly polarized antenna?
 - (c) Repeat part b if the receiving antenna is left-hand circularly polarized.
- 5.35. Repeat Problem 5.34 if the reflecting surface is water ($f = 10 \,\mathrm{MHz}$, $\varepsilon_r = 81$ and $\sigma = 4 \text{ S/m}$).
- 5.36. A parallel polarized plane wave traveling in a dielectric medium with ε_1 , μ_1 is incident obliquely on a planar interface formed by the dielectric medium with ε_2 , μ_2 such that $\varepsilon_2\mu_2 < \varepsilon_1\mu_1$. Assuming that the incident angle θ_i is equal to or greater than the critical angle θ_c of (5-35b), derive expressions for the reflection coefficient Γ^b_{\parallel} and transmission coefficient T_{\parallel}^{b} , and the incident $\mathbf{S}_{\parallel}^{i}$, reflected $\mathbf{S}_{\parallel}^{r}$, and transmitted $\mathbf{S}_{\parallel}^{t}$ average power densities respectively.
- A perpendicularly polarized uniform plane wave traveling inside a free-space medium is obliquely incident, at an incident angle $\theta_i = 60^\circ$, upon a planar dielectric medium with constitutive parameters of $\varepsilon_2 = 4\varepsilon_0$, $\mu_2 = \mu_0$. Using Figure 5-2 as a reference geometry, determine the:
 - (a) Wave impedance of the:
 - · Incident wave
 - · Reflected wave
 - Transmitted wave
 - (b) Directional impedance in the +z and +x directions, respectively, of the:

 - Incident wave Z_{to}^{+z}, Z_{to}^{+x}
 Transmitted wave Z_t^{+z}, Z_t^{+x}

- (c) Reflection coefficient Γ_{in}^{+z} in the +zdirection (magnitude and phase) inside the free-space medium based on:
 - The directional impedances
 - An alternate equation
 - Compare the two answers. Are the answers the same or different in both magnitude and phase? Should they be the same or different in magnitude and phase?
- (d) SWR inside the free-space medium.
- 5.38. A uniform plane wave of either parallel or perpendicular polarization, as shown respectively in Figures 5-2 and 5-4, traveling in free space is incident upon a dielectric/magnetic material such that the product of the relative permittivity and permeability of the dielectric/magnetic material is much greater than unity; that is

$$\varepsilon_r \mu_r \gg 1$$

The intrinsic impedances of the two media are, respectively, η_0 (free space) and η (dielectric/magnetic material).

- (a) Determine an approximate value of the refraction angle θ_t (in degrees) for:
 - 1. Perpendicular polarization.
 - 2. Parallel polarization.
- (b) Obtain simplified expressions, in terms η_0 and η , of the Brewster angle $\theta_i = \theta_R$
 - 1. Perpendicular polarization.
 - 2. Parallel polarization.
- 5.39. A dielectric slab of polystyrene ($\varepsilon_r = 2.56$), of any thickness, is bounded on both of its sides by air. In order to eliminate reflections on each of its interfaces, the slab is covered on each of its faces with a dielectric

At a frequency of 10 GHz, determine, for each dielectric material that must cover each of the faces of the slab, the:

- (a) Thickness (in λ_i ; wavelength in the corresponding dielectric).
- (b) Thickness (in cm).
- (c) Dielectric constant.
- (d) Intrinsic impedance of its medium.
- (e) SWR created in air when a plane wave impinges at normal incidence from one of its sides when the slab is covered with the selected cover material.
- 5.40. For Example 5-10, determine the bandwidth, and the lower and upper frequencies of the

bandwidth, over which the system can operate so that the magnitude of the reflection coefficient is equal to:

- (a) 0.05
- (b) 0.10

Assume a center frequency of 10 GHz within the bandwidth.

- **5.41.** For the one-slab reflection problem of Figure 5-11*a*, write the expressions for the:
 - (a) Exact transmission-line model.
 - (b) Exact ray-tracing model.
 - (c) Approximate ray-tracing model.

For Example 5-9, when d=0.9375 cm, plot the magnitude of the input reflection coefficient for 5 GHz $\leq f \leq$ 15 GHz using the:

- (d) Exact transmission line-model.
- (e) Exact ray-tracing model.
- (f) Approximate ray-tracing model.

For Example 5-10, when $d = \lambda_{20}/4$ at the center frequency $f_0 = 10$ GHz, plot the magnitude of the input reflection coefficient for 5 GHz $\leq f \leq$ 15 GHz using the:

- (g) Exact transmission line-model.
- (h) Exact ray-tracing model.
- (i) Approximate ray-tracing model.
- 5.42. A dielectric slab of thickness d, as shown in Figure 5-11a, is surrounded with air on its left and with a dielectric material, whose dielectric constant (relative permittivity) is 16, on its right. You are asked as an electromagnetic engineer/scientist to design a dielectric slab with the smallest nonzero thickness that will reduce the input reflection coefficient, at normal incidence, to zero at a frequency of 1 GHz.

What should one set of parameters of the dielectric slab be that will reduce the reflection coefficient to zero? State the:

- (a) Smallest thickness of the slab in terms of the wavelength in the dielectric slab.
- (b) Smallest thickness of the slab, in cm, at 1 GHz.
- (c) Dielectric constant of the dielectric material of the slab.

Justify your answers. Assume that the permeability of all three media is the same as free space.

5.43. A symmetrical three-layer dielectric slab is bounded at both sides by air, and it is designed to filter the signal that can pass through it. The dielectric constant of all the 5 media, including the medium to the left (air), the 3 slabs, and the medium to the

right (air) are, respectively, $\varepsilon_{r0} = 1$, $\varepsilon_{r1} = 4$, $\varepsilon_{r2} = 9$, $\varepsilon_{r3} = 4$, $\varepsilon_{r4} = 1$.

Assuming that at the operating frequency the width d_m , n = 1, 2, 3, of each layer is one quarter-of-a wavelength in its respective medium, determine the:

- (a) Corresponding intrinsic reflection coefficients at each interface (Γ₀₁, Γ₁₂, Γ₂₃, Γ₃₀).
- (b) Approximate total input reflection coefficient at the leading interface between air and the first layer (Γ_{in}) at the center operating frequency.
- **5.44.** A uniform plane wave traveling in air, whose amplitude of the magnetic field is E_o , is incident normally upon a perfect electric conductor that is coated with a lossless dielectric material with $\varepsilon = 4\varepsilon_o$, $\mu = \mu_o$, $\sigma = 0$, and thickness of $\lambda/8$ (λ is the wavelength in the dielectric). Just to the left of the air side of the air-dielectric interface, determine the:
 - (a) Exact reflection coefficient looking normally just to the left of the air/dielectric interface $(z = -d^-)$, i.e., toward the conductor).
 - (b) SWR looking normally just to the left of the air/dielectric interface ($z = -d^-$, i.e., toward the conductor).

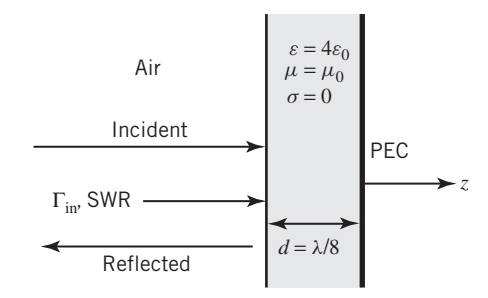


Figure P5-44

- **5.45.** Two vertical lossless dielectric slabs, each of thickness equal to $\lambda_0/4$ at a center frequency of $f_0 = 2$ GHz, are sandwiched between a lossless semi-infinite medium of dielectric constant $\varepsilon_r = 2.25$ to the left and air to the right. Assume a fractional bandwidth of 0.5 and a binomial design.
 - (a) Find the magnitude of the maximum reflection coefficient within the allowable bandwidth.
 - (b) Determine the magnitude of the reflection coefficients at each interface (junction).

- (c) Compute the intrinsic impedances, dielectric constants, and thickness (in centimeters) of each dielectric slab.
- (d) Determine the lower and upper frequencies of the bandwidth.
- (e) Plot the magnitude of the reflection coefficient inside the dielectric medium with $\varepsilon_r = 2.25$ as a function of frequency (within $0 \le f/f_0 \le 2$).
- **5.46.** It is desired to design a three-layer (each layer of $\lambda_0/4$ thickness) impedance transformer to match a semi-infinite dielectric medium of $\varepsilon_r = 9$ on one of its sides and one with $\varepsilon_r = 2.25$ on the other side. The maximum SWR that can be tolerated inside the dielectric medium with $\varepsilon_r = 9$ is 1.1. Assume a center frequency of $f_0 = 3$ GHz and a binomial design.
 - (a) Determine the allowable fractional bandwidth and the lower and upper frequencies of the bandwidth.
 - (b) Find the magnitude of reflection coefficients at each junction.
 - (c) Compute the magnitude of the maximum reflection coefficient within the bandwidth.
 - (d) Determine the intrinsic impedances, dielectric constants, and thicknesses (in centimeters) of each dielectric slab.
 - (e) Plot the magnitude of the reflection coefficient inside the dielectric medium with $\varepsilon_r = 9$ as a function of frequency (within $0 \le f/f_0 \le 2$).
- **5.47.** Repeat Example 5-11 using a Tschebyscheff design.
- **5.48.** Repeat Problem 5.45 using a Tschebyscheff design.
- **5.49.** Repeat Problem 5.46 using a Tschebyscheff design.
- **5.50.** A right-hand (CW) elliptically polarized wave traveling in free space is obliquely incident at an angle $\theta_i = 30^\circ$, measured from the normal, on a flat perfect electric conductor of infinite extent. If the incident field has an axial ratio of -2, determine the polarization of the reflected field. This is to include the axial ratio as well as its sense of rotation. Assume that the time-phase difference between the components of the incident field is 90° .

- **5.51.** Repeat Problem 5.50 if the reflecting surface is a flat lossless ($\sigma_2 = 0$) ocean ($\varepsilon_2 = 81\varepsilon_0$ and $\mu_2 = \mu_0$) of infinite extent. Also find the polarization of the wave transmitted into the water.
- **5.52.** A uniform plane wave is normally incident upon a Perfect Electric Conductor (PEC) medium. The incident electric field is given by

$$\mathbf{E}^{i}(z) = (\hat{\mathbf{a}}_z + j2\hat{\mathbf{a}}_y) E_o e^{-j\beta_o x}$$

where β_o and E_o are real constants. Assuming a $e^{+j\omega t}$ time convention:

- (a) Write an expression for the reflected electric field.
- (b) For the incident wave, determine the:
 - Polarization (linear, circular, or elliptical). Justify your answer.
 - Sense of rotation of the incident wave (CW or CCW). Justify your answer.
 - Axial Ratio (AR). Justify your answer.
- (c) For the reflected wave, determine the:
 - Polarization (linear, circular or elliptical). Justify your answer.
 - Sense of rotation of the incident wave (CW or CCW). Justify your answer.
 - Axial Ratio (AR). Justify your answer.

For all of the above, be sure to justify your answers. Verify with the MATLAB computer program Polarization_Refl_Trans.

5.53. A uniform plane wave is normally incident upon a Perfect Magnetic Conductor (PMC). The incident electric field is given by

$$\mathbf{E}^{i}(z) = (2\hat{\mathbf{a}}_{x} - j\hat{\mathbf{a}}_{z}) E_{o} e^{-j\beta_{o}y}$$

where β_o and E_o are real constants. Assuming a $e^{+j\omega t}$ time convention:

- (a) Write an expression for the reflected electric field.
- (b) For the incident wave, determine the:
 - Polarization (linear, circular, or elliptical). Justify your answer.
 - Sense of rotation of the incident wave (CW or CCW). Justify your answer.
 - Axial Ratio (AR). Justify your answer.
- (c) For the reflected wave, determine the:
 - Polarization (linear, circular, or elliptical). Justify your answer.

- Sense of rotation of the incident wave (CW or CCW). Justify your answer.
- Axial Ratio (AR). Justify your answer.

For all of the above, be sure to justify your answers. Also verify with MATLAB computer program **Polarization_Refl_Trans.**

- **5.54.** A left-hand (CCW) circularly polarized wave traveling inside a lossless earth, with a dielectric constant of 9, is incident upon a planar interface formed by the earth and air. The angle of incidence is 18.43495°. Determine the:
 - (a) Polarization of the reflected wave (linear, circular, elliptical).
 - (b) Sense of rotation of the reflected wave;(CW or CCW), if appropriate.
 - (c) Polarization of the transmitted wave (linear, circular, elliptical).
 - (d) Sense of rotation of the transmitted wave; (CW, CCW), if appropriate.

As an option, you do not have to use too many analytical equations as long as you can

justify the correct answers using words/text (you can keep the formulations minimal).

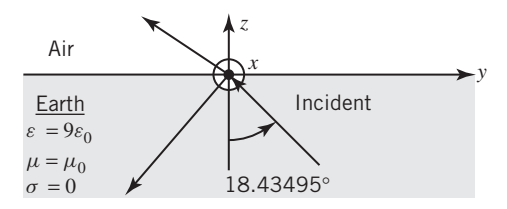


Figure P5-54

- **5.55.** Repeat Problem 5.54 when the incident wave is right-hand (CW) circularly polarized.
- **5.56.** Derive the transmission coefficient for the dielectric slab of Example 5-15.
- **5.57.** For a planar interface formed by DPS-DNG materials and assuming parallel polarization wave incidence, write expressions for the wavenumbers and Poynting vectors, similar in form to the ones of Figure 5-29, (5-110a) through (5-110c) and (5-111a) through (5-111c). Examine the directions of the wavenumbers and Poynting vectors of the transmitted wave and compare with those for a DPS-DPS interface.